INVESTIGATING ROLES OF THE BRG1-ASSOCIATED FACTOR (BAF) CHROMATIN REMODELING COMPLEX DURING MAMMALIAN HEART VALVE DEVELOPMENT

by

BRYNN NICOLE-YOSHIKO AKERBERG

A DISSERTATION

Presented to the Department of Biology
and the Graduate School of the University of Oregon
in partial fulfillment of the requirements
for the degree of
Doctor of Philosophy

September 2015

DISSERTATION APPROVAL PAGE

Student: Brynn Nicole-Yoshiko Akerberg

Title: Investigating Roles of the Brg1-Associated Factor (BAF) Chromatin Remodeling Complex during Mammalian Heart Valve Development

This dissertation has been accepted and approved in partial fulfillment of the requirements for the Doctor of Philosophy degree in the Department of Biology by:

Victoria Herman	Chairperson
Kryn Stankunas	Advisor
Chris Doe	Core Member
Eric Selker	Core Member
Tom Stevens	Institutional Representative

and

Scott L. Pratt	Dean of the Graduate School

Original approval signatures are on file with the University of Oregon Graduate School.

Degree awarded September 2015

DISSERTATION ABSTRACT

Brynn Nicole-Yoshiko Akerberg

Doctor of Philosophy

Department of Biology

September 2015

Title: Investigating Roles of the Brg1-Associated Factor (BAF) Chromatin Remodeling Complex during Mammalian Heart Valve Development

The integration of chromatin regulation into the gene regulatory networks that progressively transform endocardial cushions into highly structured valves is poorly understood. To investigate contributions of chromatin remodeling to valve development, we use two endocardial Cre lines to conditionally delete floxed *Brg1*, the core subunit of the Brg1-associated factor complex. In an early-deleting *Tie2:Cre* model, loss of *Brg1* disrupts endocardial-mesenchymal transformation (EMT) in both the proximal outflow tract (pOFT) and atrioventricular canal (AVC) cushions. EMT appears to initiate normally in the absence of Brg1, but endocardial cells fail to switch from an epithelial to mesenchymal gene expression program. In a later-deleting *Nfatc1*^{Cre} model, *Brg1*-deficient mice develop thickened, malpatterned and frequently bicuspid semilunar valves while showing normal AVC-derived valves. Fate mapping experiments demonstrate that the enlarged semilunar valves result from an expansion of non-*Nfatc1*^{Cre}-lineage mesenchyme. Paradoxically, until E14.5, these same embryos have smaller semilunar valves, *originating* from a moderate deficiency of pOFT EMT. Depletion of this mesenchyme sub-population precludes formation of the valves' base and hinge regions and disrupts growth regulatory networks, causing the valves to *progress* to a diseased

state. RNA-seq of E14.5 *Nfatc1*^{Cre};*Brg1*$^{F/F}$ cardiac cushions identifies novel transcripts that may coordinate cellular interactions that direct growth and patterning stages of semilunar valve development. We propose that early disruption of EMT in the pOFT is sufficient to trigger secondary responses that culminate in commonly observed valve phenotypes in both mouse genetic models and human disease.

This dissertation includes previously published and unpublished co-authored material.

CURRICULUM VITAE

NAME OF AUTHOR: Brynn Nicole-Yoshiko Akerberg

GRADUATE AND UNDERGRADUATE SCHOOLS ATTENDED:

University of Oregon, Eugene

University of Washington, Seattle

DEGREES AWARDED:

Doctor of Philosophy, Biology, 2015, University of Oregon

Bachelor of Science, Molecular, Cellular and Developmental Biology, 2009, University of Washington

AREAS OF SPECIAL INTEREST:

Molecular, Cellular and Developmental Biology

Developmental Cardiovascular Biology Research

GRANTS, AWARDS, AND HONORS:

Department of Biology Travel Award, 2015

Predoctoral Fellowship, American Heart Association, 2012 to 2014

Weinstein Cardiovascular Conference 'Best poster presentation' award, 2013

Developmental Biology Training Grant, National Institutes of Health, 2010 to 2011

Boeing Employees' Credit Union Scholars Award, University of Washington, 2005 to 2007

PUBLICATIONS:

Akerberg BN, Sarangam ML, Stankunas K. 2015. Endocardial Brg1 disruption illustrates the developmental origins of semilunar valve disease. *Developmental Biology, accepted articles* 1–15.

Chen HI, Sharma B, Akerberg BN, Numi HJ, Kivela R, Saharinen P, Aghajanian H, McKay AS, Bogard PE, Chang AH, et al. 2014. The sinus venosus contributes to coronary vasculature through VEGFC-stimulated angiogenesis. *Development* 141: 4500–4512.

ACKNOWLEDGMENTS

I would like to sincerely thank my advisor, Dr. Kryn Stankunas, for his mentorship and guidance during my time in his lab. Many thanks goes to Vidusha Devasthali for her technical assistance and friendship during the early years of the Stankunas lab and thereafter. I thank all the Stankunas lab members for critical feedback on the *Developmental Biology* manuscript and for their technical support. I greatly appreciate the advice and feedback from my dissertation advisory committee members: Doctors Tory Herman, Chris Doe, Eric Selker and Tom Stevens. I am grateful for all of my friends and family and my most heartfelt appreciation goes out to my co-worker and husband, Alex Akerberg. It is his persistence to make me laugh and put up with my (now our) inbred shih-tzu that make me truly lucky. A special acknowledgement to my parents, Rhonda and Jim Simek and my sister Carissa for all of their support during my time in Eugene, Oregon.

These projects originated in the laboratory of Dr. Ching-Pin Chang and benefited from his early technical and intellectual input. Dr. Bin Zhou shared the *Nfatc1*-based Cre lines in advance of publication. The UO ACISS computing cluster used for RNA-Seq analyses was NSF-supported (OCI-0960354). I was funded by an American Heart Association (AHA) predoctoral fellowship (12PRE11800017) from 2012-2014. Undergraduate researcher, Maithri Sarangam, received an AHA summer research award. The March of Dimes (Basil O'Connor Award) and the National Institutes of Health (4R00HL087598 and 1R01HL115294) provided funding (K.S. lab).

TABLE OF CONTENTS

Chapter Page

Chapter Page

LIST OF FIGURES

CHAPTER I

INTRODUCTION

Congenital heart defects (CHD) are the number one cause of deaths in infants and congenital valve disease (CVD) affects nearly 2% of the world's population. The high incidence of these congenital diseases emphasizes the need to understand the cause of these common birth defects (Go et al. 2013). Often semilunar valve (SLV) disease originates as a congenital defect and is characterized by dramatically overgrown and myxomatous aortic/pulmonic valves (Stephens et al. 2012).

Mammalian valve development is a complex developmental process that initiates with the formation of primitive endocardial cushions that subsequently mature into elongated and thin valves. Cardiac cushions are temporally and spatially restricted 'swellings' between the endocardium and myocardium with a secreted proteoglycan-rich substance called cardiac jelly (Eisenberg and Markwald 1995). An endothelial-to-mesenchymal transformation (EMT) originates from the endocardium to populate the proximal-outflow tract (pOFT) and atrioventricular canal (AVC) cardiac cushions (Krug et al. 1987; Eisenberg and Markwald 1995). Beginning at embryonic day 9.5 (E9.5), a defined subset of endocardial cells undergo EMT to delaminate from the endocardium, differentiate into a mesenchymal cell and migrate into the extracellular matrix within both the AVC and pOFT cushions. This process requires several signaling molecules to

initiate and reinforce the EMT process. Misexpression of growth factor ligands inhibits EMT and similarly, loss of cardiac transcription factors and/or Notch signaling components leads to severe EMT defects on all cardiac cushions (Akhurst et al. 1990; Potts et al. 1991; Ramsdell and Markwald 1997; Rivera-Feliciano et al. 2006; Timmerman et al. 2004; Wang et al. 2013). Extensive research has described early endocardial cushion formation, but we remain perplexed about the molecular regulation of endocardial cushion maturation and remodeling stages of valve development.

The outflow tract has two distinct sets of endocardial cushions that contain mesenchyme of multiple cellular origins. The proximal outflow tract (pOFT) cushion is most adjacent to the newly looped heart and contributes to semilunar valves and septation of the ventricles. The pOFT is primarily made up of endocardial-derived mesenchyme. The distal outflow tract (dOFT) is situated farthest from the developing ventricles. The dOFT forms semilunar valves and provides material for septation of the outflow tract into the pulmonary and aortic arteries. Permanent lineage labeling studies have shown that dOFT mesenchyme primarily originates from cardiac neural crest and possibly second heart field (Kirby et al. 1983; Waldo et al. 1998; Jiang et al. 2000; Engleka et al. 2012; Sizarov et al. 2012). By E13.5, the cardiac valves begin to elongate and refine into thin cusps through the organization of extracellular matrix (ECM) into distinct regions. It is of considerable debate how the endocardial cushions mature into a valve that can withstand a lifetime of mechanical force to allow for proper blood flow. By late embryonic development, ECM begins to stratify into three distinguishable layers (Hinton et al. 2006). Collagens, proteoglycans and elastin become localized within the fibrosa, spongiosa and

ventricularis layers respectively, to generate the proper stiffness and flexibility of the individual cusps that retain form to regulate blood flow over the span of a lifetime (Gross and Kugel 1931; Broom 1978; Votteler et al. 2013). The extracellular matrix proteins are specifically distributed within the valve and their localization is often found perturbed in malformed and myxomatous valves (Wirrig et al. 2007; Tkatchenko et al. 2009; Hinton et al. 2010; Iwamoto et al. 2010; Kern et al. 2010; Dupuis et al. 2011).

Equally important as the transverse organization of the semilunar valves, is the medial-to-lateral patterning. The aortic and pulmonic valves are made up of three cusps. Each cusp can be considered as a shallow cup partially fastened within a cylindrical structure. All three of the aortic and pulmonic cusps contain a base region that fosters the connection to the smooth muscle and/or myocardium. This base region provides the rigidity and stiffness for the cusp and exhibits high expression of Tenascin C. The distal region of the cusps requires flexibility for opening and closing and display high expression of Versican and Periostin. The smooth muscle regions between the cusps are called interleaflet regions that lend support to the valve cusps. Together, the multi-dimensional organization of the semilunar valve interstitium suggests that proper formation is governed a complex set of developmental signaling cues. What is known about semilunar valve defects are primarily from studies of human diseased valves, where the disease has manifested to a myxomatous state. It is difficult to distinguish the initiation from the progression of semilunar valve disease (BAVD) and the former being the primary interest to genetic studies and the latter for therapeutic approaches. While a

number of genetic variants and disruptions have been associated with semilunar valve disease, an understanding of the role of chromatin regulators has yet to be elucidated.

Multi-subunit remodeling complexes that facilitate the activation and repression of genes through ATP-dependent nucleosome repositioning and replacement provide one mechanism of chromatin regulation. The SWI/SNF, or Brg1-associated factor (BAF) complex is a widely studied chromatin remodeling complex that is essential for development, such that complete mouse knock-out models are peri-implantation lethal (Bultman et al. 2000). Brg1 is the core ATPase subunit of the BAF complex and loss of Brg1 renders the BAF complex inactive (Kadoch and Crabtree 2013). The SWI/SNF complex is essential during mammalian heart development and studies have shown its importance in cardiomyocyte specification and ventricular trabeculation (Lickert et al. 2004; Stankunas et al. 2008; Takeuchi et al. 2011). Secondly, Brg1 is strongly expressed in a number of cell types, specifically in endocardial cells of the developing cardiac valves, which implicates a possible role for Brg1 during valvulogenesis.

The material presented in Chapter II describes a new mouse model for a common congenital heart defect, which has been accepted and recently published at *Developmental Biology* (online). Nearly all of the data presented in Chapter II was obtained and analyzed by myself, whereas Chapter III contains data (in the form of figures) obtained by myself and Vidusha Devasthali.

CHAPTER II

ENDOCARDIAL BRG1 DISRUPTION ILLUSTRATES THE DEVELOPMENTAL ORIGINS OF SEMILUNAR VALVE DISEASE

JOURNAL STYLE INFORMATION

AUTHOR CONTRIBUTIONS

I performed the experiments presented in this manuscript, with the exception of the 3-dimensional renderings of the E16.5 aortic valves. This data, presented in Fig. 1I, J and Fig. S5, was obtained and analyzed by an undergraduate researcher, Maithri Sarangam. Dr. Stankunas and I designed the experiments, prepared and wrote the manuscript.

INTRODUCTION

Congenital valve defects affect at least 2% of humans, a remarkable frequency that underlines the urgent need to understand their etiology (Hoffman and Kaplan 2002; Siu and Silversides 2010; Go et al. 2013). Frequently, developmentally abnormal valves do not progress to a pathologic state until late adulthood. For example, many cases of adult aortic valve disease characterized by thickened and myxomatous valve cusps display bicuspid rather than tricuspid arrangements originating from fusions during development

(Angelini et al. 1989; Roberts and Ko 2005). The rationale design of diagnostics and therapeutics therefore must distinguish between disrupted developmental processes, and their genetic and environmental influences, that trigger valve defects from mechanisms that drive the progression of an anatomically abnormal valve to a disease state.

Valvulogenesis is a dynamic and multistep process that transforms primitive endocardial cushions (ECs) into highly patterned valves with thin, elongated leaflets or cusps. ECs form at discrete sites of the looping heart tube by the local secretion of a specialized extracellular matrix called the cardiac jelly. The mesenchyme of atrioventricular canal ECs, which generate the mitral and tricuspid valves, originates from an endothelial-to-mesenchymal transition (EMT) of a subset of overlying endocardial cells. The outflow tract contains two pairs of neighboring ECs that together will form the semilunar valves. The proximal outflow tract (pOFT) cushions are primarily populated by EMT-derived mesenchyme. In contrast, the distal outflow tract (dOFT) cushion mesenchyme is largely derived from invading cardiac neural crest cells (NCCs) (Kirby et al. 1983; Waldo et al. 1998; Jiang et al. 2000). Additional cell populations, possibly of second heart field (SHF) origin, may contribute additional mesenchyme to the OFT cushions (Engleka et al. 2012; Sizarov et al. 2012).

EMT begins at embryonic day 9.5 (E9.5) in the AVC and soon after in the pOFT (Camenisch et al. 2002). Signaling factors, notably TGF-beta superfamily and Notch proteins, direct EMT by promoting gene expression program changes that transition endocardial cells from an interconnected epithelial to invasive mesenchymal state

(Ramsdell and Markwald 1997; Timmerman et al. 2004; Fischer et al. 2007; Venkatesh et al. 2008; Luna-Zurita et al. 2010; Chang et al. 2011; Wang et al. 2013). Deficient mesenchyme production, including when EMT is disrupted, impedes subsequent steps of valve development and leads to congenitally abnormal valves. A connection between EMT disruption and semilunar valve disease is suggested by *Notch1* being one of the few identified human aortic valve disease genes (Garg et al. 2005), although Notch signaling may also have later roles in valve development or homeostasis (Hofmann et al. 2012; Theodoris et al. 2015).

After EMT, the paired OFT ECs undergo a complex rearrangement to form two sets of symmetric tricuspid semilunar valves. By E13.5, the ECs meet and rearrange concomitantly with OFT septation to form separate pulmonic and aortic valves. The three cusps of each semilunar valve elongate and refine into thin tissues that will distend to meet and form a tight seal but have the flexibility to promptly open under pressure. Through postnatal development, the valve interstitium becomes stratified into layers of distinct extracellular matrix (ECM) composition to confer appropriate stiffness/flexibility across the cusps' short axis (Gross and Kugel 1931; Broom 1978; Hinton et al. 2006). Genetic loss or disruption of several extracellular proteins, such as Versican (Vcan) and Periostin (Postn), or their regulators, notably Adamts-family matrix proteases, produce valve defects (Tkatchenko et al. 2009; Kern et al. 2010; Dupuis et al. 2011; Cheek et al. 2012).

The semilunar valves are also patterned along their proximal-to-distal (long) axis. Each cusp of both aortic and pulmonic valves can be considered as a shallow bisected cup fastened within a cylindrical structure (Fig. S1A-B; see Appendix for all Supplemental Figures). The cusps' base region that connects them to underlying muscle is enriched with Tenascin C (Tnc), which helps confer tissue rigidity (Zhang et al. 1993; Satta et al. 2002; Hinton et al. 2006). In contrast, the flexible distal part of the cusps express high levels of Vcan and Postn (Kruzynska-Frejtag et al. 2001; Norris et al. 2008; Snider et al. 2008; Kern et al. 2010). The junction between the stiff base and flexible distal regions is commonly termed the hinge. The multi-dimensional organization of semilunar valve interstitium suggests that valve patterning requires a highly coordinated series of events that act over an extended period of development. Any of these steps could be perturbed to cause formation of a congenitally abnormal valve.

Human genetics and model organism studies, largely in mice, highlight disrupted regulatory pathways that coalesce on transcriptional changes as primary sources of SLV defects. For example, disrupted Notch signaling produces bicuspid aortic valve (BAV) in both mice and humans (Garg et al. 2005; Jain et al. 2011; Bosse et al. 2013). Additional mouse models of semilunar valve disease implicate Gata5 and Pax3 transcription factors and transcriptional effectors of Tgf-β family signaling (Jain et al. 2011; Laforest et al. 2011; Thomas et al. 2012; Dupuis et al. 2013). The molecular activities of these transcription factors, including an understanding of how they function within a chromatinized landscape to direct specific responses, are poorly understood. A role for chromatin regulation in human SLV disease is supported by the high frequency of de

novo variants in histone modifying genes in congenital heart disease (Zaidi et al. 2013). Further the sporadic inheritance patterns in afflicted families (Clementi et al. 1996; Huntington et al. 1997) suggest epigenetic influences that modify penetrance and/or expressivity of disease-causing alleles.

The Brg1-associated factor (BAF) chromatin remodeling complex facilitates activation and repression of genes by ATP-dependent nucleosome repositioning and/or replacement. The core ATPase subunit is predominantly provided by Brg1; in most cases, loss of Brg1 alone inactivates the BAF complex (Kadoch et al. 2013). Coordinately, *Brg1*-null mice are peri-implantation lethal (Bultman et al. 2000). The BAF complex has been implicated in multiple steps of heart development and disease, including cardiac specification and hypertrophy (Lickert et al. 2004; Hang et al. 2010; Takeuchi et al. 2011). Further, Brg1 is required in endocardial cells to maintain the microenvironment required for the initiation of cardiac trabeculation (Stankunas et al. 2008). Brg1 expression in endocardial and mesenchymal cells of the developing valves suggests additional roles for endocardial lineage BAF complexes during valvulogenesis.

Here, we disrupt endocardial-lineage *Brg1* in mice to demonstrate that the BAF chromatin remodeling complex is essential for semilunar valve development. Endocardial *Brg1*-deficient embryos develop thickened aortic and pulmonic valves that frequently are bicuspid and progress to a myxomatous, disease-like state. We map the origins of these defects to a partial disruption of pOFT EMT, a process an earlier deletion of endocardial *Brg1* shows the BAF complex is required for in both the pOFT and AVC. Developing

semilunar valves compensate for the deficiency of EMT-derived mesenchyme, but the responding mesenchymal populations are insufficient to fully pattern a complex, multi-origin semilunar valve interstitium. Therefore, an initial deficiency of pOFT EMT can trigger secondary responses that culminate in semilunar valve disease. By RNA-seq analysis of the *Brg1*-deficient valves, we additionally identify and characterize the expression of novel transcripts that may promote growth and patterning of semilunar valves and/or serve as biomarkers of a diseased state.

MATERIALS AND METHODS

Mice

All mouse husbandry and procedures were approved and monitored by the University of Oregon's Institutional Animal Care and Use Committee. Transgenic lines are described in Supplemental Materials.

Tissue processing and sectioning

Mouse embryos or dissected adult hearts were fixed overnight in 4% PFA/PBS at 4°C. Fixed tissue was washed thoroughly and then equilibrated overnight with PBS at 4°C. Samples were dehydrated through a graded ethanol series and cleared with xylenes prior to paraffin embedding. 7 mm paraffin sections were transferred to microscope slides for either histological or fluorescent antibody staining. Cryosections were used for RNA in situ hybridizations and occasional antibody staining (see Supplementary Materials). For cryosections, embryos were fixed as described, washed thoroughly with PBS,

equilibrated in 30% sucrose overnight at 4°C, embedded in OCT (Tissue-Tek), and sectioned (16 μm).

Histology

Hematoxylin and eosin (H&E) staining used paraffin sections and conventional reagents and methodology (Ricca Chemical Company). Masson's Trichrome staining on paraffin sections used a reagent kit following manufacturer's instructions (Electron Microscopy Sciences). Von Kossa stained paraffin sections were counterstained with Alcian Blue (pH 2.5) and Nuclear Fast Red (Vector Laboratories).

Immunostaining

Paraffin-sectioned tissue on slides was de-paraffinized and rehydrated to distilled water using a graded series of ethanol washes. Antigen retrieval was performed as described in Supplemental Materials. The slides were blocked with M.O.M protein diluent (Vector Laboratories) or 10% normal goat serum (NGS) in PBS for 1 hour at RT and then stained overnight with primary antibodies diluted in blocking buffer (sources and dilutions in Supplemental Materials). Alexa dye-conjugated fluorescent secondary antibodies (Life Technologies) were used to detect signal. Nuclei were stained with Hoechst (Life Technologies). Slides were mounted with Vectashield (Vector Laboratories). Immunofluorescent images were acquired using a widefield microscope or an Olympus FV1000 laser-scanning confocal microscope. Confocal images shown are average intensity projections of image stacks.

RNA In situ hybridization

In situ hybridizations were performed using cryosections (16 μm) except for *Nptx1*, which used paraffin sections (7 μm), as described (Stewart et al. 2014). Briefly, frozen sections were washed with PBS and PBST prior to Proteinase K treatment. Alternatively, paraffin sectioned tissue was first de-paraffinized and rehydrated. Sections were post-fixed with 4% PFA, washed, and incubated with pre-hybridization buffer at 65°C for 4 hours. Digoxigenin (DIG)-labeled RNA probes (see Supplemental Materials) were hybridized overnight at 65°C. Following multiple washes, the tissue was blocked with 1% Roche blocking buffer (Roche) and then stained with alkaline phosphatase-conjugated anti-DIG antibody (Roche) overnight at 4°C. The signal was developed after extensive TBST washes using BCIP/NBT (Promega). Tissue was counterstained with Nuclear Fast Red (Vector Laboratories) before being processed for mounting with Permount (Electron Microscopy Sciences).

Valve morphometrics

Optimally matched H&E stained sections for each studied valve of wildtype and littermate $Nfatc1^{Cre};Brg1^{F/F}$ embryos were imaged for area and distance measurements using ImageJ (NIH). Length-to-width ratios were determined as described previously (Stankunas et al. 2010). Cell numbers were counted manually. Data from multiple litters was combined by normalizing values to the mean of wildtype embryos within each letter. Statistical significance was determined using two-tailed Student's t-tests.

Valve 3D reconstructions

7 mm serial paraffin sections covering the entire E16.5 aortic valve were collected, H&E stained and imaged. All images (slices in stack) were imported into ImageJ (NIH) and aligned manually to neighboring valve sections using the Trakem2 plugin (Cardona et al. 2012). An 'area list' for each cusp (LCC, RCC, NCC) was generated manually for every layer before being merged across layers to establish 3-D shapes. Adjustments made for the z-space and thickness were standardized for a given litter to allow a direct comparison between wildtype and *Nfatc1*^{Cre}*;Brg1*$^{F/F}$ aortic valves. A two-tailed Student's t-test comparing total aortic valve volumes (all cusps) between wildtype and *Nfatc1*^{Cre}*;Brg1*$^{F/F}$ embryos used data normalized to the mean of the wildtype aortic valve volumes within each litter.

In vivo EdU labeling and proliferation assays

Pregnant females were IP injected with 50 mg/kg of 5-ethynyl-2′-deoxyuridine (EdU; Life Technologies) 2-3 hours before embryos were harvested. Paraffin sections were prepared for staining as described. For combined lineage tracing and EdU proliferation studies, slides were incubated for 10' in a pressure cooker with DAKO antigen retrieval solution (DAKO). The slides were blocked for one hour with 10% NGS/PBS after antigen retrieval followed by a Click-iT reaction (Life Technologies). Subsequently, slides were washed 6X 10' with PBS before proceeding with anti-GFP antibody staining as described in the Supplemental Materials.

EMT explant assays

Collagen gel EMT explant assays using dissected E10.0 outflow tract tissue were performed as described (Xiong et al. 2011). 1 mg/ml rat tail collagen I (BD Biosciences) matrices were supplemented with 5 mg/ml doxycycline to induce the *TRE:H2BGFP* reporter used for fluorescent lineage tracing. Explants were incubated at 37°C in 5% O_2/5% CO_2 for 48 hours before brightfield and fluorescent imaging on an inverted Nikon Eclipse Ti widefield microscope.

Quantitative RT-PCR

qRT-PCR was performed using KAPA SYBR FAST qPCR Master Mix (Kapa Biosystems) and cDNA synthesized using SuperScript III (Life Technologies) from Trizol-isolated RNA prepared from dissected valve regions. Relative mRNA expression was normalized using a control transcript (HPRT) to calculate ΔCTs (threshold cycles). Expression levels between wildtype and $Nfatc1^{Cre};Brg1^{F/F}$ hearts were compared using a ΔΔCT approach. ΔCT values were used for two-tailed Student's t-tests with a Bonferroni correction for multiple comparisons to determine statistical significance. Primer sequences are in Supplemental Materials.

Illumina RNA sequencing

The valve-containing region of E14.5 hearts was dissected under a fluorescent stereomicroscope using the guide of an endocardial-lineage nuclear GFP reporter (see Supplemental Materials). RNA was extracted using TRIzol (Life Technologies). RNA-sequencing libraries were prepared from two sets of individual paired control and

littermate *Nfatc1*^{Cre};*Brg1*$^{F/F}$ embryos as described in Supplemental Materials. The bioinformatics workflow to determine differentially gene expression is also presented therein.

RESULTS

Endocardial Brg1 is required for semilunar valve development

Prior studies of Brg1 roles in the developing endocardium showed that the BAF complex is required at embryonic day E9.5 to transcriptionally maintain a microenvironment that supports ventricular trabeculation (Stankunas et al. 2008). Persistent endocardial Brg1 expression throughout the embryonic heart suggested additional endocardial BAF complex functions in other heart regions or during later steps of cardiogenesis. The previous use of the *Tie2:Cre* line to conditionally delete floxed *Brg1* alleles precluded studying later roles due to lethality arising from hematopoietic and yolk sac vasculature defects in *Tie2:Cre;Brg1*$^{F/F}$ embryos (Stankunas et al. 2008). Therefore, we used the *Nfatc1*^{Cre} line that expresses Cre from the *Nfatc1* locus to specifically remove Brg1 from endocardial but not endothelial or hematopoietic cells (Wu et al. 2012).

Nfatc1^{Cre};*Brg1*$^{F/F}$ mice rarely survived to adulthood, accounting for 3% rather than an expected 25% of animals generated from *Nfatc1*^{Cre};*Brg1*$^{F/+}$ X *Brg1*$^{F/F}$ intercrosses (Fig. S2A, F). A decreased fraction of viable *Nfatc1*^{Cre};*Brg1*$^{F/F}$ embryos was first observed at E16.5 with few animals surviving after birth, demonstrating late embryonic or perinatal lethality. Hearts from the rare viable postnatal day 0 (P0) *Nfatc1*^{Cre};*Brg1*$^{F/F}$ were grossly larger and histologically had a thickened compact myocardium, possibly reflecting

endocardial BAF complex roles in trabecular development (Fig. S2B-E). The coronary artery network was reduced (Fig. S2G-J), consistent with known BAF complex functions in vasculogenesis (Griffin et al. 2008; Stankunas et al. 2008) and *Nfatc1*^{Cre}-driven recombination in coronary vessel endothelium of endocardial origin (Wu et al. 2012). These defects likely contributed to the perinatal lethality. In addition to these phenotypes, hearts from *Nfatc1*^{Cre}*;Brg1*$^{F/F}$ newborn mice had histologically thickened aortic and pulmonic valves (Fig. S2K-P).

We examined if the semilunar valve defects seen in *Nfatc1*^{Cre}*;Brg1*$^{F/F}$ mice manifested earlier in development by H&E staining of sectioned E16.5 embryos. The semilunar valve cusps of *Nfatc1*^{Cre}*;Brg1*$^{F/F}$ embryos were strikingly thickened and poorly elongated. The thinner "hinge" region that demarcates the boundary between the distal and basal regions of each cusp of both aortic and pulmonic valves was absent (Fig. 1A-B, D-E). In contrast, the mitral valve of *Nfatc1*^{Cre}*;Brg1*$^{F/F}$ embryos was of normal size and organization (Fig. 1C, F). Quantitatively, the left and right cusps of the pulmonic valve from *Nfatc1*^{Cre}*;Brg1*$^{F/F}$ E16.5 embryos had significantly decreased length:width ratios (0.998 vs. 0.581, $P < 1.0E-4$), were increased in area (0.998 vs. 1.76, $P < 6.0E-3$), and had a concordant modest increase in the number of interstitial cells per valve section ($P < 2.0E-3$) (Fig. 1G). Semilunar valve defects in *Nfatc1*^{Cre}*;Brg1*$^{F/F}$ embryos first became apparent at E14.5 as a decreased length:width ratio of the forming cusps although without a change in sectional area (Fig. S3B, F). E14.5 *Nfatc1*^{Cre}*;Brg1*$^{F/F}$ embryos also occasionally had a small membranous ventricular septal defect, which usually resolved by E16.5 in surviving embryos (> 90%, n= 11) (Fig. S3J-M). E16.5 *Nfatc1*^{Cre}*;Brg1*$^{F/F}$

mitral valve leaflets exhibited no significant change in morphology or cell number (Fig. 1H), even though many mitral valve endocardial and mesenchymal cells had lost Brg1 protein by E14.5 (Fig. S4A-F). The divergent effects on semilunar vs. atrioventricular canal valves suggested that the BAF complex has a unique role during semilunar valve development or that the idiosyncrasies of *Nfatc1*^{Cre} deletion kinetics only perturbed

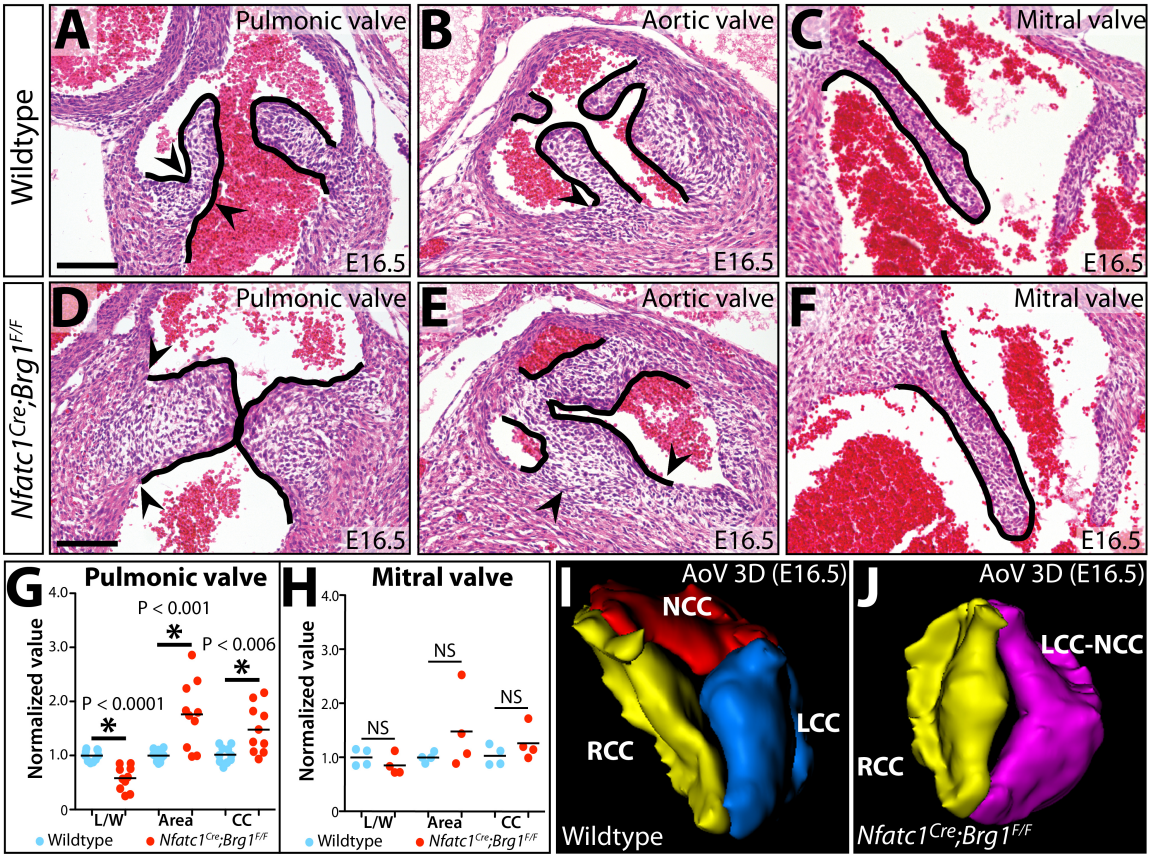

Figure 1. Endocardial-lineage *Brg1* deficient embryos exhibit semilunar valve defects. (A-F) Hematoxylin and eosin (H&E) stained sections from E16.5 wildtype and *Nfatc1*^{Cre}*;Brg1*$^{F/F}$ embryos showing indicated valves. Arrowheads mark the basal cusp regions of the semilunar valves. (G, H) Morphometric analyses of pulmonic and mitral valves from E16.5 wildtype and *Nfatc1*^{Cre}*;Brg1*$^{F/F}$ embryos. Each data point represents one valve, with values normalized to the mean of the wildtype samples from individual litters. Asterisks indicate a significant difference ($P < 0.05$, Student's two-tailed t-tests). (I, J) 3-dimensional rendering of serial sections of aortic valves from E16.5 wildtype and *Nfatc1*^{Cre}*;Brg1*$^{F/F}$ littermate embryos. AoV: aortic valve; L/W: length-to-width; CC: mesenchymal cell count; NS, not statistically significant; LCC (blue): left coronary cusp; NCC (red): non-coronary cusp; RCC (yellow): right coronary cusp; LCC-NCC (purple): bicuspid fusion between left and non-coronary cusps. Scale bars: 100 μm.

Brg1's role in a common process in the developing outflow tract.

3-D reconstruction of serial sections through the entire aortic valve of E16.5 *Nfatc1^{Cre};Brg1$^{F/F}$* and littermate embryos revealed that *Nfatc1^{Cre};Brg1$^{F/F}$* aortic valves lacked the typical thin elongated cusps and extended aortic sinuses of wildtype littermates (Fig. S5A-D). However, *Nfatc1^{Cre};Brg1$^{F/F}$* embryos retained coronary ostia with normal origins of the coronary arteries (Fig. S5E, F). Three of the six 3-D reconstructed *Nfatc1^{Cre};Brg1$^{F/F}$* aortic valves were bicuspid. In each case, the bicuspid valve originated from a fusion between the left and non-coronary cusps (LCC-NCC), with residual individual cusp attachment points to the surrounding muscle. While several *Nfatc1^{Cre};Brg1$^{F/F}$* aortic valves had larger volumes than those of paired littermates, this change was not statistically significant (Fig. S5G-R). Therefore, area changes seen by sectional analysis likely represented the bulbous shape of the valves rather than increased size, additionally highlighting how 2-D morphometric analyses of valve development can be misleading. Consistent with the valves having a normal volume, the pulmonic valve mesenchyme of E14.5/E15.5 *Nfatc1^{Cre};Brg1$^{F/F}$* mice had no change in overall proliferation (measured by EdU incorporation and phospho-histone H3 staining, Fig. S6A-D, I-J) or apoptosis (measured by TUNEL and anti-cleaved caspase 3, Fig. S6E-H, K). Collectively, these results suggested that the semilunar valve defects in *Nfatc1^{Cre};Brg1$^{F/F}$* mice primarily represent a patterning/morphogenesis defect rather than overall misregulated growth.

Bicuspid aortic valve (BAV) disease in endocardial *Brg1* deficient mice

The semilunar valve (SLV) defects present at E16.5 indicated that *Nfatc1*^{Cre};*Brg1*$^{F/F}$ mice would provide a mouse model of adult semilunar valve disease if not for the predominant perinatal lethality. Therefore, we conditionally deleted *Brg1* with the less efficient parent line, *Nfatc1*$^{Cre\text{-}PGK}$ that retains the hygromycin-resistance cassette used for gene targeting (Wu et al. 2012). As described, the majority of *Nfatc1*$^{Cre\text{-}PGK}$;*Brg1*$^{F/F}$ mice survived to adulthood, gradually losing their hair and whiskers due to a failure of hair follicle stem cell renewal (Xiong et al. 2013). While most *Nfatc1*$^{Cre\text{-}PGK}$;*Brg1*$^{F/F}$ mice had a normal

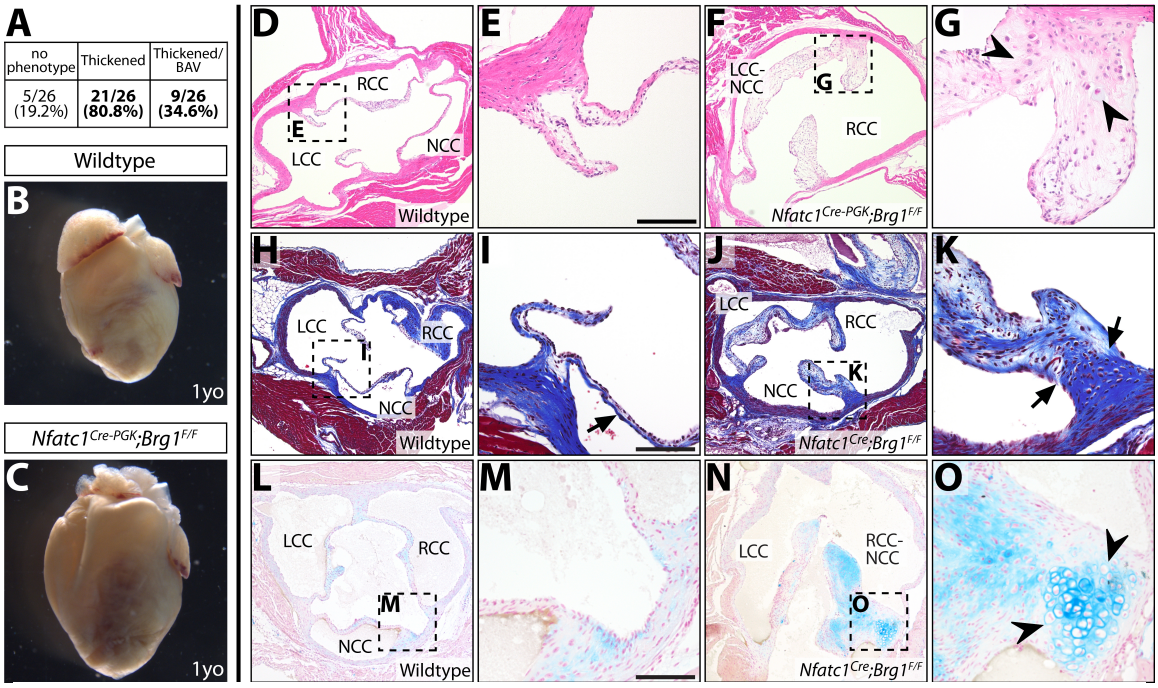

Figure 2. Endocardial-lineage *Brg1* deficient adult mice develop aortic valve disease
(A) Fraction of adult *Nfatc1*$^{Cre\text{-}PGK}$;*Brg1*$^{F/F}$ or *Nfatc1*^{Cre};*Brg1*$^{F/F}$ mice with 1) thickened/myxomatous and/or 2) bicuspid aortic valve. 0/26 littermate control animals had abnormal aortic valves. (B, C) Whole mount anterior view of hearts from one year old (1yo) wildtype and *Nfatc1*$^{Cre\text{-}PGK}$;*Brg1*$^{F/F}$ littermate mice. (D-G) H&E stained wildtype (D, E) and *Nfatc1*$^{Cre\text{-}PGK}$;*Brg1*$^{F/F}$ (F, G) aortic valve sections. (H-K) Adult aortic valve sections stained using Masson's Trichrome stain (collagen deposition in blue). Wildtype (H, I) and *Nfatc1*^{Cre};*Brg1*$^{F/F}$ (J, K) samples are shown. Black arrows mark mislocalized collagen. (L-O) Von Kossa and Alcian Blue (counterstained with Nuclear Fast Red) stained tissue sections from wildtype (L, M) and *Nfatc1*^{Cre};*Brg1*$^{F/F}$ (N, O) adult aortic valves. Black arrowheads indicate cartilaginous nodules. LCC: left coronary cusp; NCC: non-coronary cusp; RCC: right coronary cusp; LCC/RCC-NCC: bicuspid fusion between left/right and non-coronary cusps. Scale bars:

lifespan (monitored for up to two years), their hearts were frequently enlarged with thickened ventricles (Fig. 2B, C, Fig. S7A-D). This cardiomyopathy could represent cardiac hypertrophy arising from pressure overload caused by a partial outflow tract obstruction.

We examined hearts from adult *Nfatc1*$^{Cre\text{-}PGK}$*;Brg1*$^{F/F}$ mice for semilunar valve defects (Fig. 2D-G) and found that *Nfatc1*$^{Cre\text{-}PGK}$*;Brg1*$^{F/F}$ adult mice frequently had substantially thickened aortic valve cusps (21/26; 0/26 control littermates were affected). Nine had a bicuspid aortic valve (six LCC-NCC and three RCC-NCC), recapitulating the E16.5 *Nfatc1*^{Cre}*;Brg1*$^{F/F}$ embryonic phenotype. The pulmonic valves were similarly thickened, while the mitral valve appeared qualitatively normal (Fig. S7E-H).

Trichrome staining indicated that *Nfatc1*$^{Cre\text{-}PGK}$*;Brg1*$^{F/F}$ and rare surviving *Nfatc1*^{Cre}*;Brg1*$^{F/F}$ mice aortic valves had myxomatous characteristics, with extensive proteoglycan-rich material throughout the valve and intermittent and dispersed collagen deposits rather than the typical enrichment of collagen along the arterial side of the cusps. Irregular chondrocyte-like cells with large nuclei and scattered small-nucleated cells were present, especially at the lateral edges of the cusps where they contact neighboring muscle (Fig. 2H-K). Similar histologic abnormalities are seen in human aortic valve disease and additional mouse models (Satta et al. 2002; Jackson et al. 2003; Kern et al. 2010; Cheek et al. 2012; Hofmann et al. 2012; Krishnamurthy et al. 2012). We assessed if the valves became calcified, as can occur in human disease, using Von Kossa staining. Unexpectedly, we observed little or no change in calcification in adult *Nfatc1*^{Cre}*;Brg1*$^{F/F}$

aortic valves irrespective of age or severity of the valve thickening/disorganization phenotype (Fig. 2L-O). Collectively, *Nfatc1*$^{Cre\text{-}PGK}$*;Brg1*$^{F/F}$ and rare surviving *Nfatc1*^{Cre}*;Brg1*$^{F/F}$ mice establish a unique model of aortic valve disease that 1) has thickened, misorganized and myxomatous cusps, 2) forms bicuspid arrangements usually arising from LCC-NCC fusions and 3) does not become overtly calcified.

Endocardial *Brg1* deficient semilunar valves exhibit a loss of interstitial organization

We explored whether the ECM defects seen in adult *Nfatc1*$^{Cre\text{-}PGK}$*;Brg1*$^{F/F}$ adult mice manifested developmentally or reflected disease-like progression by antibody staining for ECM proteins expressed in developing valves. Vcan, which is essential for valve maturation and enriched in the medial-distal region of semilunar valve cusps(Kern et al. 2010; Dupuis et al. 2011), became diffusely localized in E16.5 *Nfatc1*^{Cre}*;Brg1*$^{F/F}$ embryos with expression extending into the base regions (Fig. 3A-H). Postn expression, another ECM protein essential for valve maturation (Norris et al. 2008; Snider et al. 2009), was both expanded and increased in *Nfatc1*^{Cre}*;Brg1*$^{F/F}$ semilunar valve cusps (Fig. 3I-L). In contrast to Vcan and Postn, Tnc was concentrated on the ventricular side and towards the base of wildtype E16.5 semilunar valve cusps (Fig. 3M, O) (Lincoln et al. 2004; Hinton et al. 2006). Reduced Tnc expression in *Nfatc1*^{Cre}*;Brg1*$^{F/F}$ embryos was especially apparent in the left cusps of both aortic and pulmonic valves (Fig. 3N, P), correlating with the sites of elevated Postn. Together, the mislocalized ECM indicates a loss of patterning of the semilunar valve cusps into distinct base and distal regions in *Nfatc1*^{Cre}*;Brg1*$^{F/F}$ embryos. Mechanistically, the disrupted ECM pattern could reflect the

misexpression of locally restricted ECM or ECM-modifying transcripts and/or altered organization of distinct valve interstitial cell populations.

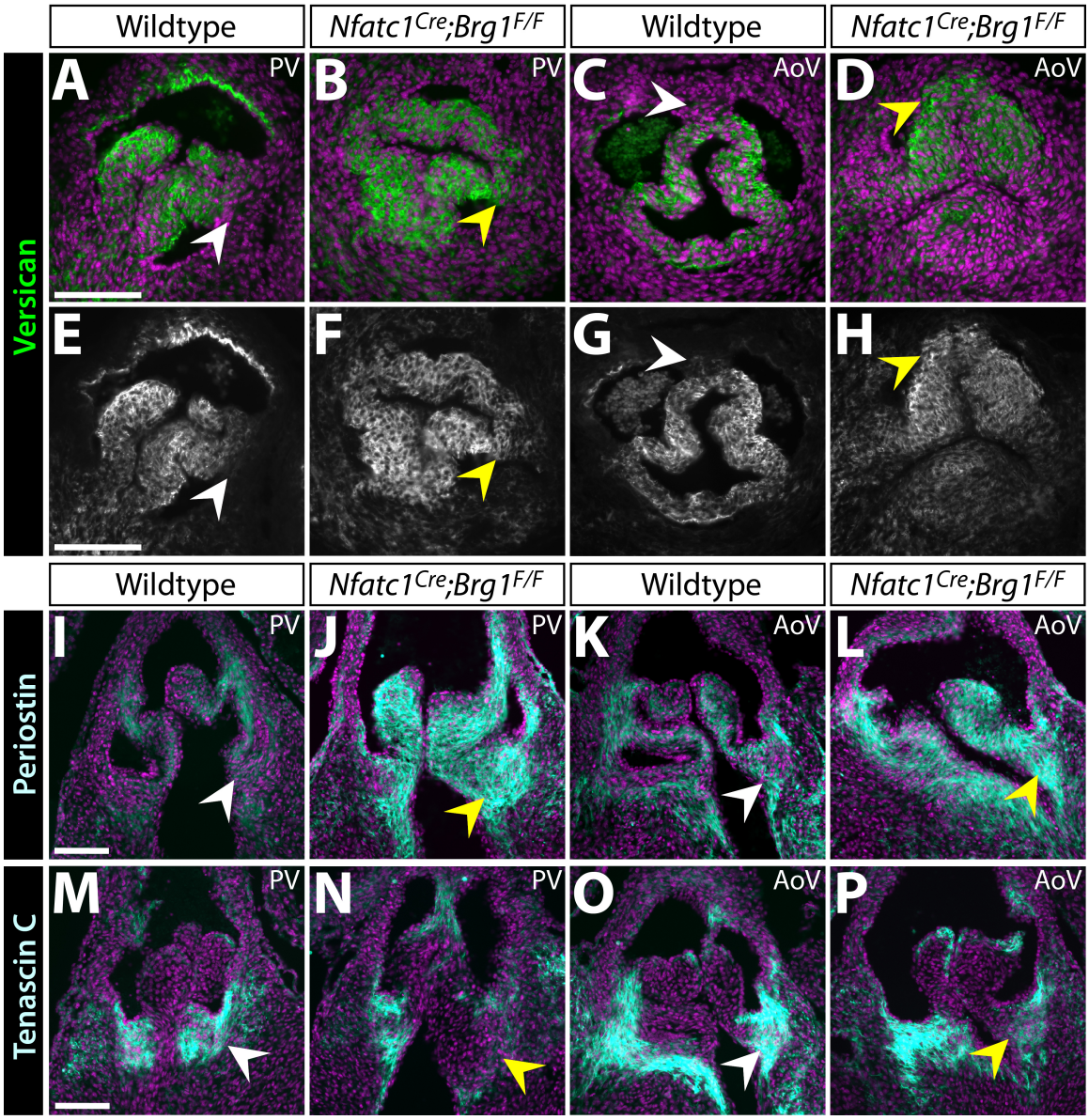

Figure 3. Altered localization and levels of ECM in *Nfatc1^{Cre};Brg1$^{F/F}$* semilunar valves. (A-H) Widefield fluorescence images of anti-Versican (Vcan) antibody stained sections of E16.5 wildtype and *Nfatc1^{Cre};Brg1$^{F/F}$* embryos. (I-P) Representative confocal imaged cryosections of E16.5 wildtype and *Nfatc1^{Cre};Brg1$^{F/F}$* semilunar valves fluorescently immunostained for Periostin (Postn) (I-L) or Tenascin C (Tnc) (M-P) (n=3, paired control and *Brg1*-deficient valves). Pulmonic (PV) or aortic (AoV) valves are shown as indicated. ECM proteins are shown in green/gray scale (A-D) or cyan (I-P). Hoechst-stained nuclei are blue. White arrowheads mark areas of normal protein expression. Yellow arrowheads show regions with broadened (Vcan), broadened/increased (Postn) or decreased (Tnc) levels. Scale bars: 100 μm.

Nfatc1^{Cre};*Brg1*$^{F/F}$ semilunar valves have reduced endocardial-derived mesenchyme

Semilunar valve mesenchyme is derived from endocardial, neural crest, and possibly additional lineages that have inconsistently been reported to populate different regions of semilunar valve cusps (Jiang et al. 2000; de Lange et al. 2004; Nakamura et al. 2006; Ma et al. 2008; Jain et al. 2011; Engleka et al. 2012; Phillips et al. 2013). To explore if the aberrant ECM pattern in *Nfatc1*^{Cre};*Brg1*$^{F/F}$ embryos reflected misorganization of distinct mesenchymal sub-populations, we fate mapped endocardial cells and their mesenchymal derivatives in *Nfatc1*^{Cre};*Brg1*$^{F/F}$ hearts using the *Rosa26R*^{mTmG} Cre reporter line (Muzumdar et al. 2007) while double-staining for Tnc and Postn. In E16.5 wildtype embryos, EMT-derived cells were scattered throughout the right and left pulmonic valve cusps but were enriched towards the Tnc-rich base of the cusp (Fig. 4A, B). In *Nfatc1*^{Cre};*Brg1*$^{F/F}$ embryos, EMT-derived cells were reduced, likely accounting for the loss of the Tnc-high field seen in the base of the left semilunar valve cusps (Fig. 4C, D). The mitral valves of *Nfatc1*^{Cre};*Brg1*$^{F/F}$ embryos had normal Tnc expression in spite of substantial loss of Brg1 protein in mitral valve mesenchyme (Figs. 4E, F and S4C, F). Therefore, the decreased Tnc in *Nfatc1*^{Cre};*Brg1*$^{F/F}$ semilunar valve cusps likely reflected depleted EMT-derived mesenchyme rather than BAF-dependent control of Tnc expression. The high Postn-expressing areas in the pulmonic valve cusps of *Nfatc1*^{Cre};*Brg1*$^{F/F}$ embryos were largely populated by non-labeled cells (Fig. 4G-J). Therefore, the increased Postn originated from a non-cell-autonomous response to endocardial-lineage *Brg1* deletion. These results further indicate that, at least for the left cusps, specialized EMT-derived mesenchyme produces the concentrated Tnc in the base of the semilunar valves. The depletion of these cells upon loss of endocardial-lineage

Brg1 accounts for the bulbous valves that lack robust basal cusp regions and therefore fail to restrain Postn-expressing cells to the distal cusp.

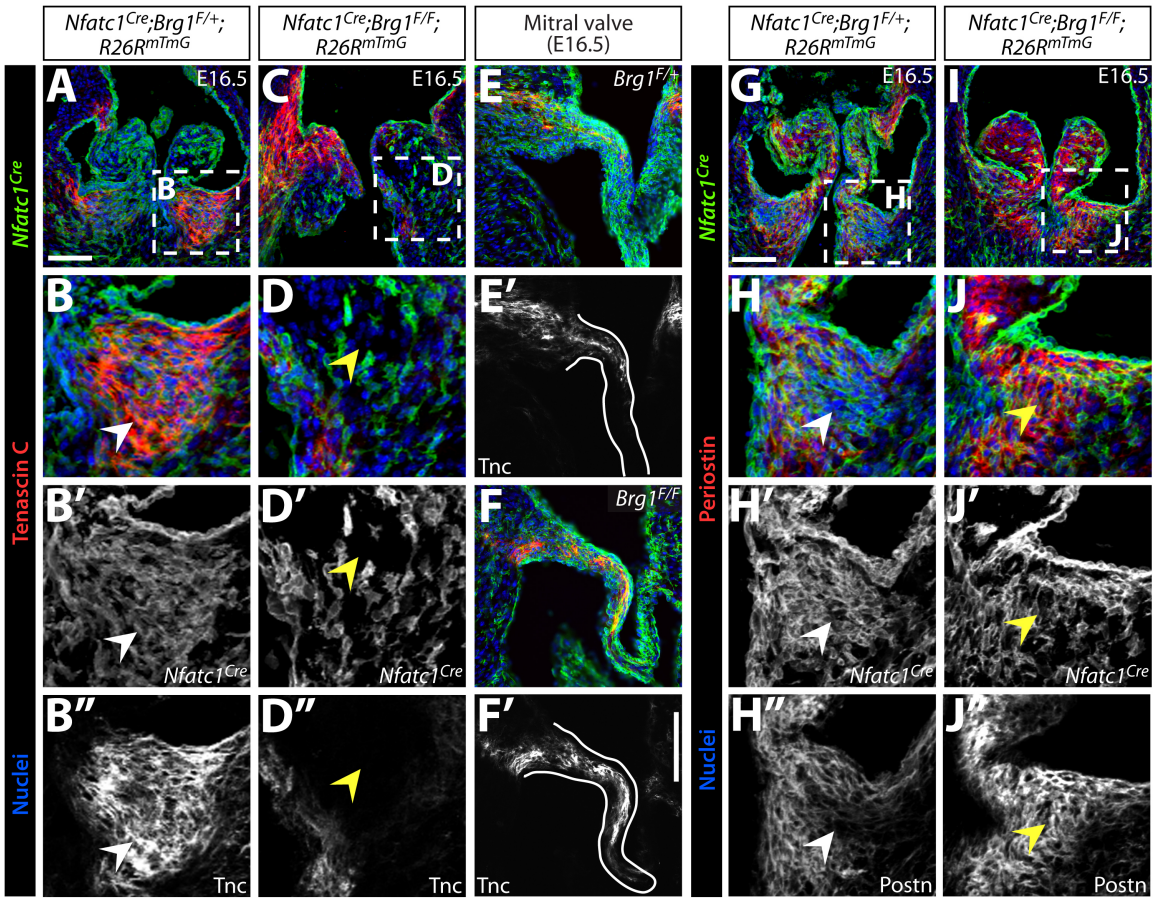

Figure 4. Disorganized extracellular matrix in endocardial *Brg1*-deficient semilunar valves reflects an altered organization of distinct mesenchymal lineages.
Immunofluorescence images of E16.5 control (*Nfatc1*^{Cre};*Brg1*$^{F/+}$;*R26R*^{mTmG}) or endocardial *Brg1*-deficient (*Nfatc1*^{Cre};*Brg1*$^{F/F}$;*R26R*^{mTmG}) embryo sections simultaneously stained for GFP to monitor *Nfatc1*^{Cre}-lineage cells and either Tenascin C (Tnc) (A-F) or Periostin (Postn) (G-J). Pulmonic valves (A-D, G-J) and mitral valves (E-F) are shown. All panels are confocal images except (E-F), which are widefield images. Overlay images show Tnc or Postn in red, GFP indicating *Nfatc1*^{Cre}-lineage cells in green, and Hoechst-stained nuclei in blue. Magnified regions are outlined in dashed boxes. White arrowheads denote normal ECM localization and yellow arrowheads represent either deficient (Tnc) or ectopic (Postn) ECM protein. Scale bars: 100 μm.

We quantitatively assessed the depletion of EMT-derived semilunar valve mesenchyme upon endocardial Brg1 deletion by scoring the fraction of GFP-labeled pulmonic valve mesenchymal cells in *Nfatc1*^{Cre};*Brg1*$^{F/F}$;*Rosa26R*^{mTmG} embryos (Fig. 5A, B). At E16.5, there was a significant decrease in the number of *Nfatc1*^{Cre}-derived mesenchymal cells in both left and right pulmonic cusps (Fig. 5E, F, J). In contrast, the mitral valve retained its full complement of EMT-derived cells (Fig. 5G, H). At E14.5, when the semilunar valve defects first became evident, a similar decrease in the number of EMT-derived cells was observed in the left cusp of *Nfatc1*^{Cre};*Brg1*$^{F/F}$ pulmonic valves (mean 33.3%; $P < 0.04$) (Fig. 5C, D, I). A comparable trend of reduced EMT-derived cells likewise was seen in the right cusp. Given *Nfatc1*^{Cre};*Brg1*$^{F/F}$ SLVs were of normal volume and cell number, the change in the ratio of mesenchyme of different origins suggested non-EMT derived mesenchyme expanded to replace the scarce EMT-derived population.

Figure 5 (next page). A depleted pool of EMT-derived mesenchyme in endocardial Brg1-deficient semilunar valves is replaced by increased proliferation of other mesenchymal lineage(s).

(A-H) Sections of *Nfatc1*^{Cre};*Brg1*$^{F/+}$;*R26R*^{mTmG} and *Nfatc1*^{Cre};*Brg1*$^{F/F}$;*R26R*^{mTmG} embryos (pulmonic valve except mitral valve in (G, H); genotype and age as indicated) immunostained for GFP (*Nfatc1*^{Cre}-lineage derived cells, green) and nuclei (Hoechst-stained, purple). Arrowheads indicate EMT-derived mesenchymal cells at the pulmonic valve cusp base near the cushion-myocardium boundary. (I, J) Quantification of the relative contribution of *Nfatc1*^{Cre}-lineage pulmonic valve mesenchyme in control (*Brg1*$^{F/+}$) and endocardial *Brg1*-deficient embryos (*Brg1*$^{F/F}$) at E14.5 (I) and E16.5 (J). Left (L-PV) and right (R-PV) cusps are scored separately. The percentile fraction of *Nfatc1*^{Cre}-lineage mesenchyme for each embryo is normalized to the mean of corresponding littermate wildtype samples. The mean absolute percentage of labeled and unlabeled cells is shown within individual bars of the chart (n=5). (K-L) E14.5 wildtype (*Nfatc1*^{Cre};*Brg1*$^{F/+}$;*R26R*^{mTmG}) (K) and *Nfatc1*^{Cre};*Brg1*$^{F/F}$;*R26R*^{mTmG} (L) pulmonic valve sections stained with GFP (*Nfatc1*^{Cre}-lineage, green), EdU-incorporating proliferating cells (red), and Hoechst (nuclei, blue). White arrows denote EdU^{+}, non-*Nfatc1*^{Cre}-lineage mesenchymal cells. (M) Quantitation of the proliferation rate of *Nfatc1*^{Cre}- and other-lineage pulmonic valve mesenchyme in E14.5 control and *Nfatc1*^{Cre};*Brg1*$^{F/F}$ embryos. The mean absolute fraction of EdU-incorporated cells for each condition is shown. For all graphs, error bars show one standard deviation of the mean. Asterisks indicate a significant difference ($P < 0.05$, two-tailed Student's t-tests). NS: not significant; GFP^{+}: *Nfatc1*^{Cre}-lineage labeled mesenchyme; Non-LL: non-*Nfatc1*^{Cre}-lineage labeled mesenchyme. Scale bars: 100 μm.

EMT-derived cells of *Nfatc1*^{Cre};*Brg1*$^{F/F}$ SLVs could be reduced due to a change in their net growth rate and/or deficient EMT when the cells were first generated. To distinguish between these possibilities, we examined proliferation rates by EdU incorporation in EMT-lineage traced wildtype and *Nfatc1*^{Cre};*Brg1*$^{F/F}$ embryos. Residual EMT-derived mesenchyme and endocardial cells proliferated normally (Fig. 5K-M). In contrast, we observed a nearly two-fold increase in EdU-incorporated non-*Nfatc1*^{Cre}-lineage-labeled mesenchymal cells (Fig. 5M). Therefore, this specialized cushion mesenchyme, likely of NCC and dOFT cushion origins, proliferated to compensate for the deficient EMT-

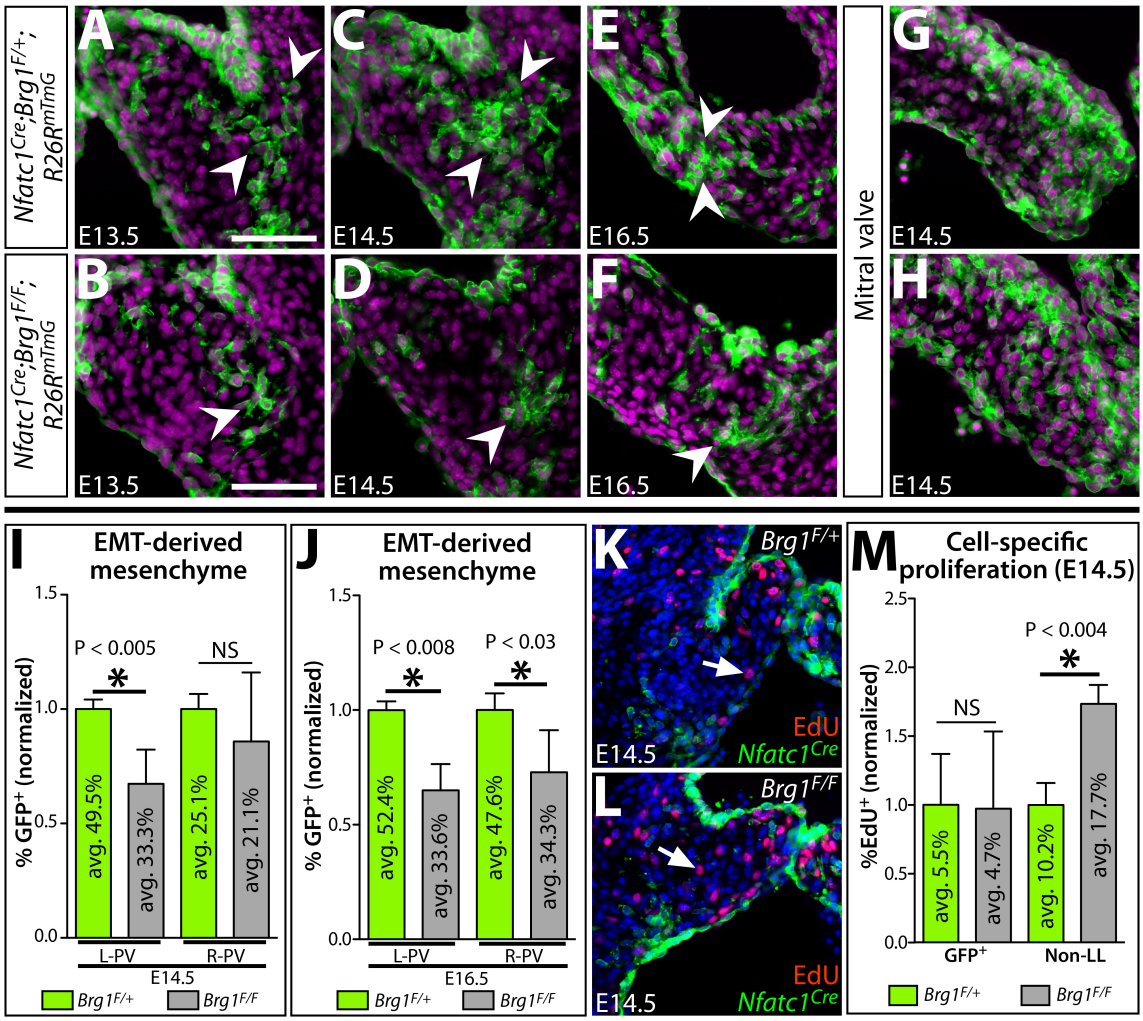

derived pool. Therefore, Brg1 is not inherently required in cushion mesenchyme for cell growth or survival and origins of the semilunar valve defects in *Nfatc1^{Cre};Brg1$^{F/F}$* embryos likely rest earlier in outflow tract development when EMT-derived cells are generated.

Semilunar valve defects originate from deficient pOFT EMT

To determine if outflow tract EMT was disrupted in *Nfatc1^{Cre};Brg1$^{F/F}$* embryos, we examined cushion development at E10.5, less than 24 hours after EMT onset. The pOFT, but not the NCC-populated dOFT cushions of *Nfatc1^{Cre};Brg1$^{F/F}$* embryos contained approximately half the normal number of mesenchymal cells ($p < 0.022$) (Fig. 6A, B, E). As expected, the AVC cushions were normal (Fig. 6C-E). We used the *Rosa26R^{mTmG}* reporter line to confirm the deficient pOFT mesenchyme in E10.5 *Nfatc1^{Cre};Brg1$^{F/F}$* embryos represented a loss of EMT-derived cells (Fig. 6F-G). A reduced pOFT with fewer lineage-traced EMT-derived cells persisted at E11.5 in endocardial *Brg1*-deficient embryos (Fig. 6H-K). We further explored a potential primary pOFT EMT defect in *Nfatc1^{Cre};Brg1$^{F/F}$* embryos using collagen gel explant assays (Runyan and Markwald 1983) and a *Nfatc1^{Cre}*-driven lineage tracing approach to brightly labeled EMT-derived cell nuclei with GFP. E10.0 *Nfatc1^{Cre};Brg1$^{F/F}$;Rosa26R^{rtTA};TRE:H2B-GFP* OFT cushion explants produced significantly fewer GFP+ mesenchymal cells ($p < 1.0E-4$) (Fig. 6L-N). These results confirmed that endocardial deletion of *Brg1* driven by *Nfatc1^{Cre}* produced a modest EMT defect in the pOFT but not AVC cushions.

We questioned whether the isolated pOFT EMT defect in *Nfatc1*^{Cre}*;Brg1*$^{F/F}$ embryos represented a specific BAF complex role in pOFT endocardium, or if the induction of Cre activity in the *Nfatc1*^{Cre} line was too late to remove Brg1 in AVC endocardial cells prior to EMT. Supporting this latter possibility, EMT occurs earlier in the AVC than pOFT (Camenisch et al. 2002). Further, *Nfatc1*^{Cre}*;Brg1*$^{F/F}$ embryos did not exhibit a widespread loss of endocardial Brg1 protein until E10.5 (Fig. S8, Fig. S9). To achieve an earlier deletion, we used *Tie2:Cre* with the floxed *Brg1* alleles to remove endocardial Brg1 by E9.5 (Stankunas et al. 2008). E9.75 *Tie2:Cre;Brg1*$^{F/F}$ embryos displayed a near complete absence of EMT in both the pOFT and AVC cushions (Fig. 6O-R). Therefore, endocardial BAF complex-mediated chromatin remodeling is required for both AVC and

---

Figure 6 (next page). Reduced EMT-derived semilunar valve mesenchyme in *Nfatc1*^{Cre}*;Brg1*$^{F/F}$ embryos originates from deficient pOFT EMT, a process that generally requires Brg1 function.

(A-D) H&E stained sagittal sections of E10.5 wildtype and *Nfatc1*^{Cre}*;Brg1*$^{F/F}$ embryos. The proximal (pOFT) and distal (dOFT) outflow tract (A, B) and atrioventricular canal (AVC) cushions (C, D) are shown. Arrowheads indicate pOFT mesenchyme. (E) Scoring of mesenchymal cells populating the pOFT or AVC cushions in E10.5 wildtype and *Nfatc1*^{Cre}*;Brg1*$^{F/F}$ embryos. Each point shows one embryo and all values are normalized to the mean of littermate wildtype samples. Asterisk denotes a significant difference (two-tailed Student's t-tests). (F-G, J-K) Widefield fluorescence images of OFT regions from transverse sectioned E10.5 (F, G) or sagittal sectioned E11.5 (J, K) embryos. Tissue is immunostained for GFP (for *Nfatc1*^{Cre}-lineage tracing, green) and Nfatc1 (endocardium, red). Nuclei are stained with Hoechst (blue). Control (*Nfatc1*^{Cre}*;Brg1*$^{F/+}$*;R26R*^{mTmG}; F, J) and *Nfatc1*^{Cre}*;Brg1*$^{F/F}$*;R26R*^{mTmG} (G, K) embryos are shown. (H, I) H&E stained sagittal sections of E11.5 wildtype and *Nfatc1*^{Cre}*;Brg1*$^{F/F}$ embryos. Arrowheads indicate pOFT mesenchyme. (L, M) Brightfield and fluorescence overlaid images of collagen gel OFT explants from E10.0 control and *Nfatc1*^{Cre}*;Brg1*$^{F/F}$ embryos (24 hours post-dissection). All embryos additionally carry *R26R*^{rtTA} and *TRE:H2B-GFP* transgenes and explants are treated with doxycycline to induce H2B-GFP expression (to label *Nfatc1*^{Cre}-lineage mesenchymal cells, green). White arrowheads denote EMT-derived (GFP^{+}) mesenchymal cells. *Brg1* is required for all cushion EMT. H&E stained sections showing AVC (O, P) and pOFT (Q, R) cushions of wildtype and *Tie2:Cre;Brg1*$^{F/F}$ E9.75 littermate embryos. Arrowheads denote either the presence or a depleted/absent pool of endocardial-derived cushion mesenchymal cells. Arrows in (Q, R) show neural crest-origin mesenchyme within the dOFT cushions. Scale bars: 100 μm.

pOFT EMT. The serendipitous timing of *Brg1* deletion at the onset of EMT accounts for the unique and partial pOFT EMT deficiency seen in *Nfatc1*^{Cre};*Brg1*$^{F/F}$ embryos.

To assess potential ongoing endocardial roles for Brg1, we used an additional Cre line, *Nfatc1enh:Cre*, to delete floxed *Brg1* in cushion endocardial cells that undergo minimal or no EMT (Wu et al. 2011). Lineage tracing experiments using *Rosa26R*^{mTmG} confirmed that *Nfatc1enh:Cre* was active only in cushion endocardial cells and not valve mesenchyme at E14.5 (Fig. S10A-D). *Nfatc1enh:Cre;Brg1*$^{F/F}$ embryos exhibited no change in semilunar valve morphology at E14.5 or E16.5 (Fig. S10E-L). The absence of major post-EMT roles for Brg1 in either endocardium or cushion mesenchyme suggests that pOFT EMT is the disrupted process that "triggers" semilunar valve defects in

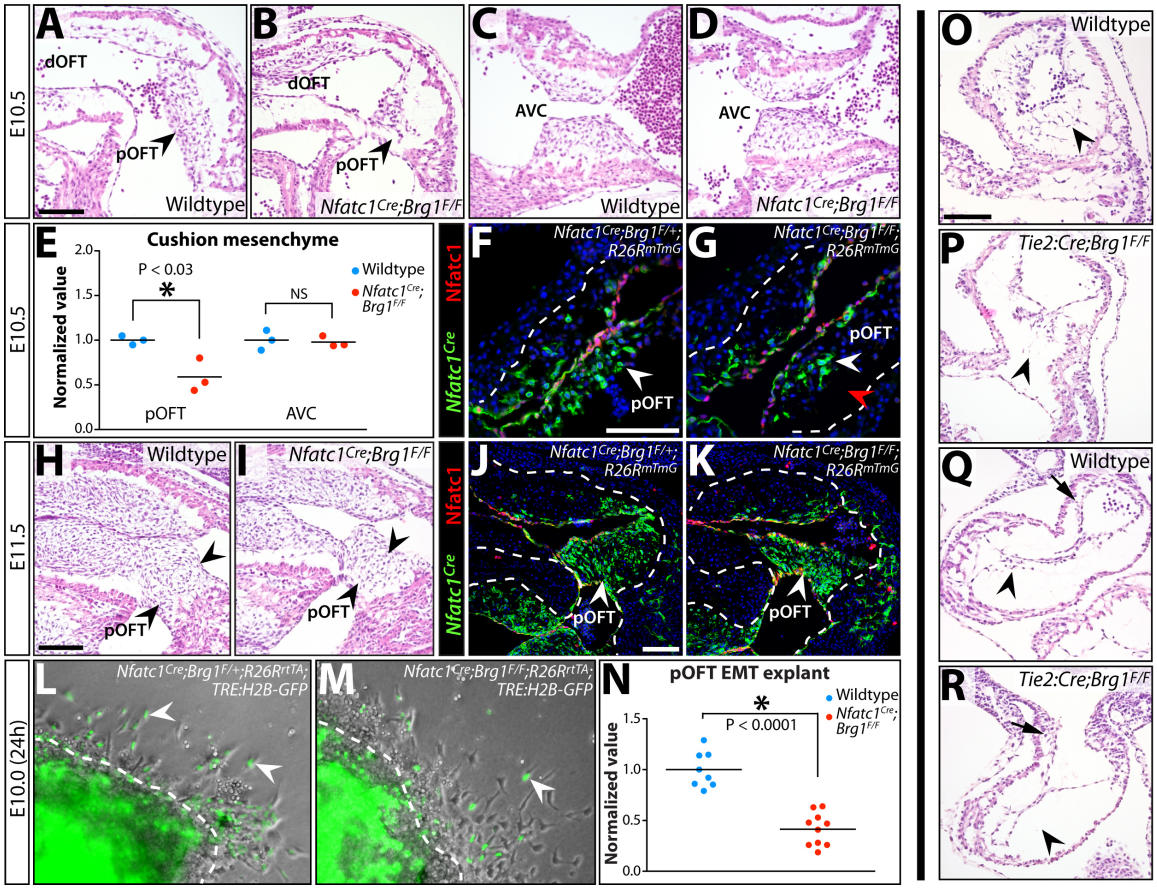

Nfatc1^{Cre};*Brg1*$^{F/F}$ embryos. The ultimate manifestation of disorganized ECM and poorly patterned valves thus represents a progression towards a disease-like state, driven by imperfect compensation by non-EMT derived and functionally distinct mesenchymal cells.

Transcriptional profiling of *Brg1*-deficient cardiac cushions reveals novel regulators

We sought to characterize misexpressed transcripts in *Nfatc1*^{Cre};*Brg1*$^{F/F}$ embryos that could characterize and/or promote the progression of their EMT-deficient SLVs into a diseased state. None amongst a select group of semilunar valve disease-associated transcripts were misexpressed by quantitative qRT-PCR at E14.5 (Fig. S11). Therefore, we used RNA-Seq to identify differences between the E14.5 SLV transcriptomes of wildtype and *Nfatc1*^{Cre};*Brg1*$^{F/F}$ embryos. We identified 43 differentially expressed genes (DEGs) (22 increased, 21 decreased; Table S1) and selected seven for further study (see Supplemental Materials). We used quantitative RT-PCR on additional sets of dissected tissue to confirm both up-regulated (*Nptx1*, *Clec7a* and *Cthrc1*) and down-regulated (*Col23a1*, *Enpp2, Irf6* and *Smoc1*) genes were significantly misexpressed at E14.5. At E16.5, *Clec7a*, *Cthrc1*, and *Nptx1* remained upregulated, suggesting they define a progressively worsening disease-like state (Fig. 7B-C). Conversely, *Col23a1*, *Enpp2* and *Smoc1* transcripts were no longer decreased at E16.5, indicating these genes were transiently misexpressed in endocardial-*Brg1* deficient embryos at the onset of overt semilunar valve defects.

To characterize the cell type-specific expression of these potential regulators of SLV development and disease, we performed in situ hybridizations on E14.5 wildtype and *Nfatc1*^{Cre};*Brg1*$^{F/F}$ embryos. *Nptx1*, a member of the neuronal pentraxin family (Omeis et al. 1996; Boles et al. 2014) was expressed in the most distal endocardial cells of the pulmonic valve and had notbly higher levels in endocardial *Brg1* mutants (Fig. 7D-E). However, no change in *Nptx1* expression was observed in the mitral valve, suggesting that *Nptx1* is an OFT endocardial-specific transcript (Fig. S12A-D). In contrast, the collagen triple helix repeat containing 1, *Cthrc1* (Pyagay et al. 2005), protein was found only in mesenchymal cells at the very base of the cusps where cushion-derived tissue met adjacent myocardium. As expected, cushion mesenchyme *Cthrc1* levels were higher in *Nfatc1*^{Cre};*Brg1*$^{F/F}$ embryos (Fig. 7F-G). Further, *Cthrc1* was increased in aortic valve mesenchyme and became ectopically expressed in both valve and ventricular endocardium (Fig. S12E-J). *Enpp2*, a secreted phospholipase required for lysophosphatidic acid production (Tokumura et al. 2002; Umezu-Goto et al. 2002), and *Irf6*, an interferon-responsive factor (Kondo et al. 2002), were both specifically expressed in endocardial cells on the arterial side of wildtype pulmonic valves. *Enpp2* and *Irf6* were largely absent in the endocardium from *Nfatc1*^{Cre};*Brg1*$^{F/F}$ semilunar valves (Fig. 7H-K, Fig. S12K, M, O, R). In contrast, pulmonic arterial endothelial expression of *Irf6* was unchanged (Fig. S12Q, T). Given their misexpression in endocardial and/or EMT-derived cells, these four DEGs could represent directly repressed (*Nptx1*, *Cthrc1*) or activated (*Enpp2*, *Irf6*) targets of BAF complex chromatin remodeling. Further studies are merited to test their potential roles in valve development and disease and/or broader utility as markers of SLV disease progression.

A

Symbol	Full Name	Fold Δ	FDR	Notes
Nptx1	neuronal pentraxin 1	5.07	2.8e-18	synaptogenesis
Cybb	cytochrome b-245, β polypeptide	3.02	4.5e-09	chronic granulomatous disease
Ctss	cathepsin s	2.52	1.6e-07	lysosomal cysteine proteinase
Clec7a	C-type lectin domain 7a	3.31	5.0e-06	inflammatory response
Myo1f	myosin IF	2.70	9.9e-05	immune response
Thbd	thrombomodulin	2.19	1.4e-04	endoth.-type I receptor for thrombin
Rims2	reg. synaptic exocytosis 2	2.47	5.9e-04	calcium-dependent exocytosis
Chn2	chimerin 2	2.12	1.7e-03	GTPase-activating protein
Cthrc1	collagen triple helix repeat containing 1	1.98	2.9e-03	target of BMP2
Parp14	poly(ADP-rib) polymerase family, member 14	2.14	1.4e-02	mono (ADP-ribosyl)ation activity
Ptpn6	tyr. phosphatase, non-receptor	2.35	7.9e-03	immune response
Ctla2a	cytotoxic T lymphocyte-associated protein 2a	2.35	1.4e-07	negative regulator of inflammatory response
Col23a1	collagen type XXIII a2	-2.58	1.3e-08	transmembrane collagen
Enpp2/Atx	autotaxin	-3.51	1.4e-08	LPA signaling
Smoc1	SPARC related modifying Ca^{2+} binding 1	-3.47	6.3e-07	BMP signaling antagonist
Mirlet7a-1	miRNA let7a-1	-2.25	9.4e-06	Tgfβ signaling antagonist
Slc22a23	solute carrier 22, member 23	-2.23	1.0e-05	ion transport
Fgf12	fibroblast growth factor 12	-3.04	1.9e-05	atypical non-secreted Fgf
Ecm2	extracellular matrix protein 2	-2.19	7.6e-05	extracellular matrix glycoprotein
Nppa	natriuretic peptide type A	-2.09	1.2e-04	extracellular fluid volume control
Mmrn2	multimerin 2	-1.82	8.6e-04	Tgfβ signaling antagonist
Irf6	inferon regulatory factor 6	-1.97	1.3e-03	Van der Woude syndrome (VWS)
Dpp4	dipeptidylpeptidase 4	-1.73	9.5e-03	intrinsic membrane glycoprotein & serine exopeptidase
Gbp4	guanylate binding protein 4	-2.41	1.2e-02	hydrolyzes GTP to GDP/GMP
Opcml	opioid binding protein	-2.29	1.7e-02	immunoglobin superfamily
Acvr1c	activin A receptor, type IC	-1.90	2.0e-02	type I receptor for Tgfβ family

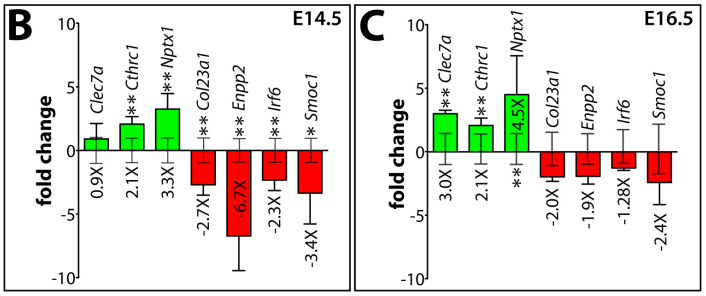

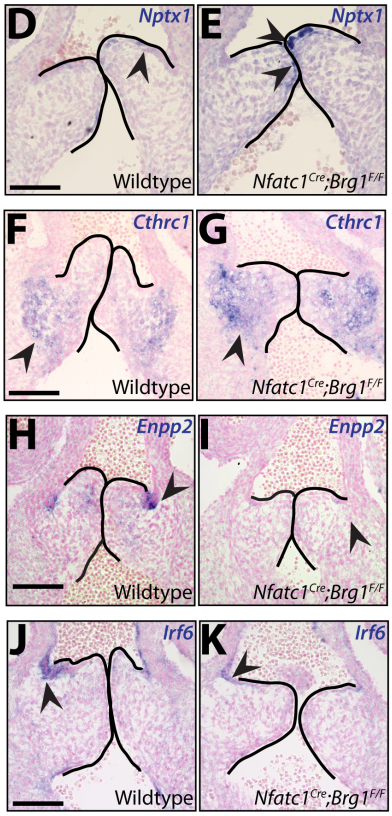

Figure 7. RNA-seq identifies novel semilunar valve expressed transcripts misexpressed in endocardial lineage *Brg1*-deficient valves.

(A) Select differentially expressed genes (DEGs) identified from an RNA-seq analysis comparing two paired samples of wildtype and *Nfatc1*^{Cre}*;Brg1*$^{F/F}$ dissected E14.5 heart valve tissue. 26 DEGs (green-upregulated; red-downregulated) are listed with fold change and false discovery rate (FDR). Transcripts of particular interest are highlighted. (B, C) Quantitative RT-PCR expression studies of the highlighted DEGs in (A) E14.5 (B) and E16.5 (C) valves. Bar heights represent the log-base-2 fold change in gene expression (linear mean fold change value indicated below bars) between *Nfatc1*^{Cre}*;Brg1*$^{F/F}$ and wildtype tissue. Error bars represent one standard deviation with the additional error bars centered along the x-axis showing the variation between wildtype samples. Double asterisks indicate a significant difference including a Bonferroni correction (one-tailed Student's t-test, n=7, $P < 0.007$); single asterisk indicates a $P < 0.05$. (D-K) RNA in situ hybridizations for indicated transcripts on pulmonic valve sections of E13.5 wildtype or littermate *Nfatc1*^{Cre}*;Brg1*$^{F/F}$ embryos. Arrowheads highlight areas of highest transcript expression. Scale bar: 100 μm.

DISCUSSION

Endocardial *Brg1* deletion establishes a model of semilunar valve disease with origins in deficient EMT

We describe a new mouse model of semilunar valve disease caused by deletion of *Brg1* in the endocardial lineage. $Nfatc1^{Cre};Brg1^{F/F}$ mice develop thickened, blunted, and occasionally fused valve cusps that become myxomatous in surviving adults. We map the origins of these phenotypes to disrupted pOFT EMT, one of the earliest steps in valve development. OFT mesenchyme of other origins, likely cardiac neural crest, compensates for the deficient EMT-derived cells by relatively increased proliferation but is incompetent to fully generate the complex 3-dimensionally patterned interstitium of a tricuspid semilunar valve. As such, the cellular and extracellular changes that characterize the abnormal semilunar valves represent secondary responses to a disrupted system, rather than reflecting later developmental or physiologic roles of Brg1.

Chromatin remodeling contributes to endocardial cushion EMT

Early deletion of floxed *Brg1* in all endocardial cells using the *Tie2:Cre* driver disrupted EMT in both the AVC and pOFT cushions. These results establish chromatin remodeling as a component of the transcriptional networks that promote EMT. Endocardial *Brg1* deletion does not have a significant effect on endocardial cell death or proliferation (Stankunas et al. 2008), suggesting that cushion endocardial BAF complexes have a relatively specific transcriptional role in EMT. A simple explanation is that the BAF complex has a common chromatin remodeling role in all EMT processes, whether in the endocardial cushions or other developmental/disease situations. Consistent with this

possibility, the Baf60c subunit of the BAF complex is required for EMT in cancer cell lines (Jordan et al. 2013) and Brg1 interacts with the Zeb1 transcription factor to promote a terminal step in the mesenchymal transition of MCF7 cells (Sánchez-Tilló et al. 2010). Alternatively, effectors of upstream EMT-inducing signaling pathways, such as TGF-beta or Notch signaling, may recruit BAF complex activity to induce EMT. In support of these possibilities, both the Smad2/3 effectors of TGF-beta signaling and activated Notch1, each of which has been implicated in both AVC and pOFT EMT, cooperate with the BAF complex and/or induce chromatin remodeling in other circumstances (Takeuchi et al. 2007; Xi et al. 2008).

The semilunar valve interstitium is organized into regions enriched with mesenchyme of different origins

Multiple lineage tracing studies suggest a complex patterning of multi-origin mesenchymal populations within semilunar valves (Jiang et al. 2000; de Lange et al. 2004; Nakamura et al. 2006; Jain et al. 2011; Phillips et al. 2013). Our simultaneous study of the localization of valve ECM components with *Nfatc1*-based lineage tracing indicates that the patterned ECM composition of semilunar valves is conferred by the regulated organization of mesenchymal cells with differential competency to produce ECM proteins. For example, EMT-derived cells likely produce the Tnc-enriched base of the left semilunar valve cusps that is depleted in $Nfatc1^{Cre};Brg1^{F/F}$ embryos. As a corollary, the increased Postn seen in $Nfatc1^{Cre};Brg1^{F/F}$ embryos could reflect an expanded non-EMT origin (likely neural crest-derived) mesenchyme that continues to fulfill its normal role of secreting Postn. This general concept of semilunar valve

patterning provides a framework to understand when and how valve regulators function and comprehend how various mechanisms can generate valve defects.

Interpreting mouse models of semilunar valve disease

A number of other mouse models exhibit either bicuspid aortic valve and/or semilunar valve disease-like phenotypes. When bicuspid, the aortic valves of *Nfatc1*^{Cre}*;Brg1*$^{F/F}$ embryos display either a RCC-NCC or, more frequently, what in humans is the rarest LCC-NCC subtype (Fernandes et al. 2004; Fernández et al. 2009; Kang et al. 2013). Grewal et al. proposed that the "type I" subtype showing fusions between RCC-LCC cusps is caused by a deficiency of NCCs (Jain et al. 2011; Phillips et al. 2013; Grewal et al. 2014). In contrast, "type II" fusions (RCC-NCC) are suggested to be of second heart field (SHF) origin, which could encompass pOFT EMT defects given the outflow tract's SHF origins. Consistent with this idea, the *Nos3*-deficient mouse model of BAV develops RCC-NCC fusions and may, like the *Brg1*-deficient model, originate from defective EMT (Fernández et al. 2009). Whether a RCC-NCC or LCC-NCC fusion occurs could reflect the severity of the EMT disruption, reflected by the variable *Brg1* deletion in *Nfatc1*^{Cre}*;Brg1*$^{F/F}$ embryos.

Could other mouse models of thickened and disorganized semilunar valves also have origins in pOFT EMT defects? Supporting this hypothesis, several other models disrupt known or potential EMT regulators, including the TGF-b effector *Smad2* (combined with *Adamts5*), TGF-b family receptors (*Alk2*), Gata-family transcription factors (*Gata5*), Notch signaling, and BMP signaling (*BMP4*) (Camenisch et al. 2002; Timmerman et al.

2004; Ma et al. 2005; Wang et al. 2005; McCulley et al. 2008; Laforest and Nemer 2011; Moskowitz et al. 2011; Thomas et al. 2012; Bosse et al. 2013; Dupuis et al. 2013). Testing this idea would require directly examining these mice for pOFT EMT defects as well as monitoring their valves for a deficient Tnc-expressing base region, as observed in the endocardial *Brg1*-deficient model. Another set of models, for instance $Cxcr7^{KO}$, $Egfr^{KO};Ptpnll^{+/-}$ and $Hb\text{-}egf^{KO}$ have clear hyperplastic semilunar valve cusps (Chen et al. 2000; Jackson et al. 2003; Yu et al. 2011), which we did not observe in $Nfatc1^{Cre};Brg1^{F/F}$ embryos by EdU incorporation and cusp volume measurements. We postulate that this manifestation of a semilunar valve defect likely originates in misregulated proliferative signals rather than deficient EMT. However, our combined EdU incorporation and lineage tracing of $Nfatc1^{Cre};Brg1^{F/F}$ valves does show how a subset population of semilunar valve mesenchyme can have an increased proliferative rate even while overall mesenchyme proliferation is unchanged. In endocardial *Brg1*-deficient mice, this effect is non-autonomous, with non-EMT derived mesenchyme increasing their relative rate of proliferation to compensate for the deficient EMT-derived cells. This observation also supports the idea that different valve mesenchymal populations communicate to modulate each other's growth and organization (Jain et al. 2011; Wu et al. 2011). By extension, neural crest (or other origin) mesenchyme could also be genetically perturbed in semilunar valve disease, as indicated by *Rho kinase* and *Pax3* deficient models (Jain et al. 2011; Phillips et al. 2013).

RNA-Seq of the endocardial *Brg1*-deficient valves uncovers potential novel regulators of semilunar valve development and disease

Our transcriptomics study of E14.5 *Nfatc1^{Cre};Brg1$^{F/F}$* valve regions identified a number of such potential novel regulators of valve development and/or disease biomarkers. For example, we found misexpressed negative regulators of both BMP signaling (*Smoc1*, (Thomas et al. 2009) and TGF-beta signaling (*Mirlet7a-1*, (Colas et al. 2012), two pathways that can be aberrantly active in mesenchyme of developmentally abnormal valves (Conway et al. 2011). Our subsequent RNA ISH analysis revealed that several of the misexpressed genes had highly specific and unique expression patterns, showing the high degree of cellular specialization within semilunar valves. For example, *Nptx1* was expressed only in distal tip endocardium of both semilunar valves. Similarly, *Enpp2*, and *Irf6* also are normally expressed in subsets of endocardial cells. In contrast, *Cthrc1* transcripts were restricted to mesenchyme at the base of the semilunar valve. Given their altered expression in endocardial or possible EMT-derived cells (*Cthrc1*) of *Nfatc1^{Cre};Brg1$^{F/F}$* valves, each of these genes may be a direct target of BAF complex activation or repression. Indeed, Brg1 binds near the 5' end of both *Irf6* and *Nptx1* genes by ChIP-Seq studies of E11.5 hearts (Li et al. 2013).

Endocardial *Brg1*-deficient model of semilunar valve disease distinguishes between the origins and progression of semilunar valve disease

Our interpretation of the valve defects in *Nfatc1^{Cre};Brg1$^{F/F}$* embryos provides an explanation for how semilunar valve disease, including thickened and fused cusps, could commonly originate in a sensitive EMT process of early valvulogenesis. Disease

progression then represents the "best effort" of robust developmental networks to produce and maintain a functional valve. As such, a genetic understanding of inherited semilunar valve disease may frequently reflect EMT mechanisms, while efforts to therapeutically attenuate disease progression may merit focusing on manipulating compensating cell lineages and/or their ECM products. For the former goal, mutations in BAF component genes themselves are unlikely to be causes of aortic valve disease given the pleiotropic roles of BAF complex driven chromatin remodeling. However, interacting transcription factors and target genes of BAF-direct chromatin regulation during EMT would represent attractive candidate disease genes. For the latter goal, our RNA-Seq analysis of progressively worsening valves in endocardial *Brg1*-deficient mice has identified new candidate regulators with highly specific expression patterns that may characterize or even drive progression of an anatomically abnormal valve into a disease state.

BRIDGE TO CHAPTER III

My work in Chapter II demonstrates that the BAF complex is required for patterning of the semilunar valves. I show that *Nfatc1*^{Cre}-expressing EMT-derived cells are essential for regulating other mesenchymal populations during OFT valve maturation and ECM organization. Loss of Brg1 in the endocardium results in deficient number of endocardial-derived mesenchymal cells during cushion formation. In Chapter III, I will describe the mechanism of Brg1-dependent EMT in endocardial cells.

CHAPTER III

BRG1 IS REQUIRED FOR TERMINAL STEPS OF ENDOCARDIAL-TO-MESENCHYMAL TRANSFORMATION

AUTHOR CONTRIBUTIONS

I performed the experiments for this project, which include the genetic crosses, histology, fluorescent immunostaining, imaging and data analysis. Additionally, I wrote and prepared the figures in this chapter. Vidusha Devasthali performed a number of fluorescent immunostaining and microscopy assays. Dr. Kryn Stankunas initiated the project while a postdoctoral fellow with Dr. Ching-Pin Chang at Stanford University. He also provided guidance with experimental design, data analysis, and preparing the text and figures.

INTRODUCTION

Cardiac valve development is a complex, multistep process that gives rise to two distinct sets of heart valves in mammals. These intricate structures govern blood flow within the heart, as well as to other regions of the body. The semilunar valves (aortic and pulmonic) are morphologically distinct than that of the atrioventricular-derived valves (mitral and tricuspid). Differences in formation and functions of these valves are attributed to

dissimilarities of mesenchyme origin and formation of these specific structures is precisely regulated during development.

Valvulogenesis first requires the formation of primitive endocardial cushions, which subsequently undergo a morphogenesis process to remodel the cushions into intricate valve structures. The formation of endocardial cushions is driven by an endothelial-to-mesenchymal transformation (EMT) of specialized endocardial cells surrounding 'swellings' of cardiac jelly (proteoglycan-rich) regions beginning at embryonic day 9.5 (E9.5) (Eisenberg and Markwald 1995). The atrioventricular canal (AVC) cushion is entirely populated by endocardial-derived mesenchymal cells (Person et al. 2005). Conversely, the outflow tract (OFT) cardiac cushion is populated with similarly transforming endocardial cells in its proximal cushions (pOFT) and migratory cardiac neural crest-derived mesenchymal cells within the distal cushions (dOFT). Additional studies suggest a possible third mesenchymal origin by drawing attention to the conflicting data presented by a number of different lineage labeling experiments (Kirby et al. 1983; Jiang et al. 2000; Jain et al. 2011; Engleka et al. 2012).

The cellular signals that direct and reinforce EMT during endocardial cushion formation have been studied extensively. Particularly, activated Notch and Tgfβ signaling effectors in the endocardium are essential for induction of EMT in the AVC cushion (Ramsdell and Markwald 1997; Camenisch et al. 2002; Timmerman et al. 2004; Chang et al. 2011). Additionally, myocardial Bmp2 is required to initiate and restrict endocardial cushion formation through activation of Tbx2 (Yamada et al. 2000; Ma et al. 2005). The

transcriptional regulation of how these signaling pathways cooperate to promote endocardial cushion formation have been studied considerably, but an understanding of chromatin structure and regulation during this process remains to be investigated.

Gene activation or repression can, in part, be facilitated by chromatin state and chromatin remodeling proteins that promote nucleosome repositioning or replacement (Tolstorukov et al. 2013). An important chromatin remodeling complex, Brg1-associated factor (BAF) complex is required for early embryonic development, such that null alleles for the core ATPase subunit, Brg1, are peri-implantation lethal (Bultman et al. 2000).

Brg1 is required in the endocardium for both AVC and pOFT cardiac cushion formation. *Tie2:Cre;Brg1*$^{F/F}$ embryos exhibit impaired endothelial-to-mesenchymal transformation in both the atrioventricular canal (AVC) and the proximal-outflow tract (pOFT) endocardial cushions (Akerberg et al. 2015b). However, the mechanism is unknown. Here, we show that loss of Brg1 in endocardial cells results in a failure to complete mesenchymal transformation. *Brg1*-deficient transforming endocardial cells activate early mesenchymal transcription factors, such as Twist1, but unsuccessfully upregulate Sox9 and fail to downregulate endocardial genes. The intermediate mesenchymal cells remain associated with the endocardium and the result is a 'stacking' phenotype of the accumulating *Brg1*-deficient cells. We propose that Brg1 is required for a terminal process of EMT in transforming endocardial cells.

MATERIAL AND METHODS

Mice

Brg1-floxed mice were generated from Dr. Pierre Chambon's laboratory and *Tie2:Cre* mice were obtained from Jackson Laboratory (Sumi-Ichinose et al. 1997; Kisanuki et al. 2001). Mouse husbandry and procedures were permitted and monitored by the University of Oregon's Institutional Animal Care and Use Committee.

Tissue processing and sectioning

Mouse embryos were fixed overnight in 4% PFA/PBS at 4°C. Fixed tissue was washed 3-5X with PBS and then equilibrated overnight with PBS at 4°C. Embryos were dehydrated with a stepwise ethanol series the following day to 100% ethanol and left overnight at 4°C. Tissue was cleared with xylenes the next day, prior to paraffin embedding. 7 μm paraffin sections were used for histological or immunofluorescent staining.

Histology

Paraffin tissue sections were used for hematoxylin and eosin (H&E) staining with standard regents and procedure (Ricca Chemical Company; Sigma-aldrich). Slides were mounted with glass coverslips and permount mounting media after stain (Electron Microscopy Sciences).

Immunostaining

Paraffin tissue sections were de-paraffinized with xylenes and gradually rehydrated with an ethanol series to distilled water. Pressure cooker-based (10' incubation) antigen

retrieval methods were performed for all immunofluorescent stains in either a citrate-based 1X DAKO (Dako) or 1mM EDTA, 0.1% Tween-20 solutions and slowly brought to room temperature. Tissue was blocked with 10% normal goat serum (NGS) in PBS for at least 1 h at room temperature and incubated with primary antibodies overnight at 4°C (anti-Beta-catenin [1:250], CST; anti-Brg1 [1:500], SCBT; anti-Cleaved caspase 3 [1:250], CST; anti-cTnT [1:250], DSHB; anti-Lef1 [1:250], CST; anti-Nfatc1 [1:250], Abcam; anti-PCNA [1:500], Sigma-aldrich; anti-Twist1 [1:100], SCBT; anti-Sox9 [1:250], SCBT; anti-Vimentin [1:250], GeneTex. Fluorescent Alexa-conjugated antibodies were used at 1:500 (Life Technologies). All antibodies were diluted in PBS and 5% NGS during incubation with slides.

RESULTS

As previously described, *Tie2:Cre;Brg1*$^{F/F}$ embryos exhibit extreme cardiovascular and hematopoietic defects (Griffin et al. 2008; Stankunas et al. 2008). These studies showed that endothelial Brg1-deficient embryos exhibit severe vascular defects and fail to properly form ventricular trabeculae. Our recently published data suggests that *Tie2:Cre;Brg1*$^{F/F}$ embryos exhibit an endocardial cushion EMT defect (Akerberg et al. 2015b). We sought to characterize this defective step in valvulogenesis more rigorously. Loss of Brg1 protein in all endothelial and hematopoietic cells can cause early embryonic lethality by E10.5. *Tie2:Cre;Brg1*$^{F/F}$ embryos appeared smaller and less vascularized than wildtype littermates at E10.25 (Fig. 1A, F). By E9.75, we observed that nearly all endocardial cells and EMT-derived cells in the developing heart were void of Brg1 protein (Fig. 1B, C, E, F). Hematoxylin and eosin (H&E) histology staining revealed that

Tie2:Cre;Brg1$^{F/F}$ displayed severe endothelial-to-mesenchymal transformation (EMT) defects in the atrioventricular canal (AVC) and proximal-outflow tract (pOFT) cardiac cushions compared to wildtype littermates (Fig. 1G, H, J, K). We quantified the EMT defect in *Brg1*-deficient AVC cushions compared to normal wildtype littermates and found that *Tie2:Cre;Brg1*$^{F/F}$ embryos exhibited a significant defect in EMT at E9.75 with nearly 52% decrease in the number of migrating mesenchymal cells (Fig. 1I). This data reinforces that Brg1 is required in the endocardium during EMT in both developing cardiac cushions.

To determine whether the diminished mesenchyme in the AVC of *Tie2:Cre;Brg1*$^{F/F}$ embryos was a result of transformed cells failing to proliferate, we tested for changes in rates of proliferation. We were interested in whether there was a mesenchymal role for Brg1 to promote proliferation of the AVC mesenchymal population at E9.75. We performed fluorescent immunostaining for proliferating cell nuclear antigen (PCNA) and an endocardial marker (Nfatc1). *Tie2:Cre;Brg1*$^{F/F}$ AVC cushions displayed normal wildtype levels of PCNA in both the endocardium and transforming mesenchymal cells at E9.75 (Fig. 2A-D). This data further supports our previous findings that *Brg1*-deficient mesenchymal cells (*Nfatc1*^{Cre}*;Brg1*$^{F/F}$ embryos) within the developing pulmonic valve exhibit no significant difference in the rate of proliferation by EdU incorporation (Akerberg et al. 2015a). Taken together, our data shows that Brg1 is dispensable for proliferation of mesenchymal cells in the developing AVC.

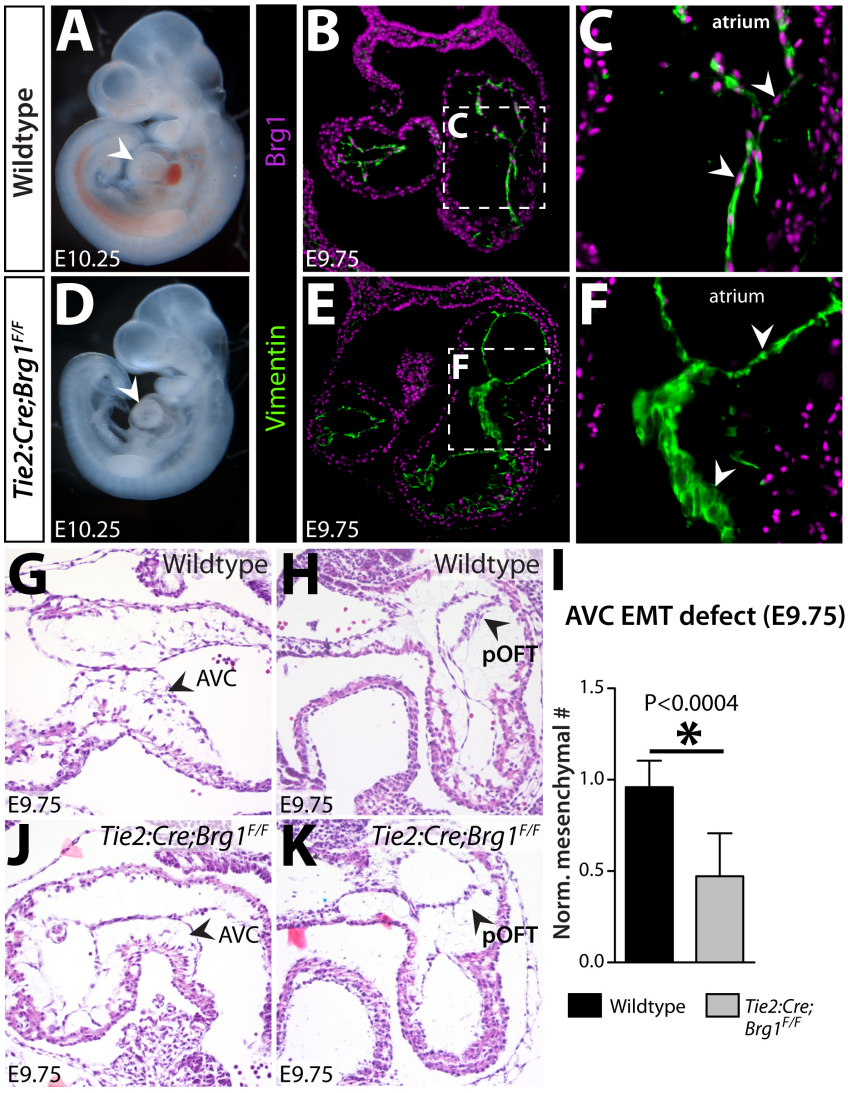

Figure 1. Brg1 is required in endocardial cells for atrioventricular canal and outflow-tract cushion endocardial-mesenchymal transformation.
(A, D) Darkfield wholemount images of *Tie2:Cre;Brg1*$^{F/F}$ and wildtype embryos at E10.25. Arrowheads point to developing heart. (B, C, E, F) Embryos were antibody stained for Brg1 (magenta) protein and Vimentin (green) in *Brg1*- and wildtype at E9.75. Zoom in panels (C, H) depict matched atrioventricular canal (AVC) cushions. White arrowheads indicate Brg1 expression in (C) wildtype AVC and loss of protein in (H) *Tie2:Cre;Brg1*$^{F/F}$ AVC. (G, H, J, K) Matching H&E stained paraffin sections of wildtype and *Brg1*- sagittal cardiac cushions at E9.75. Wildtype (D) AVC and (E) pOFT cushions compared to *Tie2:Cre;Brg1*$^{F/F}$ (I) AVC and (J) pOFT cushions. Black arrowheads indicate presence or depletion of population mesenchyme. (I) Quantification of the EMT defect observed in the AVC of *Tie2:Cre;Brg1*$^{F/F}$ embryos compared to wildtype littermates at E9.75. Data was normalized to wildtype mesenchymal cell number within each litter and statistical significance was analyzed using student's t-test, $p < 0.05$. AVC, atrioventricular canal cushion; pOFT, proximal-outflow tract cushion.

We hypothesized that an additional reason for decreased mesenchymal cells in in *Tie2:Cre;Brg1*$^{F/F}$ AVC endocardial cushions was due to an increase in programmed apoptosis. Analysis of programmed cell death marker, cleaved caspase 3, in *Tie2:Cre;Brg1*$^{F/F}$ cardiac AVC cushions revealed an increased fluorescent signal within the partially transformed mesenchymal populations (Fig. 2E, F). We speculated that *Brg1*-mutant AVCs have a unique defect in the EMT process, such that initiation of endothelial-mesenchymal transformation is not affected but the migration and complete differentiation appears to be hindered. We frequently observed a "stacking" phenotype in *Tie2:Cre;Brg1*$^{F/F}$ AVC cushions, which we defined as migrating endocardial-derived cells that remain associated with the endocardium (seen in Fig. 1C, H).

This phenotype is different than other EMT deficiencies described by loss of signaling molecules and cardiac transcriptions factors, which fail to initiate EMT (Timmerman et al. 2004; Ma et al. 2005; Niessen et al. 2008). Furthermore, these findings support our previous studies that loss of *Brg1* in the endocardium is required for the endothelial-to-mesenchymal transformation process to populate the OFT and AVC cardiac cushions.

We next investigated if *Tie2:Cre;Brg1*$^{F/F}$ AVC cushions displayed changes in known transcription factors that are required for endothelial-to-mesenchymal transformation. Since loss of *Brg1* appeared to affect a specific step of EMT, we hypothesized that transcription factors involved in initiating the process would not be changed in *Brg1*-deficient AVC cushions. We first analyzed any expression changes for the helix-loop-helix transcription factor, Twist1 and lymphoid enhancer-binding factor 1, Lef1 transcription factor that has been linked to the high motility group protein-1.

Tie2:Cre;Brg1$^{F/F}$ embryos displayed normal levels of Twist1 in the expected regions for EMT-induced endocardium in the AVC compared to wildtype AVC (Fig. 3A-D). Lef1

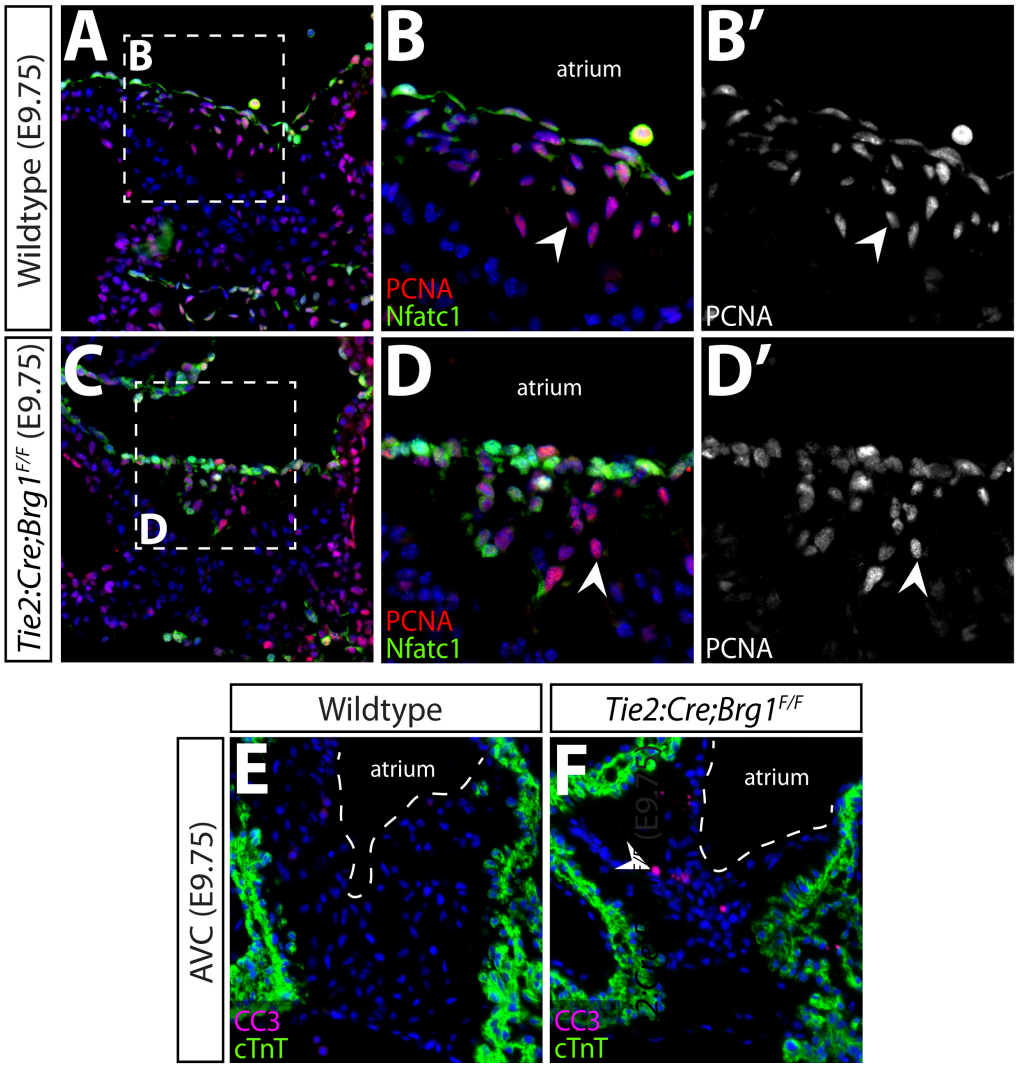

Figure 2. Brg1 is not required for proliferation of endocardial nor mesenchymal cells in *Tie2:Cre;Brg1*$^{F/F}$ atrioventricular canal cushions

(A-D) E9.75 paraffin tissue sections of *Tie2:Cre;Brg1*$^{F/F}$ and wildtype AVC cushions immunostained for proliferating cell nuclear antigen (PCNA) and the endocardial marker Nfatc1 (green). (A) Wildtype AVC cushion and zoom in (B) on atrial side-endocardium. (C) Matched section of *Brg1*-deficient AVC and similarly magnified (D) regions compared for positive PCNA (red, greyscale) staining. (E, F) E9.75 matching paraffin sections of *Tie2:Cre;Brg1*$^{F/F}$ and wildtype littermate AVC antibody stained for cleaved caspase 3 (CC3, green) and myocardial marker, cardiac troponin T (cTnT, pink). White arrowhead denotes positive CC3 staining in AVC mesenchyme.

expression was restricted to transformed mesenchymal cells and adjacent myocardium in wildtype AVC cushions. (Fig. 3B). AVC cushions of *Tie2:Cre;Brg1*$^{F/F}$ embryos exhibited no change in Lef1 expression (Fig. 3D). These results further validate our hypothesis that transcriptional initiation of EMT is intact in *Tie2:Cre;Brg1*$^{F/F}$ and does not require functional BAF protein complex.

To determine if a late step during EMT was disrupted by loss of Brg1 in the endocardium, we tested whether AVC of *Tie2:Cre;Brg1*$^{F/F}$ embryos exhibited changes in the sex-

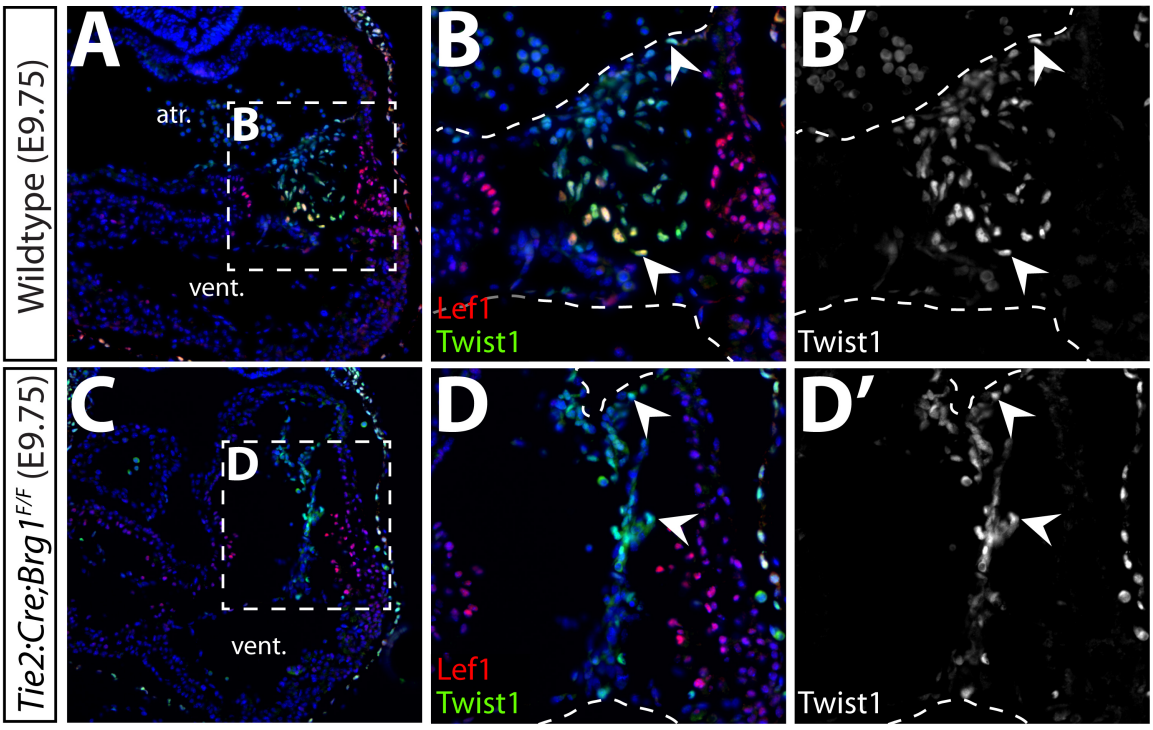

Figure 3. *Tie2:Cre;Brg1*$^{F/F}$ atrioventricular canal cushions express EMT-specific transcription factors
(A-D) E9.75 paraffin tissue sections of *Tie2:Cre;Brg1*$^{F/F}$ and wildtype AVC immunostained for Twist1 (green/grayscale) and Lef1 (red) transcription factor expression. (A, B) Wildtype and (C, D) *Tie2:Cre;Brg1*$^{F/F}$ AVC cushions with Twist1 (green/grayscale) Lef1 (red) protein expression in transforming endocardial cells. White dashed lines denote endocardium-chamber boundaries. White arrowheads indicate Twist1 expressing cells in the endocardium and mesenchyme. atr, atrium; vent, ventricle.

determining region Y (Sox9) transcription factor (Wright et al. 1993). Targeted deletions for *Sox9* have shown it's required for EMT in the AVC through regulating extracellular matrix composition and controlling terminal steps of EMT (Akiyama et al. 2004; Lincoln et al. 2007). Sox9 is normally present in mature mesenchymal cell and not as widely expressed as Twist1, which appeared in the majority of endocardial cells in the AVC. In E9.5 *Tie2:Cre;Brg1*$^{F/F}$ AVC cushions, fewer transforming endocardial cells expressed Sox9 protein (Fig. 4A-D). Wildtype transforming endocardial cells displayed high levels of Sox9 when fully migratory and coincident with downregulated endocardial gene expression (Fig. 4B).

We tested a hypothesis that transforming endocardial cells in *Brg1*-deficient AVCs remained associated with the endocardium due to a failure to downregulate cell adhesionproperties. *Tie2:Cre;Brg1*$^{F/F}$ AVC cushions were immunostned for Twist1 and β-catenin, a component of adherens junctions, at E9.75 and showed drastic changes in β-catenin cellular localization. *Brg1*-deficient embryos exhibited increased expression of β-catenin at the cell-cell contact regions of the intermediate transforming endocardial cells, compared to wildtype mesenchymal cells that displayed largely nuclear and cytoplasmic β-catenin (Fig. 5A-D). These data suggest that Brg1 directly activates Sox9, which would promote completion of EMT in the developing AVC. Further, the inability for *Tie2:Cre;Brg1*$^{F/F}$ AVC cushions to repress endocardial-specific genes is likely due to a direct role for Sox9 protein, as null alleles for *Sox9* show an inability of endocardial cells to repress Nfatc1 (Akiyama et al. 2004).

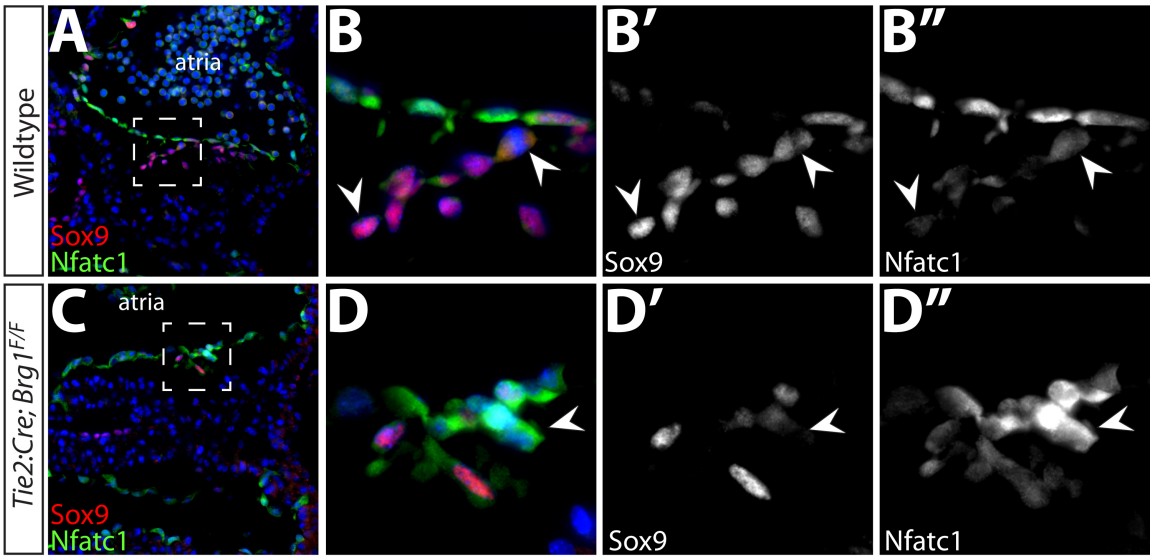

Figure 4. *Brg1*-deficient transforming endocardial cells fail to express Sox9
(A-D) E9.75 wildtype and *Tie2:Cre;Brg1*$^{F/F}$ atrioventricular canal (AVC) cushions immunostained for transcription factor, Sox9 (red, grayscale) and endocardial marker, Nfatc1 (green, grayscale). Wildtype (A, B) paraffin tissue compared to *Tie2:Cre;Brg1*$^{F/F}$ (C, D) tissue. White arrowheads indicate Sox9-positive, Nfatc1-depleted cells in wildtype panels and Nfatc1-positive cells in *Brg1*-deficient tissue.

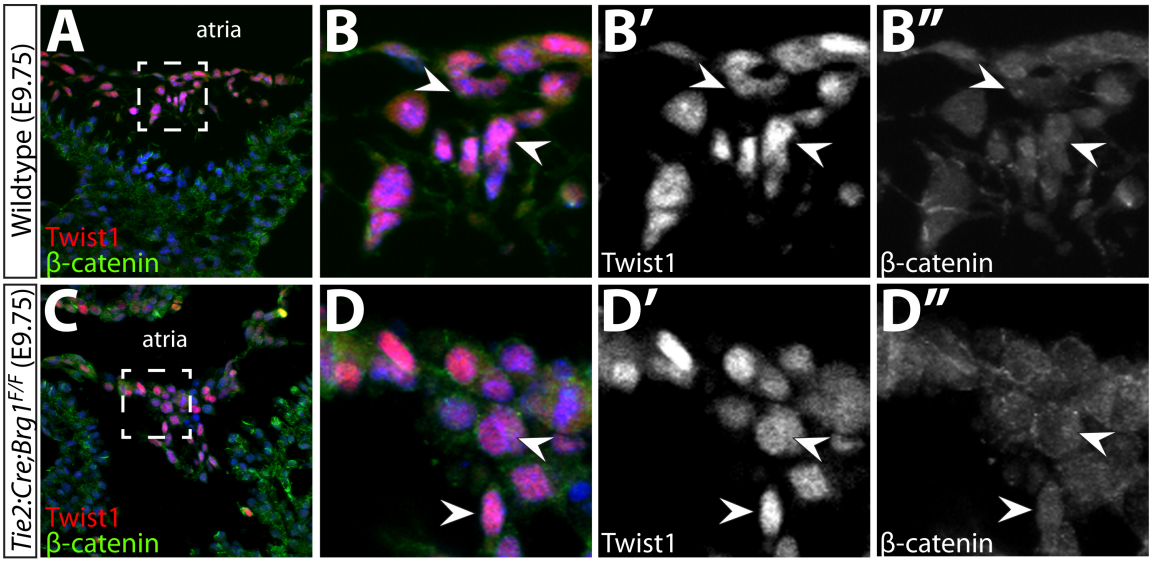

Figure 5. *Tie2:Cre;Brg1*$^{F/F}$ atrioventricular canal cushions retain cell-adhesion properties
(A-D) E9.75 paraffin tissue sections of *Tie2:Cre;Brg1*$^{F/F}$ and wildtype AVC immunostained for Twist1 (red, grayscale) and β-catenin (green, grayscale). (A, B) Wildtype AVC were assayed with (C, D) *Tie2:Cre;Brg1*$^{F/F}$ mutant AVC for changes in β-catenin, which was used to observe cell-adhesion properties. White arrowheads denote Twist1-positive transforming mesenchyme with cytoplasmic/nuclear or cell membrane β-catenin expression in wildtype and *Tie2:Cre;Brg1*$^{F/F}$ AVC tissue respectively.

DISCUSSION

Our results indicate that endocardial AVC cushions of *Tie2:Cre;Brg1*$^{F/F}$ embryos exhibit a specific endothelial-to-mesenchymal defect with a failure to complete transformation to a mesenchymal state. The result is a 'stacking' phenotype where partially transformed endocardial cells remain associated with the endocardium. We show that AVC cushions of *Tie2:Cre;Brg1*$^{F/F}$ embryos express relatively normal levels of EMT-inducing transcription factors, such as Lef1 and Twist1. However, transforming cells *Brg1*-mutant endocardial cells fail to downregulate their endocardial gene expression patterns. We attribute this to the inability to activate Sox9 in developing endocardial cushions of *Tie2:Cre;Brg1*$^{F/F}$ embryos.

Sox9 loss of function studies have demonstrated that endocardial cells fail to repress genes associated with their endocardial cell identity and fully migrate into the cardiac jelly (Akiyama et al. 2004). Furthermore, Sox9 is required to promote ECM remodeling in certain types of cancer for metastasis and represses genes associated with epidermal identity (Larsimont et al. 2015). We hypothesize that the BAF complex is essential for EMT in the developing endocardial cushion to activate the Sox9 locus, which in turn is required to repress endocardial-specific genes.

In other systems, loss of Brg1 or other BAF complex subunits can lead to an EMT defect. For instance, Baf60c is required to promote epithelial-to-mesenchymal transformation through induction of the Wnt5a ligand (Jordan et al. 2013). Similarly, Brg1 appears to

have an important role in repressing epithelial cadherins during epithelial EMT (Sánchez-Tilló et al. 2010).

CHAPTER IV

CONCLUSIONS

Here, I describe two important findings about the requirements of endocardial Brg1 in the valve development and disease. By conditionally targeting Brg1 with two temporally distinct endocardial-Cre recombinases, we have identified that the BAF complex is initially required in the endocardial cushions during endothelial-to-mesenchymal transformation. Secondly, a depletion of these endocardial-derived mesenchymal cells gives rise to progressive mispatterning of the aortic and pulmonic valves. The findings in Chapter II suggest that semilunar valve disease, characterized by malformed and myxomatous valve tissue, can arise from 1) an initial disruption in endocardial cushion formation that 2) can progress to myxomatous and disrupted valve cusps. We propose that a number of mouse models, which produce bicuspid aortic valves (BAV), might exhibit an early endocardial cushion defect. Identifying whether other mouse models display a distinct 'origin' of the valve defect may allow us to categorize these types of bicuspid valves, which could lead to insights about the initiation of those disease models. Furthermore, I describe in Chapter II how a subtle, yet significant, endothelial-mesenchymal transformation (EMT) defect in the proximal-outflow tract (pOFT) of *Nfatc1*^{Cre};*Brg1*$^{F/F}$ mutant mice ultimately leads to mispatterning of the semilunar valve mesenchyme.

Nfatc1^{Cre};*Brg1*$^{F/F}$ mutant mice display a semilunar valve defect phenotype at E16.5 that we observed as significantly less 'elongated' valve cusps that showed an increase in overall 2-D area and number of mesenchymal cells. We attribute this defect to a change in valve morphology, rather than a hyperplastic phenotype, given that 3-D reconstruction of embryonic aortic valves showed no significant increase in volume in the *Nfatc1*^{Cre};*Brg1*$^{F/F}$ mutants. By using a transgenic *Nfatc1enh:Cre* transgenic mouse that expresses only in the endocardium of the valves, we further demonstrate that loss of Brg1 in only endocardial cells is not sufficient to generate SLV defects. Thus, endocardial-derived mesenchymal cells are necessary for proper interstitial organization of the valves. *Nfatc1*^{Cre};*Brg1*$^{F/F}$ adult mice provide a mouse model for left-coronary cusp/non-coronary cusp (LCC-NCC) fusions of bicuspid aortic valve disease, where LCC-NCC BAVD is the most rare cusp fusion for BAV.

My findings in Chapter II depict a cell autonomous role for the BAF complex in semilunar valve formation. Loss of Brg1 in the endocardium causes a significant deficiency of EMT-derived mesenchyme in the base-regions of the aortic and pulmonic valve cusps that are important for proper extracellular matrix patterning and correlates with a depletion of Tenascin C (Tnc). *Nfatc1*^{Cre};*Brg1*$^{F/F}$ semilunar valves respond to compensate for the lack of Nfatc1-derived mesenchymal cells, but ultimately do not generate a functional and properly patterned valve. Whole transcriptome analysis identified a number of differentially changed transcripts in E14.5 *Brg1*-mutant valves that provides insights into potential transcripts that may be associated with the progression of the semilunar valve defect.

The study in Chapter III aims to address how Brg1 regulates endothelial-to-mesenchymal transformation (EMT). The EMT defect present in the *Nfatc1*^{Cre}*;Brg1*$^{F/F}$ mice was only present in the pOFT and can be explained by the timing of *Nfatc1*^{Cre} at the onset of EMT in the outflow tract. In contrast, the EMT process was well underway in the AVC at the time cells *Nfatc1*^{Cre} begun to label cells and excise floxed *Brg1* alleles. Thus providing an explanation for an unperturbed AVC cushion in *Nfatc1*^{Cre}*;Brg1*$^{F/F}$ mice, as well as generating a variable EMT defect phenotype. These results, supported by the *Tie2:Cre;Brg1*$^{F/F}$ embryos exhibiting EMT defects in all cardiac cushions, drove us to utilize the endothelial-specific Cre-recombinase (*Tie2:Cre*) for our studies to determine how Brg1 integrates into EMT mechanisms. In Chapter III, we demonstrate that Brg1 is essential for a terminal step during EMT in atrioventricular and proximal-outflow tract cushions. Specifically, *Tie2:Cre;Brg1*$^{F/F}$ mutants exhibit an EMT phenotype that results in the 'stacking up' of transforming endocardial cells near the endocardium. We propose that Brg1 is required for a terminal step of EMT and that the initiation of EMT does not require a functional BAF complex.

We further show that *Tie2:Cre;Brg1*$^{F/F}$ AVC cushions express normal levels of early EMT transcription factors, such as Twist1, yet are incompetent to downregulate endothelial gene expression. Furthermore, *Tie2:Cre;Brg1*$^{F/F}$ AVCs retained beta-catenin expression at the cell membrane in transforming endocardial cells, as well as failed to repress endocardial marker, Nfatc1. A transcription factor expressed only in completely transformed mesenchymal cells, Sox9, appears downregulated in E9.75 *Brg1*-mutant

AVC cushions. We hypothesize that Sox9 is directly regulated by the BAF complex and loss of Brg1 hinders Sox9 activation, thus fostering an intermediate EMT phenotype, which ultimately leads to programmed apoptosis.

In conclusion, my data has shown a requirement for Brg1 to generate EMT-derived mesenchyme for proper semilunar valve maturation. From the findings presented in Chapter II, we found that the myxomatous valve phenotype observed in $Nfatc1^{Cre};Brg1^{F/F}$ mice was due to a compensation mechanism of the cardiac neural crest mesenchyme. Moreover, my work in Chapter II characterizes the bicuspid aortic valve (BAV) defects that resulted from the semilunar valve defect progressing towards the diseased state. The data in Chapter III illustrates the requirement for Brg1 in the EMT process and attempts to identify where the BAF complex interfaces within the activation cascade of EMT.

APPENDIX

SUPPLEMENTAL MATERIAL (CHAPTER II)

SUPPLEMENTAL FIGURES

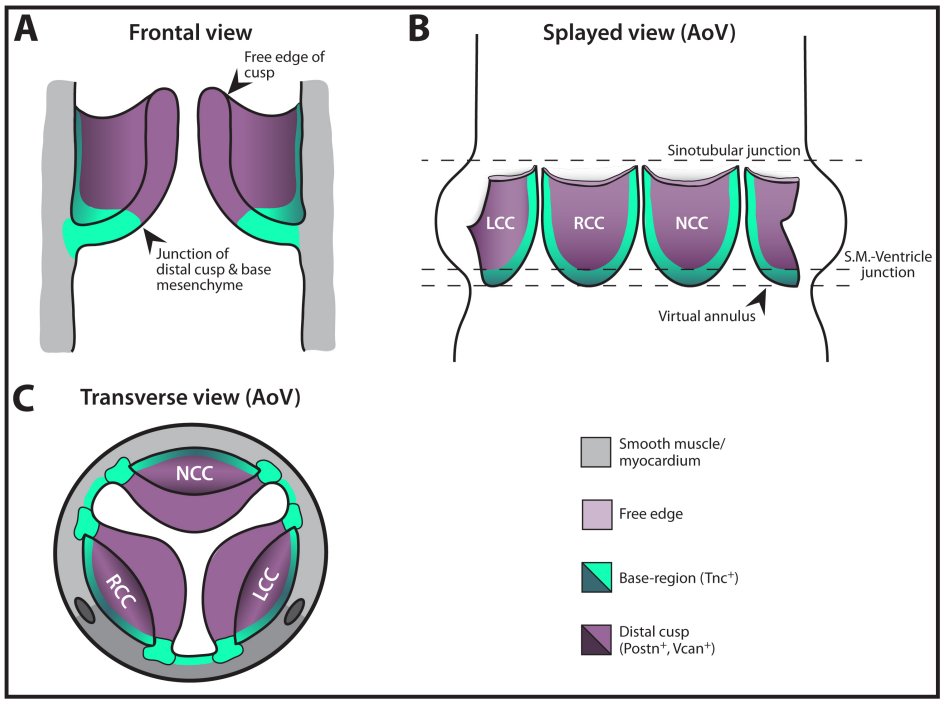

Figure S1. Schematic of semilunar valve anatomy.
(A) Frontal cross-sectional view of a semilunar valve. Each of the three cusps extends from the underlying muscle to form a bisected hemi-cup-like structure enclosing an aortic sinus on the arterial side. Each cusp has a flexible distal cusp (purple) and a stiffer base-region (basal cusp, green) where the cusp meets the adjacent myocardium/smooth muscle. The basal cusp, which has a distinct extracellular matrix composition, begins approximately where the cusp angle shifts from being largely parallel to perpendicular with the underlying muscle. The junction between the distal and basal cusp appears as a narrowing in sectional views and is sometimes called the "hinge". (B) A splayed or open view of the aortic valve showing the 3-D organization of the distal and basal regions of the three cusps. The basal cusp region extends along the entire muscle-attached edge of the cusp. The distal cusp extends from the base to the free edge. (C) Transverse section aortic valve schematic. Base-regions of the aortic and pulmonic valves are enriched with Tenascin C (green), whereas Versican and Periostin predominantly localize within the distal cusp regions (purple). AoV: aortic valve; LCC: left-coronary cusp; NCC: non-coronary cusp; RCC: right-coronary cusp; S.M.: smooth muscle; Tnc: Tenascin C; Postn: Periostin; Vcan, Versican.

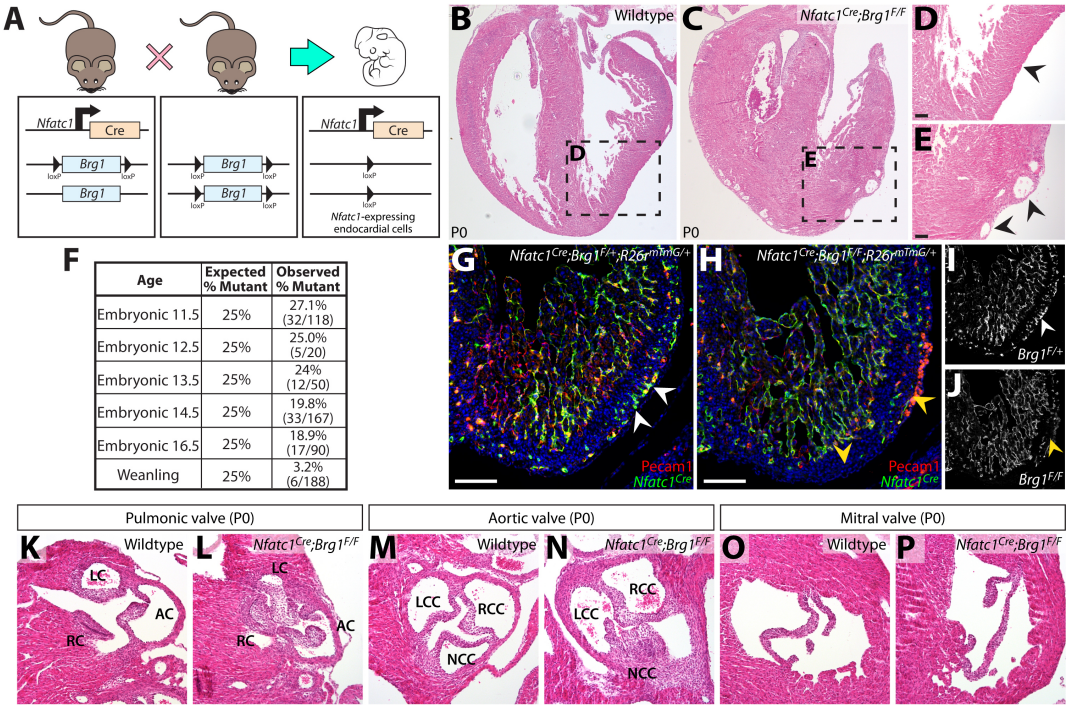

Age	Expected % Mutant	Observed % Mutant
Embryonic 11.5	25%	27.1% (32/118)
Embryonic 12.5	25%	25.0% (5/20)
Embryonic 13.5	25%	24% (12/50)
Embryonic 14.5	25%	19.8% (33/167)
Embryonic 16.5	25%	18.9% (17/90)
Weanling	25%	3.2% (6/188)

Figure S2. *Nfatc1*^{Cre}*;Brg1*$^{F/F}$ mice have congenital heart abnormalities.
(A) Mouse mating scheme used to conditionally delete floxed *Brg1* alleles in endocardial cells using *Nfatc1*^{Cre}. (B-E) Hematoxylin and eosin (H&E) stained sections of hearts from P0 wildtype and *Nfatc1*^{Cre}*;Brg1*$^{F/F}$ mice. Endocardial *Brg1*-deficient mice have a thickened ventricular myocardium containing dilated coronary veins (black arrowheads), indicative of coronary artery disease. (F) Observed versus expected frequency of mice of genotype *Nfatc1*^{Cre}*;Brg1*$^{F/F}$ harvested at indicated developmental stages from genetic crosses outlined in (A). Endocardial *Brg1*-deficient mice die between late embryonic development and birth producing few viable *Nfatc1*^{Cre}*;Brg1*$^{F/F}$ mice at weaning age and beyond. (G-J) Widefield fluorescence images of anti-Pecam (red) and anti-GFP (green, *Nfatc1:Cre*-lineage cells marked using *R26R*^{mTmG} transgene) antibody stained heart sections from E16.5 control and *Nfatc1*^{Cre}*;Brg1*$^{F/F}$ mice. Nuclei are stained with Hoechst (blue). (I, J) Gray scale images showing the *Nfatc1*^{Cre} lineage labeling alone from (G, H) respectively. Wildtype embryos form lineage-labeled endocardial-derived coronary arteries in the left ventricle myocardium (white arrowheads). The reduced coronary artery network in *Nfatc1*^{Cre}*;Brg1*$^{F/F}$ mice (yellow arrowheads) reflects a decrease of endocardial-origin coronary artery endothelium. Coronary artery defects may contribute to the perinatal lethality of endocardial *Brg1*-deficient mice. (K-P) H&E stained sections showing indicated valves of P0 wildtype and viable *Nfatc1*^{Cre}*;Brg1*$^{F/F}$ mice. Endocardial *Brg1*-deficient mice have thickened and poorly organized pulmonic (L) and

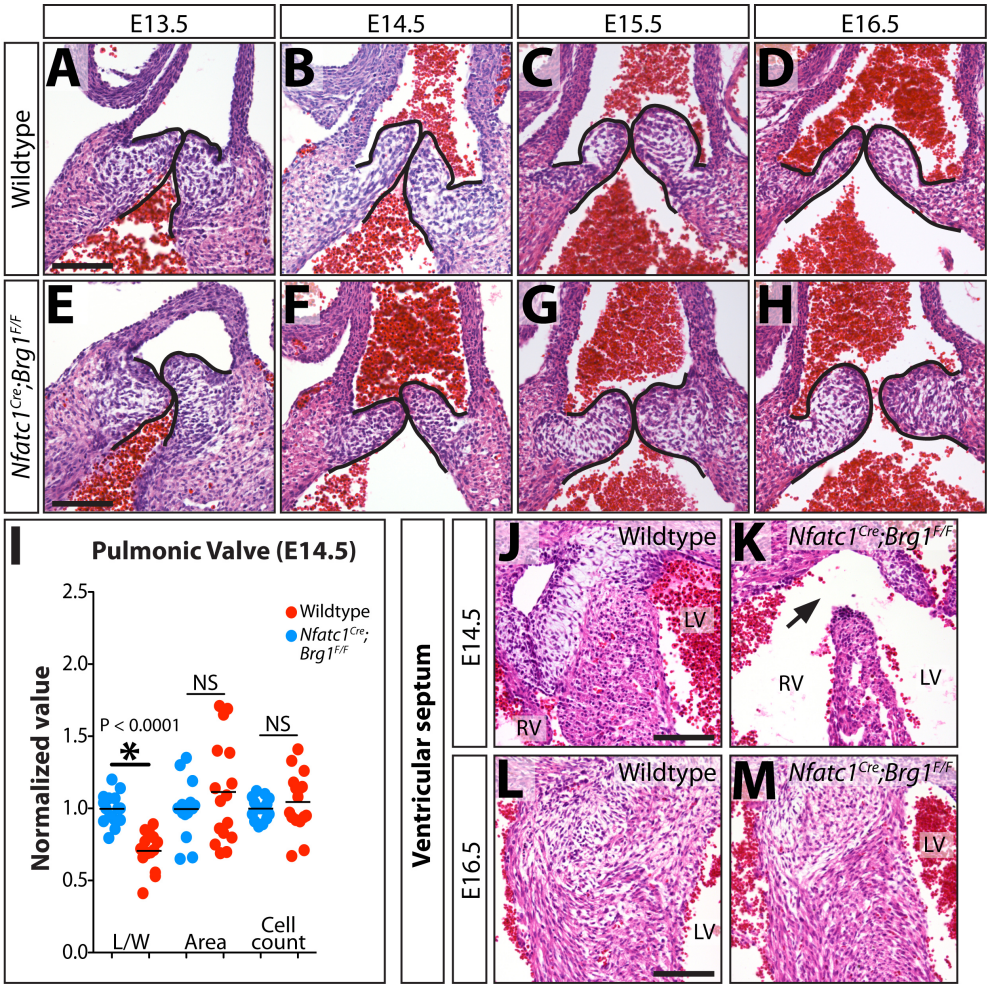

Figure S3. Semilunar valve defects in *Nfatc1^{Cre};Brg1$^{F/F}$* embryos first manifest at E14.5. (A-H) Hematoxylin and eosin (H&E) stained paraffin sections through pulmonic valves (PV) of wildtype and *Nfatc1^{Cre};Brg1$^{F/F}$* embryos (transverse oriented) at indicated embryonic stages. PV defects in *Nfatc1^{Cre};Brg1$^{F/F}$* embryos are first apparent at E14.5, when the PV is qualitatively shorter (less elongated) and lacks the distinct distal and base/hinge regions of wildtype littermate embryos. The phenotype progressively becomes more dramatic, with the PVs from E16.5 *Nfatc1^{Cre};Brg1$^{F/F}$* embryos also appearing larger in a sectional view. (I) Morphometric analyses of E14.5 wildtype and *Nfatc1^{Cre};Brg1$^{F/F}$* PVs. Endocardial *Brg1*-deficient PVs have a significantly decreased length:width (29% mean reduction) but no change in sectional area or total number of mesenchymal cells / section. Each graph point represents one valve, with values normalized to the mean of littermate wildtype embryos (n=8). The asterisk indicates a significant difference between groups (P value calculated by two-tailed Student's t-test). (J-M) H&E sectioned E14.5 (J, K) or E16.5 (L, M) hearts showing the ventricular septum of wildtype and *Nfatc1^{Cre};Brg1$^{F/F}$* embryos. Endocardial *Brg1*-deficient embryos frequently show a membranous ventricular septal defect (arrows in K) at E14.5, which almost always resolves by E16.5 in surviving embryos. NS: not significant; L/W: length-to-width; RV: right ventricle; LV: left ventricle. Scale bars: 100 μm.

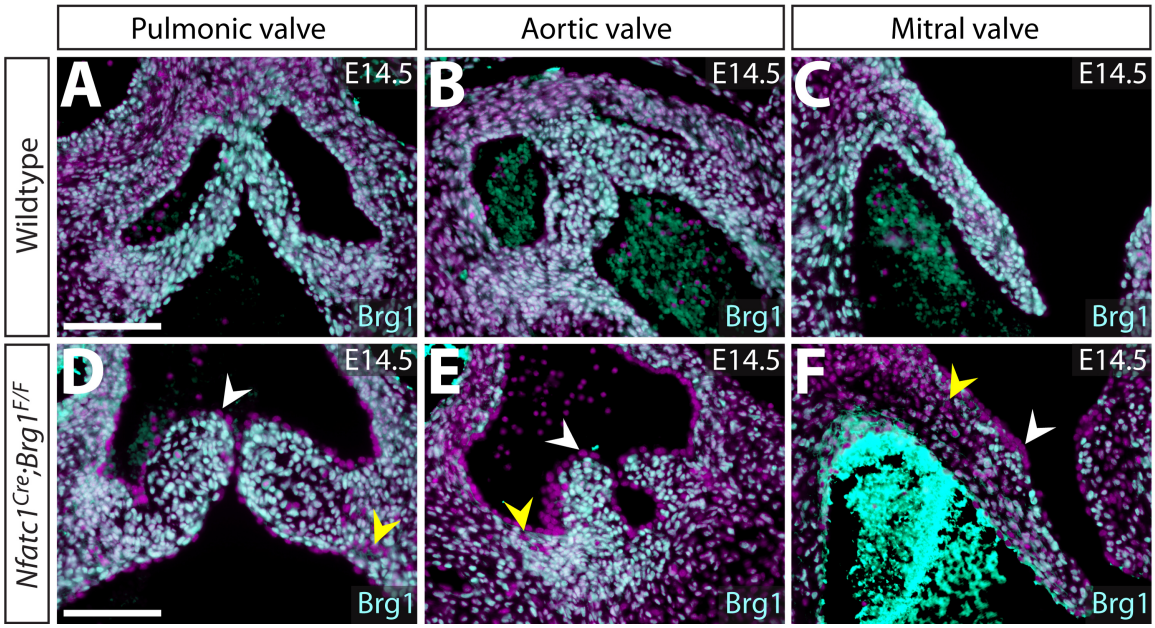

Figure S4. *Nfatc1:cre*-mediated deletion of endocardial-lineage Brg1 protein at E14.5. (A-F) Widefield fluorescence images of E14.5 embryo sections through indicated cardiac valves immunostained for Brg1 protein (gray) with Hoechst-stained nuclei in purple. (A-C) Brg1 is normally expressed in all endocardial cells and mesenchymal cells of the pulmonic, aortic, and mitral valves. (D-F) *Nfatc1*^{Cre}*;Brg1*$^{F/F}$ cardiac valves at E14.5. (D, E) Brg1 expression is lost in all endocardial cells of the semilunar valves (white arrowheads) and some mesenchymal cells concentrated at the base of the valve cusps (yellow arrowheads). (F) The atrioventricular canal-derived mitral valve exhibits a more substantial but still partial loss of Brg1 in valve mesenchyme (white arrowhead). As with the semilunar valves, Brg1 is largely removed from endocardial cells (white arrowhead). Scale bars: 100 μm.

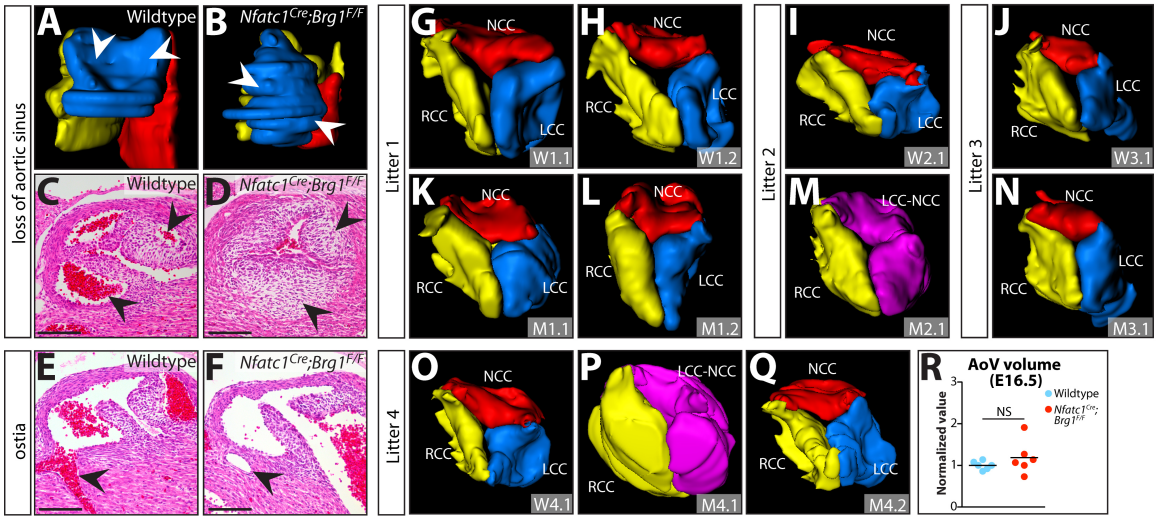

Figure S5. 3-D reconstructed valves show the variability of semilunar valve defects in endocardial-lineage *Brg1*-deficient embryos.

3-dimensional renderings of E16.5 wildtype and *Nfatc1*^{Cre};*Brg1*$^{F/F}$ and wildtype aortic valves reconstructed using serial hematoxylin and eosin (H&E) stained paraffin tissue sections. (A-D) View from the muscle wall-side (muscle hidden, arterial side up) of the left coronary cusps of E16.5 wildtype and *Nfatc1*^{Cre};*Brg1*$^{F/F}$ embryos. Sections from the same embryos are shown in (C, D). Both views show the greatly reduced aortic sinus in endocardial *Brg1*-deficient embryos. The aortic channel is narrowed but not occluded. (E, F) *Nfatc1*^{Cre};*Brg1*$^{F/F}$ E16.5 embryos retain coronary artery ostia. (G-Q) Arterial-side views of 3-D rendered E16.5 aortic valves of wildtype and *Nfatc1*^{Cre};*Brg1*$^{F/F}$ embryos. Reconstructed valves from embryos representing four litters, as denoted, are shown. "W" and "M" represent "wildtype" and/or *Nfatc1*^{Cre};*Brg1*$^{F/F}$ "mutant", respectively. (R) Volume measurements from 3-D rendered aortic valves. There is no significant increase in total aortic valve volume in *Nfatc1*^{Cre};*Brg1*$^{F/F}$ embryos. AoV: aortic valve; LCC (blue): left coronary cusp; NCC (red): non-coronary cusp; RCC (yellow): right coronary cusp; LCC-NCC (purple): bicuspid fusion between left and non-coronary cusps; W*X.X*, wildtype embryo; M*X.X*, *Nfatc1*^{Cre};*Brg1*$^{F/F}$ embryo; first number (***X***.*X*) represents litter and second number (*X.**X***) refers to embryo identifier; NS, not statistically significant. Scale bars: 100 μm.

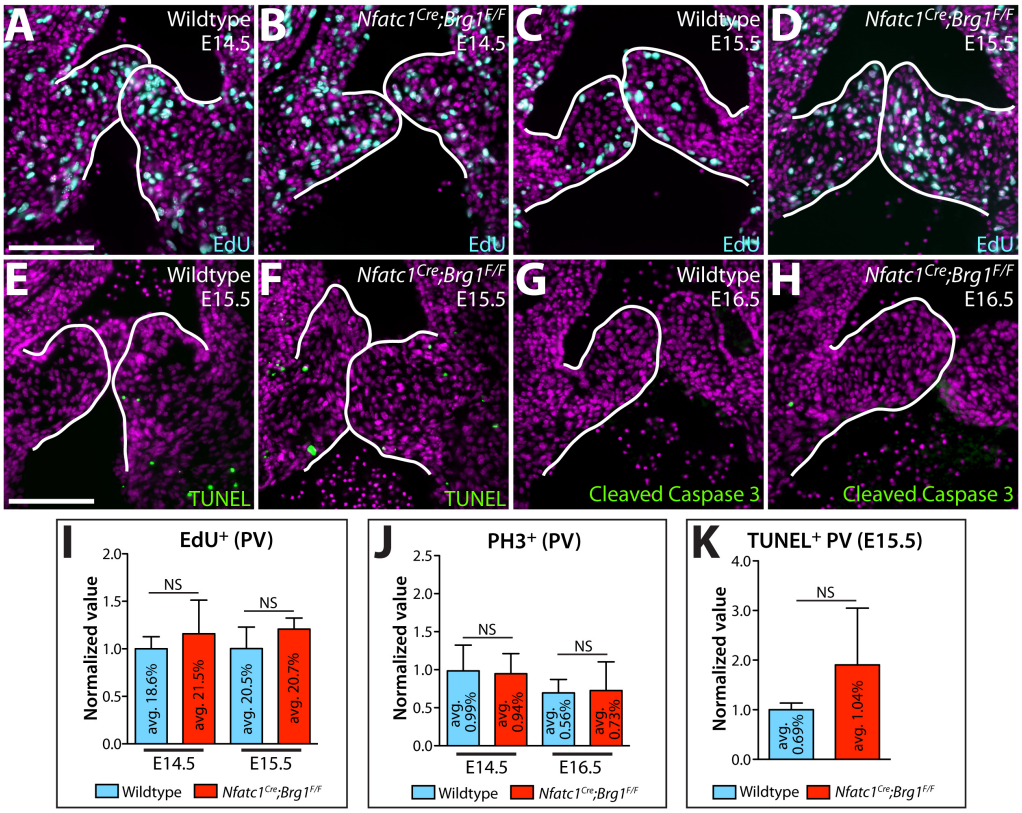

Figure S6. Pulmonic valves of endocardial *Brg1*-deficient embryos exhibit no change in overall mesenchymal cell proliferation or programmed cell death.
(A-D) Proliferation assays on pulmonic valve (PV) paraffin sections by 5-ethynyl-2'-deoxyuridine (EdU) incorporation detected using Click-iT reagents (cyan). Nuclei are Hoechst-stained and shown in purple. EdU was injected into pregnant females two hours prior to embryo harvesting. *Nfatc1*^{Cre}*;Brg1*$^{F/F}$ embryos exhibit unchanged overall PV mesenchyme proliferation at E14.5 or E15.5, as quantified in (I). (E, F) Terminal deoxynucleotidyl transferase dUTP nick end labeling (TUNEL) staining on paraffin sections of wildtype and *Nfatc1*^{Cre}*;Brg1*$^{F/F}$ pulmonic valves at E15.5. Only rare and dispersed TUNEL^{+} apoptotic cells (green, ~1% of cells, see (K)) are found in both wildtype and *Nfatc1*^{Cre}*;Brg1*$^{F/F}$ semilunar valves. (G, H) Immunostaining for an additional cell death marker, cleaved caspase 3 (green), further shows the normal and sparse amount of apoptosis in *Nfatc1*^{Cre}*;Brg1*$^{F/F}$ PVs. (I-K) Bar graphs of the normalized percentage of EdU^{+} (I), phospho-histone H3^{+} (K), and TUNEL^{+} (L) mesenchymal cells in E14.5/E15.5/E16.5 (as indicated) wildtype and *Nfatc1*^{Cre}*;Brg1*$^{F/F}$ PVs. Data is normalized to the mean of wildtype samples within each litter. The absolute mean percentage of positive cells is shown within each bar. (J) Phospho-histone H3 immunostaining at E14.5 and E16.5 shows no statistically significant change in the number of mitotic mesenchymal cells in *Nfatc1*^{Cre}*;Brg1*$^{F/F}$ PVs. NS: not significant; PH3+: phospho-histone H3. Scale bars: 100 µm.

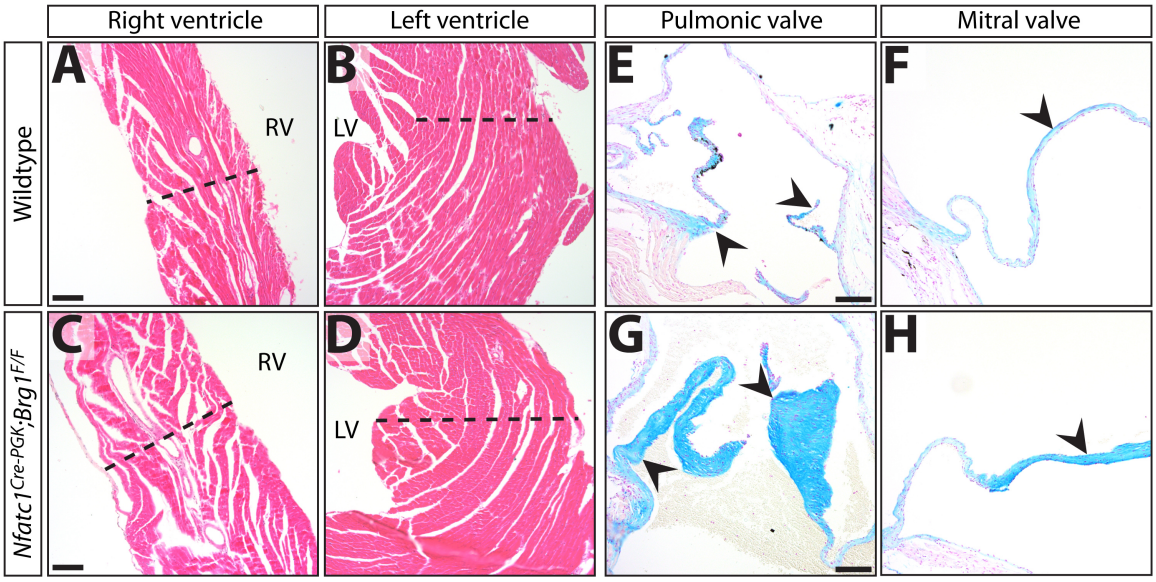

Figure S7. *Nfatc1*$^{Crw\text{-}PGK}$*;Brg1*$^{F/F}$ adult mice show a thickened myocardium and myxomatous but not calcified pulmonic valves.
(A-D) Hematoxylin and eosin (H&E) stained adult heart sections from wildtype and *Nfatc*$^{Cre\text{-}PGK}$*;Brg1*$^{F/F}$ littermates that highlight the outer walls of the right and left ventricles. The dashed line indicates wall thickness. The right and left ventricles of *Nfatc1*$^{Cre\text{-}PGK}$*;Brg1*$^{F/F}$ mice have a thickened myocardium. (E-H) Von Kossa stained heart sections containing the pulmonic or mitral valve of 1 year old (1 yo) wildtype or *Nfatc1*$^{Cre\text{-}PGK}$*;Brg1*$^{F/F}$ mice. (E, G) Endocardial *Brg1*-deficient hearts have thickened and extensively Alcian blue-positive PV cusps (black arrowheads) that, however, do not become calcified. (F, H) Conversely, *Nfatc1*$^{Cre\text{-}PGK}$*;Brg1*$^{F/F}$ mitral valves are qualitatively normal. These observations are consistent with the embryonic data using the related but more effective *Nfatc1*^{Cre} line to delete *Brg1*. RV, right ventricle; LV, left ventricle. Scale bars: 100 μm.

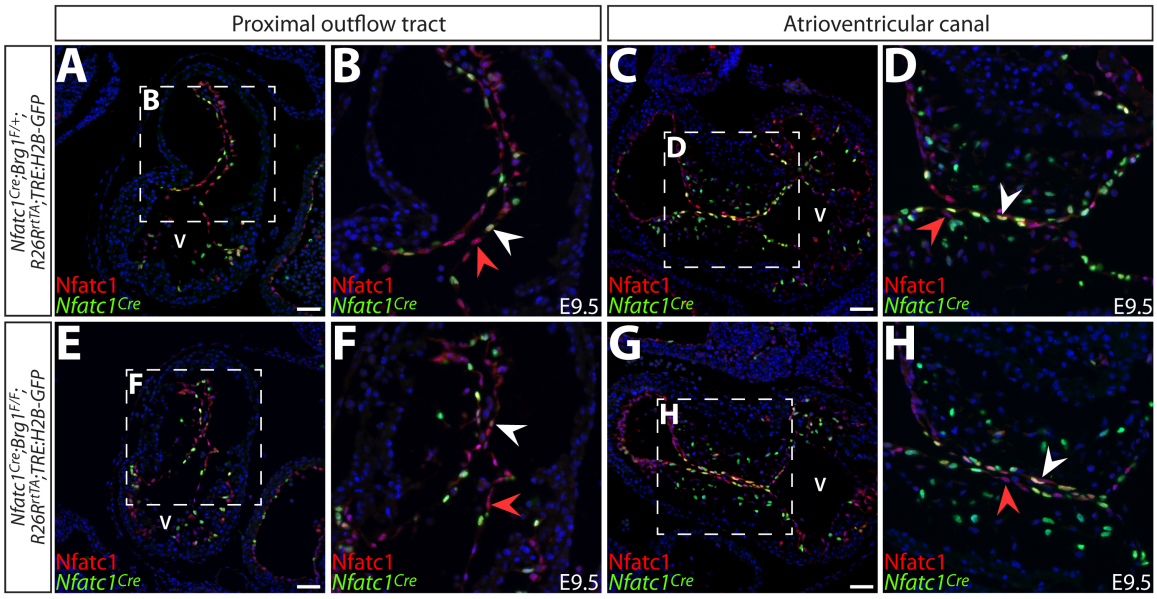

Figure S8. *Nfatc1*^{Cre} activity in endocardial cells precedes the onset of EMT in both outflow tract and atrioventricular canal cushions.

(A-H) Widefield immunofluorescence images of E9.5 hearts stained for Nfatc1 protein (endocardial cells, red) and GFP (*Nfatc1:Cre*-lineage labeled nuclei, green). Nuclear lineage labeling is provided by the combination of Cre-dependent expression of the reverse tetracycline transactivator (rtTA) using the *R26R*^{rtTA} line, a tetracycline-responsive *TRE:H2B-GFP* line, and treating pregnant mice with doxycycline (25 mg/kg IP-injected and 100 µg/ml in drinking water) 24 hours prior to harvesting embryos. Both the outflow tract (OFT; A, B, E, F) and atrioventricular canal (AVC; C, D, G, H) are shown. (A-D) Nfatc1 protein is expressed in all endocardial cells by E9.5. *Nfatc1*^{Cre} activity partially lags, driving incomplete H2B-GFP expression in endocardial cells of the E9.5 OFT (A, B) and more extensive but still partial expression in AVC cushion endocardium (C, D). Resultantly, the majority of EMT-derived mesenchyme is labeled in the AVC cushion. EMT has only just initiated in the proximal OFT so few mesenchymal cells are observed. However, the overlap of Nfatc1 and *Nfatc1:Cre*-lineage labeling in the pOFT endocardium does indicate *Nfatc1*^{Cre} is capable of driving target gene recombination in many endocardial cells prior to pOFT EMT onset. (E-H) *Nfatc1*^{Cre}*;Brg1*$^{F/F}$ embryos show similar patterns of Nfatc1 protein and *Nfatc1*^{Cre} activation within the OFT and AVC. The persistence of lineage-labeled AVC mesenchyme in *Nfatc1*^{Cre}*;Brg1*$^{F/F}$ embryos shows how *Nfatc1*^{Cre}-promoted Brg1 protein loss-of-function is delayed, allowing EMT to complete even while the otherwise essential *Brg1* gene is in the process of being recombined into a null allele. White and red arrowheads show GFP-positive and negative endocardial cells, respectively. V: ventricular chamber. Scale bars: 100 µm.

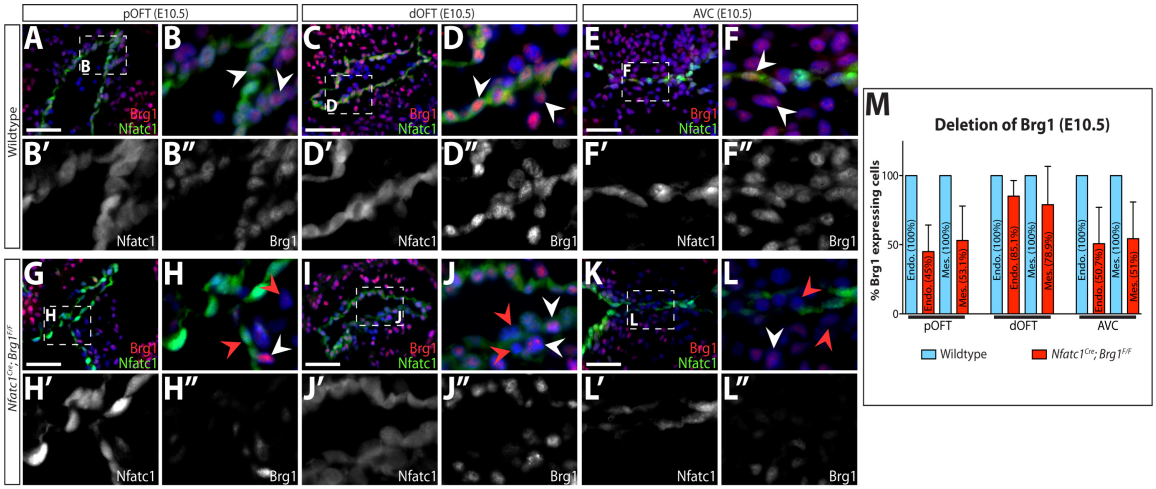

Figure S9. Partial loss of endocardial Brg1 in the E10.5 proximal outflow tract and atrioventricular canal following *Nfatc1*^{Cre}-mediated recombination.
(A-L) Paraffin sections of E10.5 wildtype and *Nfatc1*^{Cre}*;Brg1*$^{F/F}$ outflow tract (OFT) and atrioventricular canal (AVC) cushions immunostained for Brg1 (red/grayscale) and Nfatc1 (green/grayscale). Hoechst-stained nuclei are in blue. Channels are separated and in gray scale in the panels showing magnified regions (marked by dashed boxes). (A-F) Brg1 protein is expressed in all endocardial and mesenchymal cells of wildtype proximal OFT (pOFT), distal OFT (dOFT) and AVC cushions at E10.5. (G, H) Approximately half of *Nfatc1*^{Cre}*;Brg1*$^{F/F}$ pOFT endocardial (55%) and mesenchymal (47%) cells lose detectable Brg1 protein by E10.5. (I, J) A higher percentage of *Nfatc1*^{Cre}*;Brg1*$^{F/F}$ dOFT endocardial (85.1%) and mesenchymal (78.9%) cells retain Brg1. This difference is likely because dOFT endocardial cells have been more recently established from non-*Nfatc1* expressing progenitor cells and much of the dOFT mesenchyme is not EMT-derived. (K-M) Mirroring the OFT, 50.7% of endocardial cells and 51% of mesenchymal cells in E10.5 *Nfatc1*^{Cre}*;Brg1*$^{F/F}$ AVC cushions remained Brg1-expressing. (M) Bar graph displaying the normalized percentage of endocardial cells and mesenchymal cells retaining Brg1 protein in wildtype (control) and *Nfatc1*^{Cre}*;Brg1*$^{F/F}$ pOFT, dOFT, and AVC cardiac cushions. Error bars show one standard deviation from the mean. Red arrowheads mark Brg1-deleted cells. White arrowheads denote Brg1-retaining cells. Endo.: endocardium; mes.: mesenchyme. Scale bars: 100 μm.

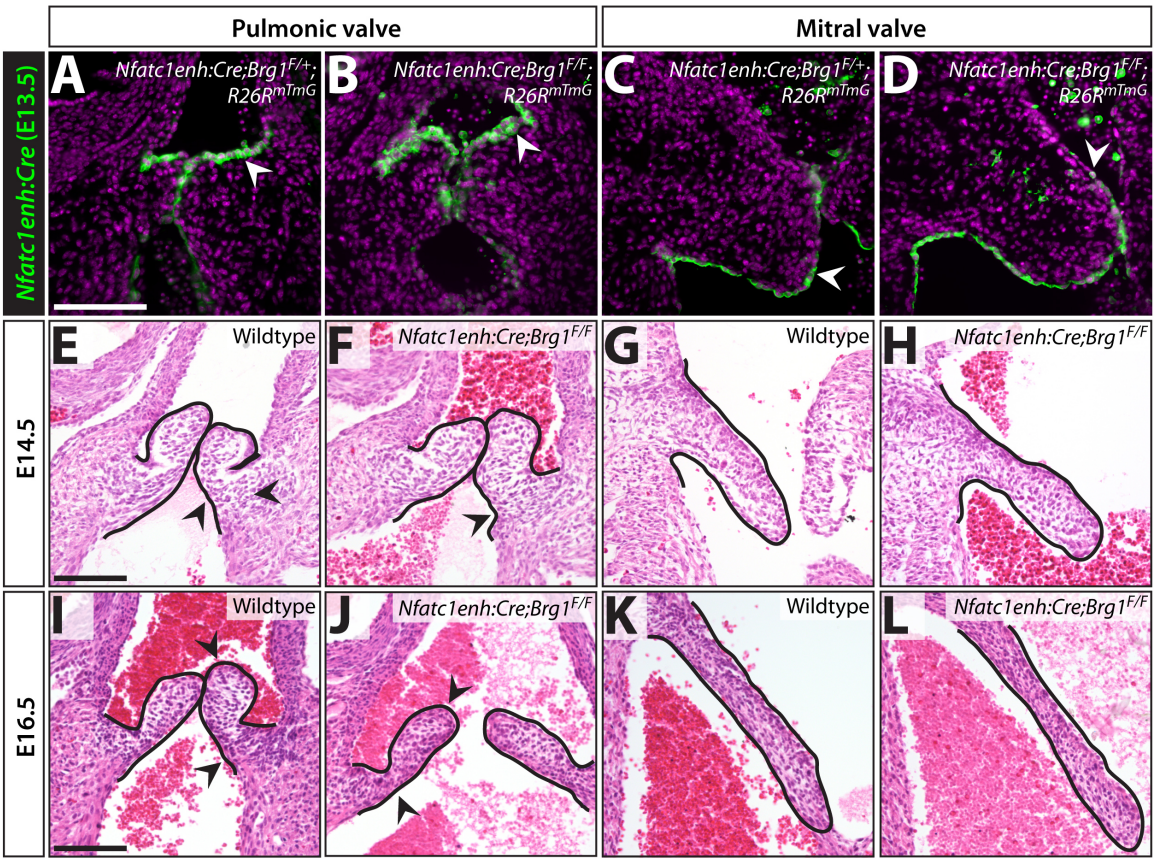

Figure S10. *Brg1* deletion in non-EMT programmed valve endocardial cells does not result in semilunar valve defects.

(A-D) Lineage tracing by immunostaining for GFP (green) on pulmonic (A, B) or mitral valve (C, D) sections of E13.5 wildtype (*Nfatc1enh:Cre;Brg1*$^{F/+}$*;R26R*^{mTmG}) and *Brg1*-deficient (*Nfatc1enh:Cre;Brg1*$^{F/F}$*;R26R*^{mTmG}) embryos. Hoechst-stained nuclei are in purple. White arrowheads indicate endocardial cells. As expected, the *Nfatc1enh:Cre* line promotes recombination exclusively in valve endocardium and not cushion mesenchyme. The Cre reporter pattern is unchanged in *Nfatc1enh:Cre;Brg1*$^{F/F}$ embryos. (E-L) H&E stained paraffin tissue sections from wildtype and *Nfatc1enh:Cre;Brg1*$^{F/F}$ at E14.5 (E-H) and E16.5 (I-L). Black arrowheads show the base/hinge region of pulmonic valves. Both the pulmonic and mitral valves of *Nfatc1*^{enh}*:Cre;Brg1*$^{F/F}$ embryos are indistinguishable from those of control littermates at all stages. Scale bars: 100 μm.

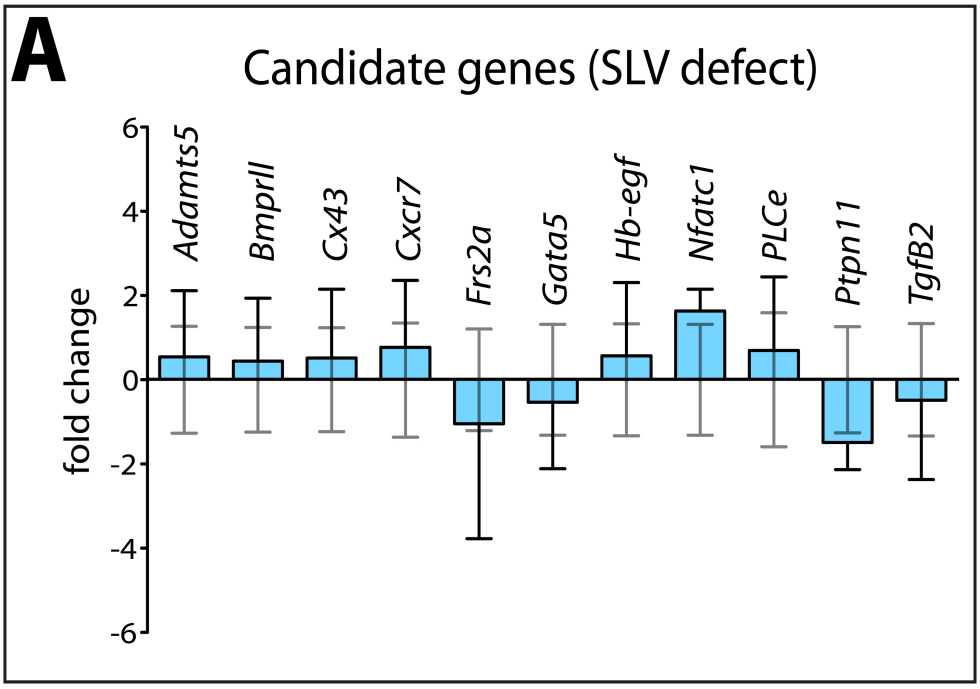

Figure S11. Known semilunar valve disease promoting genes are expressed normally in *Nfatc1^{Cre};Brg1$^{F/F}$* embryos.

A bar graph of a quantitative RT-PCR study comparing the expression of indicated genes between control and *Nfatc1^{Cre};Brg1$^{F/F}$* dissected E14.5 heart valve regions. Genes were selected based on mouse model studies connecting them with semilunar valve defects. These studies include germline null mutations *(Adamts5^{KO}, Cx43^{KO}, Hb-egf^{KO}, Plce^{KO}, Ptpnll$^{KO/+}$, Tgfb2^{KO})* or cell type-specific targeted alleles (*Tie2:Cre* (endocardial cells) targeted deletion of *Bmprll* and *Cxcr7*; *Nkx2.5:Cre* (second heart field) deletion of *Frs2a*) that produce thickened, myxomatous, and/or bicuspid valves (Ya et al. 1998; Iwamoto et al. 2003; Jackson et al. 2003; Tadano et al. 2005; Zhang et al. 2010; Azhar et al. 2011; Dupuis et al. 2011). *Gata5* and *Ptpn11* have both loss of function mouse models that result in semilunar valve defects and are genetically linked to human valve disease (Chen et al. 2000; Laforest et al. 2011; Lauriol and Kontaridis 2011; Padang et al. 2012). Fold changes are normalized to the mean of wildtype samples within each litter to allow combining data. Black and gray error bars show one standard deviation for *Nfatc1^{Cre};Brg1$^{F/F}$* and wildtype samples, respectively. Two-tailed Student's t-tests using ΔCTs identified no significantly misexpressed transcripts.

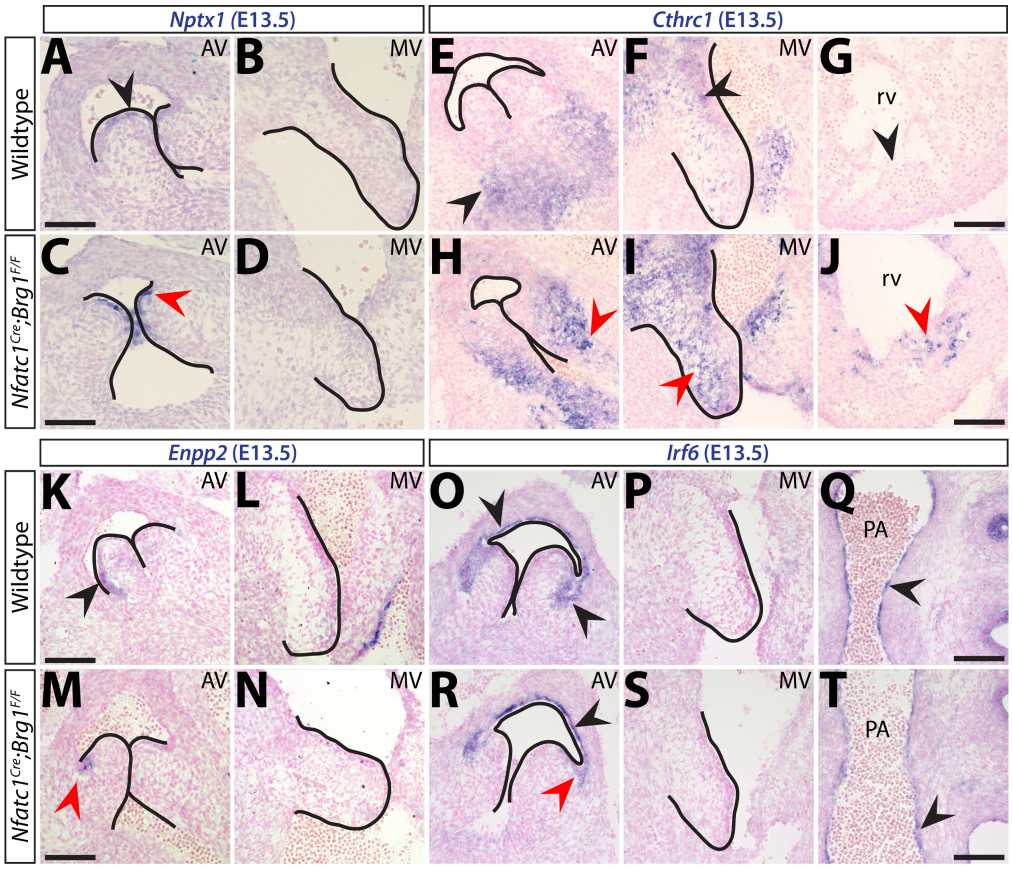

Figure S12. Novel SLV-expressed genes identified by whole transcriptome sequencing show specific and unique expression patterns in developing hearts.
Additional in situ hybridizations to those shown in Fig. 7 for the indicated transcripts on frozen sections (except A-D, which are paraffin) from E13.5 wildtype and *Nfatc1*^{Cre};*Brg1*$^{F/F}$ embryos. Aortic valves (AV), mitral valves (MV), right ventricle (RV, G, J), or pulmonic artery (PA) are shown, as noted. (A-D) *Nptx1* expression is increased in *Nfatc1*^{Cre};*Brg1*$^{F/F}$ embryos but retains its normal pattern concentrated in distal endocardial cells of the AV. *Nptx1* has little to no expression in the MV. (E-J) *Cthrc1* is restricted to mesenchyme in the base of the AV cusp and/or in muscle surrounding the valve in wildtype embryos. Expression levels are increased in AV mesenchyme in endocardial lineage *Nfatc1*^{Cre};*Brg1*$^{F/F}$ embryos. In the MV of wildtype embryos, *Cthrc1* is concentrated in arterial-side mesenchyme at the leaflet base. *Nfatc1*^{Cre};*Brg1*$^{F/F}$ embryos have expanded and increased *Cthrc1* levels in MV mesenchyme. *Cthrc1* is ectopically expressed in ventricular endocardium of *Nfatc1*^{Cre};*Brg1*$^{F/F}$ embryos. (K-N) *Enpp2* is specific to a subset of endocardial cells adjacent to the base-region of the wildtype AV. *Enpp2* AV expression is decreased in *Nfatc1*^{Cre};*Brg1*$^{F/F}$ embryos. Endocardial expression of *Enpp2* on the ventricular side of the parietal mitral valve leaflet is also decreased with endocardial-specific deletion of *Brg1*. (O-T) *Irf6* is expressed in aortic artery endothelium, which extends through the arterial-side endocardium of the aortic valve. *Irf6* is not detectably expressed on the ventricular side of AV. *Nfatc1*^{Cre};*Brg1*$^{F/F}$ embryos exhibit decreased *Irf6* in endocardium associated with the AV with no change in artery endothelial cells. The mitral valve does not express *Irf6* in wildtype or *Nfatc1*^{Cre};*Brg1*$^{F/F}$ embryos and PA endothelial *Irf6* is unchanged in *Nfatc1*^{Cre};*Brg1*$^{F/F}$ embryos. For all panels, black and red arrowheads show sites of normal or misexpressed/mislocalized transcript expression, respectively. Scale bars: 100 μm.

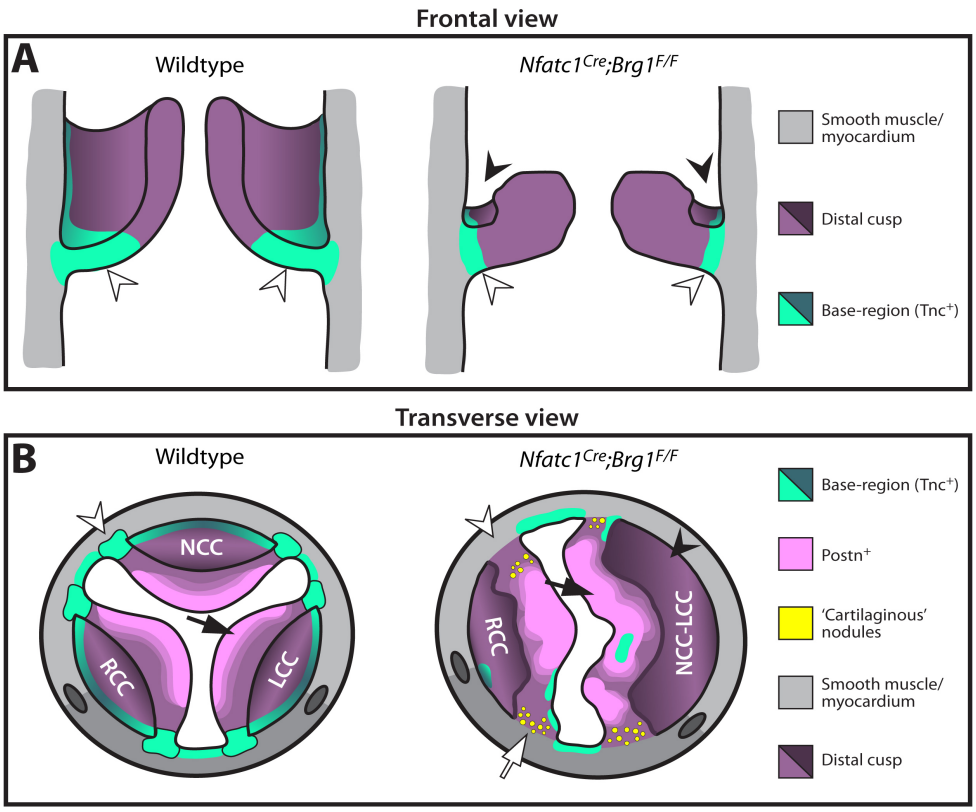

Figure S13. Schematic summary of semilunar valve disease-like phenotypes observed in endocardial *Brg1*-deficient mice.

(A, B) Frontal and transverse schematics depicting the semilunar valve disease-like phenotypes in *Nfatc1*^{Cre}*;Brg1*$^{F/F}$ mice compared to the wildtype state. Semilunar valves (SLVs) of *Nfatc1*^{Cre}*;Brg1*$^{F/F}$ embryos and surviving adults have shortened or lost sinuses (black arrowheads). The SLV cusps have reduced or absent Tenascin (Tnc) rich base-regions (white arrowheads), particularly in the left cusps of both the aortic and pulmonic valves. This defect originates from a deficiency of endocardial-to-mesenchymal transformation (EMT)-derived mesenchyme that reflects a requirement for Brg1 in the initial EMT process. Mesenchyme of other origins (presumably, cardiac neural crest cells) that normally concentrates in the distal cusp expands to replace the lost base-region mesenchyme. Effectively, the cusps become of entirely "distal cusp identity", unable to form a fully patterned SLV. The SLV defects progress to a myxomatous state that includes the presence of cartilaginous nodules in the atypical base-regions (white arrows) and increased/disorganized Postn throughout the cusps (black arrows). Additionally, endocardial *Brg1*-deficient embryos frequently have fused semilunar valve cusps. When bicuspid, the aortic valve most commonly exhibits a LCC-NCC cusp fusion arrangement. Coronary ostia remain present in *Nfatc1*^{Cre}*;Brg1*$^{F/F}$ mice. Tnc: Tenascin C; Postn: Periostin; LCC: left coronary cusp; NCC: non-coronary cusp; RCC: right coronary cusp.

SUPPLEMENTAL MATERIAL AND METHODS

Transgenic Mice

Nfatc1^{Cre}, *Nfatc1*$^{Cre\text{-}PGK}$, and *Nfatc1enh:Cre* mice were provided by Dr. Bin Zhou (Wu et al. 2011; 2012). *Brg1*-floxed allele mice originate from Dr. Pierre Chambon's laboratory (Sumi-Ichinose et al. 1997). *R26R*^{mTmG} (Muzumdar et al. 2007), *R26R*^{rtTA} (Belteki et al. 2005), *Tie2:Cre* (Kisanuki et al. 2001), and *TRE:H2B-GFP* (Tumbar et al. 2004) mice were acquired from the Jackson Laboratory.

qRT-PCR primer sequences

Hprt 5' GCTGGTGAAAAGGACCTCT 3', 5' CACAGGACTAGAACACCTGC 3' (Stankunas et al. 2008); *Cx40* 5' AGTTGAACAGCAGCCAGAGC 3', 5' GACTGTGG-AGTGCTTGTGGA 3'; *Cxcr7* 5' GGTCAGTCTCGTGCAGCATA 3', 5' GTGCGGTG-AAGTAGGTGAT 3' (Sierro et al. 2007); *PLCe* 5' TCAGTGCCTGGAGCAGCAG 3', 5' CTTGAAGGGGATCTTGGTTG 3' (Tadano et al. 2005); *Hb-egf* 5' AGGTGTCATG-GGCTGACTCT 3', 5' CACGCCCAACTTCACTTTCT 3'; *Nfatc1* 5' AGTTATGGCC-AGACAGCACCATCT 3', 5' TGTGCAGCTACACGGTTACTTGGA 3' (Stankunas et al. 2008); *Adamts5* 5' GCTGCTGGTAGCATCGTTACTG 3', 5' GAGTGTAGCGC-GCATGCTT 3' (Wang et al. 2009); *Bmprll* 5' GAAACGATAATCATTGTTTGGC 3', 5' CCCTGTTTCCGGTCTCCTGT3' (Yu et al. 2005); *TgfB2* 5' CTGTACCTTCGTGC-CGTCTAATAA 3', 5' TGCCATCAATACCTGCAAATCT 3' (Wang et al. 2009); *Frs2a* 5' CAGTCGGTGAAGAGTCCACA 3', 5' GGGGTTACTCGGCTCTTCTT 3'; *Gata5* 5' ACATGAGTTCCGACGTAGCC 3', 5' CGCAGGCATTGCATAGATAG 3' (Flagg et al. 2007); *Ptpn11* 5' GGGCAGCTGAAAGAGAAGAA 3', 5' TCTCTCGAA-

CGAGGAAGCTG 3'; *Cx43* 5' GCCGGCTTCACTTTCATTA 3', 5' GCCACCTCTCA-TCTTCACCT 3' (Kumai et al. 2000); *Enpp2* 5' GCCTCCATTTGAAAACATTGA 3', 5' TTGTGCGTAGCAGGTGATTC 3'; *Col23a1* 5' GTCCCAAAGGACCAAAAGGA 3', 5' CAGGCTCTCTTGTAGATGGTCA 3'; *Cthrc1* 5' GACCAAGGAAGCCCTGAG-TT 3', 5' ACCCAGATGGCCACATCTAC 3'; *Nptx1* 5' AGGGTGGCAATGGAGAGA-AC 3', 5' GGTCCCAGATGTTGAAATGG 3'; *Clec7a* 5' GGAAATTCCTGGTATGG-AGT 3', 5' CATGGCCCTTCACTCTGATT 3'; *Smoc1* 5' ACACTGTCCCAGGACTC-AGC 3', 5' CACTCTGGGACAAACACAGC 3'; *Irf6* F: 5' GCACCCATTCAACCCTT-CTA 3', 5' GGGTTGCTCACCGTCATAGT 3'

Fluorescent immunostaining

Paraffin sections were deparaffinized with xylenes for 10' and tissue was rehydrated by 3' sequential washes with a graded ethanol series (100%, 95%, 70%, 50%, 25%) to distilled water. Antigens were retrieved by pressure-cooking slides for 10' in 1X DAKO antigen retrieval solution (DAKO) (for Brg1, Cleaved Caspase 3, GFP, PH3, and Versican antibodies). A 5' incubation in 0.25% Trypsin solution (Life Technologies) was used for antigen retrieval for double Pecam1 and GFP antibody staining. Primary antibodies used were: Brg1 (1:100, SCBT), Cleaved Caspase 3 (1:250, Cell Signaling Technologies), GFP (1:250, Aves), Nfatc1 (1:250, Abcam), Pecam1 (1:100, BD Biosciences), PH3 (1:250, Millipore), Versican (1:250, Millipore). Frozen sections (16 mm, University of Oregon histology facility) were used for GFP (1:500, Aves), Periostin (1:100, SCBT), and Tenascin C (1:100, US Biological) antibody staining without antigen retrieval.

Alexa-conjugated fluorescent secondary antibodies (Life Technologies) were used at 1:500.

TUNEL staining

Apoptosis was assayed using the Roche '*In situ* cell death detection kit'. Rehydrated paraffin sections were proteinase K (20 mg/ml) treated in 10 mM Tris pH 7.5 at room temperature. Slides were sequentially washed twice with 100 mM glycine and PBS. The TUNEL reaction was performed at 37°C for one hour. Subsequently, sectioned tissue was washed thoroughly with PBS, Hoechst stained, and coverslip-mounted for imaging and quantification.

RNA probe synthesis

In situ probes were synthesized from PCRII-based (Life Technologies) template plasmids containing PCR-cloned cDNA fragments. The following primers were used to amplify PCR products from embryonic mouse cDNA. *Enpp2* 5' TCCAAAGGGTCTTGGTGAAG 3', 5' CGCAGATGAATGCACCTTTA 3'; *Irf6* 5' GACCCAGGGCTCTGTCATTA 3', 5' CTGTCAAAGGACCGGGTAAA 3'; *Cthrc1* 5' ATGTGTCTACAAGGACCAGCAG 3', 5' ATGGCATTCCAATATATAGGCTTAAAA 3'; *Nptx1* 5' GATGGCACCACCTACCAATC 3', 5' AACCTGCTCCTGTTGAGGAA 3'. PCRII plasmids were digested with BamHI or NotI to linearize plasmid for digoxigenin-11-dUTP (DIG) (Roche) labeled RNA synthesis using Sp6/T7 RNA polymerases (Fisher Scientific). Synthesized DIG-labeled probes were DNAse treated and LiCl precipitated.

RNA was resuspended in RNase/DNase free water and 1-2 ml was used per slide for each in situ hybridization assay.

Illumina RNA sequencing and bioinformatics

RNA sequencing was performed using RNA isolated from E14.5 dissected heart valve regions from wildtype and *Nfatc1*^{Cre};*Brg1*$^{F/F}$ embryos. 0.5-1.0 mg of total RNA was subjected to Ribo-Zero magnetic bead rRNA-depletion (Epicentre). The rRNA-depleted samples were used to generate index-specific Illumina libraries using the ScriptSeq v2 RNA-seq Library kit following the manufacturer's protocol (Epicentre). Agencourt AMPure magnetic beads (Beckman Coulter) were used for nucleic acid purifications at all necessary steps. Illumina sequencing was performed at the University of Oregon Genomics and Cell Characterization facility. Raw fastq files are deposited at the NCBI Gene Expression Omnibus. (http://www.ncbi.nlm.nih.gov/geo/query/acc.cgi?token=czerwoqixfenxul&acc=GSE67786).

All computational analysis was performed using the ACISS computing cluster at the University of Oregon (http://aciss.uoregon.edu). Reads were quality checked with FASTX-Toolkit (http://hannonlab.cshl.edu/fastx_toolkit/) and low-quality reads were discarded. Reads were aligned to the *Mus musculus* reference genome (mm10) with Bowtie2 (Langmead and Salzberg 2012), SAMtools (Li et al. 2009), and TopHat2 (Roberts et al. 2012). For all four samples (two pairs of E14.5 dissected heart valve regions from one wildtype and one littermate *Nfatc1*^{Cre};*Brg1*$^{F/F}$ embryo), over 60 million

reads were recovered. TopHat 2 aligned reads output (mapped reads/accepted hits files) was used to generate a counts table with HTSeq (Anders et al. 2014). Differential expression between wildtype and *Nfatc1*^{Cre}*;Brg1*$^{F/F}$ tissue was determined with edgeR using a paired-sample repeats matrix design (Robinson et al. 2009). From the 43 differentially expressed genes (DEGs), we highlighted 26 genes based on their expression in E14.5 hearts (Eurexpress atlas, (Diez-Roux et al. 2011) and/or literature linking them to morphogenesis, cell signaling, or gene regulation. We disregarded any of these DEGs that showed ubiquitous expression or were hematopoietic lineage-enriched transcripts that could represent blood pooling or secondary inflammatory responses in *Nfatc1*^{Cre}*;Brg1*$^{F/F}$ embryos. The remaining seven most up- or down- regulated genes were selected for further study using qRT-PCR and RNA in situ hybridization.

REFERENCES CITED

Akerberg BN, Sarangam ML, Stankunas K. 2015b. Endocardial Brg1 disruption illustrates the developmental origins of semilunar valve disease. *Developmental Biology* 1–15.

Akhurst RJ, Lehnert SA, Faissner A, Duffie E. 1990. TGF beta in murine morphogenetic processes: the early embryo and cardiogenesis. *Development* **108**: 645–656.

Akiyama H, Chaboissier M-C, Behringer RR, Rowitch DH, Schedl A, Epstein JA, de Crombrugghe B. 2004. Essential role of Sox9 in the pathway that controls formation of cardiac valves and septa. *Proc Natl Acad Sci USA* **101**: 6502–6507.

Anders S, Pyl PT, Huber W. 2014. *HTSeq - A Python framework to work with high-throughput sequencing data*. bioRxiv.

Angelini A, Ho SY, Anderson RH, Devine WA, Zuberbuhler JR, Becker AE, Davies MJ. 1989. The morphology of the normal aortic valve as compared with the aortic valve having two leaflets. *The Journal of Thoracic and Cardiovascular Surgery* **98**: 362–367.

Azhar M, Brown K, Gard C, Chen H, Rajan S, Elliott DA, Stevens MV, Camenisch TD, Conway SJ, Doetschman T. 2011. Transforming growth factor Beta2 is required for valve remodeling during heart development. *Developmental Dynamics* **240**: 2127–2141.

Belteki G, Haigh J, Kabacs N, Haigh K, Sison K, Costantini F, Whitsett J, Quaggin S, Nagy A. 2005. Conditional and inducible transgene expression in mice through the combinatorial use of Cre-mediated recombination and tetracycline induction. *Nucleic Acids Research* **33**: e51–e51.

Boles NC, Hirsch SE, Le S, Corneo B, Najm F, Minotti AP, Wang Q, Lotz S, Tesar PJ, Fasano CA. 2014. NPTX1 Regulates Neural Lineage Specification from Human Pluripotent Stem Cells. *CellReports* **6**: 724–736.

Bosse K, Hans CP, Zhao N, Koenig SN, Huang N, Guggilam A, LaHaye S, Tao G, Lucchesi PA, Lincoln J, et al. 2013. Endothelial nitric oxide signaling regulates Notch1 in aortic valve disease. *Journal of Molecular and Cellular Cardiology* **60**: 27–35.

Broom ND. 1978. The observation of collagen and elastin structures in wet whole mounts of pulmonary and aortic leaflets. *The Journal of Thoracic and Cardiovascular Surgery* **75**: 121–130.

Bultman SJ, Gebuhr T, Yee D, La Mantia C, Nicholson J, Gilliam A, Randazzo F, Metzger D, Chambon P, Crabtree GR, et al. 2000. A Brg1 null mutation in the mouse reveals functional differences among mammalian SWI/SNF complexes. *Molecular Cell* **6**: 1287–1295.

Camenisch TD, Molin DGM, Person A, Runyan RB, Gittenberger-de Groot AC, McDonald JA, Klewer SE. 2002. Temporal and Distinct TGFβ Ligand Requirements during Mouse and Avian Endocardial Cushion Morphogenesis. *Developmental Biology* **248**: 170–181.

Cardona A, Saalfeld S, Schindelin J, Arganda-Carreras I, Preibisch S, Longair M, Tomancak P, Hartenstein V, Douglas RJ. 2012. TrakEM2 Software for Neural Circuit Reconstruction ed. A. Samuel. *PLoS ONE* **7**: e38011.

Chang ACY, Fu Y, Garside VC, Niessen K, Chang L, Fuller M, Setiadi A, Smrz J, Kyle A, Minchinton A, et al. 2011. Notch Initiates the Endothelial-to-Mesenchymal Transition in the Atrioventricular Canal through Autocrine Activation of Soluble Guanylyl Cyclase. *Developmental Cell* **21**: 288–300.

Cheek JD, Wirrig EE, Alfieri CM, James JF, Yutzey KE. 2012. Journal of Molecular and Cellular Cardiology. *Journal of Molecular and Cellular Cardiology* **52**: 689–700.

Chen B, Bronson RT, Klaman LD, Hampton TG, Wang JF, Green PJ, Magnuson T, Douglas PS, Morgan JP, Neel BG. 2000. Mice mutant for Egfr and Shp2 have defective cardiac semilunar valvulogenesis. *Nature Genetics* **24**: 296–299.

Clementi M, Notari L, Borghi A, Tenconi R. 1996. Familial congenital bicuspid aortic valve: a disorder of uncertain inheritance. *Am J Med Genet* **62**: 336–338.

Colas AR, McKeithan WL, Cunningham TJ, Bushway PJ, Garmire LX, Duester G, Subramaniam S, Mercola M. 2012. Whole-genome microRNA screening identifies let-7 and mir-18 as regulators of germ layer formation during early embryogenesis. *Genes & Development* **26**: 2567–2579.

Conway SJ, Doetschman T, Azhar M. 2011. The Inter-Relationship of Periostin, TGFβ, and BMP in Heart Valve Development and Valvular Heart Diseases. *The Scientific World JOURNAL* **11**: 1509–1524.

de Lange F, Moorman AFM, Anderson RH, Manner J, Soufan A, de Gier-de Vries C, Schneider MD, Webb S, van der Hoff MJB, Christoffels VM. 2004. Lineage and Morphogenetic Analysis of the Cardiac Valves. *Circulation Research* **95**: 645–654.

Diez-Roux G, Banfi S, Sultan M, Geffers L, Anand S, Rozado D, Magen A, Canidio E, Pagani M, Peluso I, et al. 2011. A High-Resolution Anatomical Atlas of the Transcriptome in the Mouse Embryo ed. G.S. Barsh. *PLoS Biol* **9**: e1000582.

Dupuis LE, McCulloch DR, McGarity JD, Bahan A, Wessels A, Weber D, Diminich AM, Nelson CM, Apte SS, Kern CB. 2011. Altered versican cleavage in ADAMTS5 deficient mice; A novel etiology of myxomatous valve disease. *Developmental Biology* **357**: 152–164.

Dupuis LE, Osinska H, Weinstein MB, Hinton RB, Kern CB. 2013. Insufficient versican cleavage and Smad2 phosphorylation results in bicuspid aortic and pulmonary valves. *Journal of Molecular and Cellular Cardiology* **60**: 50–59.

Eisenberg LM, Markwald RR. 1995. Molecular regulation of atrioventricular valvuloseptal morphogenesis. *Circulation Research* **77**: 1–6.

Engleka KA, Manderfield LJ, Brust RD, Li L, Cohen A, Dymecki SM, Epstein JA. 2012. Islet1 Derivatives in the Heart Are of Both Neural Crest and Second Heart Field Origin. *Circulation Research* **110**: 922–926.

Fernandes SM, Sanders SP, Khairy P, Jenkins KJ, Gauvreau K, Lang P, Simonds H, Colan SD. 2004. Morphology of bicuspid aortic valve in children and adolescents. *Journal of the American College of Cardiology* **44**: 1648–1651.

Fernández B, Durán AC, Fernández-Gallego T, Fernández MC, Such M, Arqué JM, Sans-Coma V. 2009. Bicuspid Aortic Valves With Different Spatial Orientations of the Leaflets Are Distinct Etiological Entities. *Journal of the American College of Cardiology* **54**: 2312–2318.

Fischer A, Steidl C, Wagner TU, Lang E, Jakob PM, Friedl P, Knobeloch KP, Gessler M. 2007. Combined Loss of Hey1 and HeyL Causes Congenital Heart Defects Because of Impaired Epithelial to Mesenchymal Transition. *Circulation Research* **100**: 856–863.

Flagg AE, Earley JU, Svensson EC. 2007. FOG-2 attenuates endothelial-to-mesenchymal transformation in the endocardial cushions of the developing heart. *Developmental Biology* **304**: 308–316.

Garg V, Muth AN, Ransom JF, Schluterman MK, Barnes R, King IN, Grossfeld PD, Srivastava D. 2005. Mutations in NOTCH1 cause aortic valve disease. *Nature* **437**: 270–274.

Go AS, Mozaffarian D, Roger VL, Benjamin EJ, Berry JD, Borden WB, Bravata DM, Dai S, Ford ES, Fox CS, et al. 2013. Heart Disease and Stroke Statistics--2013 Update: A Report From the American Heart Association. *Circulation* **127**: e6–e245.

Grewal N, DeRuiter MC, Jongbloed MRM, Goumans MJ, Klautz RJM, Poelmann RE, Gittenberger-de Groot AC. 2014. Normal and abnormal development of the aortic wall and valve: correlation with clinical entities. *Neth Heart J* **22**: 363–369.

Griffin CT, Brennan J, Magnuson T. 2008. The chromatin-remodeling enzyme BRG1 plays an essential role in primitive erythropoiesis and vascular development. *Development* **135**: 493–500.

Gross L, Kugel MA. 1931. Topographic anatomy and histology of the valves in the human heart. *The American Journal of Pathology* 445–473.

Hang CT, Yang J, Han P, Cheng H-L, Shang C, Ashley E, Bin Zhou, Chang C-P. 2010. Chromatin regulation by Brg1 underlies heart muscle development and disease. *Nature* **466**: 62–67.

Hinton RB, Adelman-Brown J, Witt S, Krishnamurthy VK, Osinska H, Sakthivel B, James JF, Li DY, Narmoneva DA, Mecham RP, et al. 2010. Elastin Haploinsufficiency Results in Progressive Aortic Valve Malformation and Latent Valve Disease in a Mouse Model. *Circulation Research* **107**: 549–557.

Hinton RB, Lincoln J, Deutsch G, Osinska H, Manning P, Benson DW, Yutzey KE. 2006. Extracellular Matrix Remodeling and Organization in Developing and Diseased Aortic Valves. *Circulation Research* **98**: 1431–1438.

Hoffman JIE, Kaplan S. 2002. The incidence of congenital heart disease. *Journal of the American College of Cardiology* **39**: 1890–1900.

Hofmann JJ, Briot A, Enciso J, Zovein AC, Ren S, Zhang ZW, Radtke F, Simons M, Wang Y, Iruela-Arispe ML. 2012. Endothelial deletion of murine Jag1 leads to valve calcification and congenital heart defects associated with Alagille syndrome. *Development* **139**: 4449–4460.

Huntington K, Hunter AGW, Chan K-L. 1997. A prospective study to assess the frequency of familial clustering of congenital bicuspid aortic valve. *JACC* **30**: 1809–1812.

Iwamoto R, Mine N, Kawaguchi T, Minami S, Saeki K, Mekada E. 2010. HB-EGF function in cardiac valve development requires interaction with heparan sulfate proteoglycans. *Development* **137**: 2205–2214.

Iwamoto R, Yamazaki S, Asakura M, Takashima S, Hasuwa H, Miyado K, Adachi S, Kitakaze M, Hashimoto K, Raab G, et al. 2003. Heparin-binding EGF-like growth factor and ErbB signaling is essential for heart function. *Proc Natl Acad Sci USA* **100**: 3221–3226.

Jackson LF, Qiu TH, Sunnarborg SW, Chang A, Zhang C, Patterson C, Lee DC. 2003. Defective valvulogenesis in HB-EGF and TACE-null mice is associated with aberrant BMP signaling. *EMBO J* **22**: 2704–2716.

Jain R, Engleka KA, Rentschler SL, Manderfield LJ, Li L, Yuan L, Epstein JA. 2011. Cardiac neural crest orchestrates remodeling and functional maturation of mouse semilunar valves. *J Clin Invest* **121**: 422–430.

Jiang X, Rowitch DH, Soriano P, McMahon AP, Sucov HM. 2000. Fate of the mammalian cardiac neural crest. *Development* **127**: 1607–1616.

Jordan NV, Prat A, Abell AN, Zawistowski JS, Sciaky N, Karginova OA, Zhou B, Golitz BT, Perou CM, Johnson GL. 2013. SWI/SNF Chromatin-Remodeling Factor Smarcd3/Baf60c Controls Epithelial-Mesenchymal Transition by Inducing Wnt5a Signaling. *Molecular and Cellular Biology* **33**: 3011–3025.

Kadoch C, Crabtree GR. 2013. Reversible Disruption of mSWI/SNF (BAF) Complexes by the SS18-SSX Oncogenic Fusion in Synovial Sarcoma. *Cell* **153**: 71–85.

Kadoch C, Hargreaves DC, Hodges C, Elias L, Ho L, Ranish J, Crabtree GR. 2013. Proteomic and bioinformatic analysis of mammalian SWI/SNF complexes identifies extensive roles in human malignancy. *Nature Genetics* **45**: 592–601.

Kang JW, Song HG, Yang DH, Baek S, Kim DH, Song JM, Kang DH, Lim TH, Song JK. 2013. Association Between Bicuspid Aortic Valve Phenotype and Patterns of Valvular Dysfunction and Bicuspid Aortopathy. *JCMG* **6**: 150–161.

Kern CB, Wessels A, McGarity J, Dixon LJ, Alston E, Argraves WS, Geeting D, Nelson CM, Menick DR, Apte SS. 2010. Reduced versican cleavage due to Adamts9 haploinsufficiency is associated with cardiac and aortic anomalies. *Matrix Biology* **29**: 304–316.

Kirby ML, Gale TF, Stewart DE. 1983. Neural crest cells contribute to normal aorticopulmonary septation. *Science* **220**: 1059–1061.

Kisanuki YY, Hammer RE, Miyazaki J-I, Williams SC, Richardson JA, Yanagisawa M. 2001. Tie2-Cre Transgenic Mice: A New Model for Endothelial Cell-Lineage Analysis in Vivo. *Developmental Biology* **230**: 230–242.

Kondo S, Schutte BC, Richardson RJ, Bjork BC, Knight AS, Watanabe Y, Howard E, Ferreira de Lima RLL, Daack-Hirsch S, Sander A, et al. 2002. Mutations in IRF6 cause Van der Woude and popliteal pterygium syndromes. *Nature Genetics* **32**: 285–289.

Krishnamurthy VK, Opoka AM, Kern CB, Guilak F, Narmoneva DA, Hinton RB. 2012. Maladaptive matrix remodeling and regional biomedical dysfunction in a mouse model of aortic valve disease. *Matrix Biology* **31**: 197–205.

Krug EL, Mjaatvedt CH, Markwald RR. 1987. Extracellular matrix from embryonic myocardium elicits an early morphogenetic event in cardiac endothelial differentiation. *Developmental Biology* **120**: 3488–3355.

Kruzynska-Frejtag A, Machnicki M, Rogers R, Markwald RR, Conway SJ. 2001. Periostin (an osteoblast-specific factor) is expressed within the embryonic mouse heart during valve formation. *Mechanisms of Development* **103**: 183–188.

Kumai M, Nishii K, Nakamura K, Takeda N, Suzuki M, Shibata Y. 2000. Loss of connexin45 causes a cushion defect in early cardiogenesis. *Development* **127**: 3501–3512.

Laforest B, Andelfinger G, Nemer M. 2011. Loss of Gata5 in mice leads to bicuspid aortic valve. *J Clin Invest* **121**: 2876–2887.

Laforest B, Nemer M. 2011. GATA5 interacts with GATA4 and GATA6 in outflow tract development. *Developmental Biology* **358**: 368–378.

Langmead B, Salzberg SL. 2012. Fast gapped-read alignment with Bowtie 2. *Nature Methods* **9**: 357–359.

Larsimont J-C, Youssef KK, Sánchez-Danés A, Sukumaran V, Defrance M, Delatte B, Liagre M, Baatsen P, Marine J-C, Lippens S, et al. 2015. Sox9 Controls Self-Renewal of Oncogene Targeted Cells and Links Tumor Initiation and Invasion. *Stem Cell* **17**: 60–73.

Lauriol J, Kontaridis MI. 2011. PTPN11-Associated Mutations in the Heart: Has LEOPARD Changed Its RASpots? *TCM* **21**: 97–104.

Li H, Handsaker B, Wysoker A, Fennell T, Ruan J, Homer N, Marth G, Abecasis G, Durbin R, 1000 Genome Project Data Processing Subgroup. 2009. The Sequence Alignment/Map format and SAMtools. *Bioinformatics* **25**: 2078–2079.

Li W, Xiong Y, Shang C, Twu K, Hang CT, Yang J, Han P, Lin C-Y, Lin C-J, Tsai Y-P, et al. 2013. Brg1 governs distinct pathways to direct multiple aspects of mammalian neural crest cell development. Vol. 110 of, pp. 1738–1743.

Lickert H, Takeuchi JK, Both Von I, Walls JR, McAuliffe F, Adamson SL, Henkelman RM, Wrana JL, Rossant J, Bruneau BG. 2004. Baf60c is essential for function of BAF chromatin remodelling complexes in heart development. *Nature* **432**: 107–112.

Lincoln J, Alfieri CM, Yutzey KE. 2004. Development of heart valve leaflets and supporting apparatus in chicken and mouse embryos. *Developmental Dynamics* **230**: 239–250.

Lincoln J, Kist R, Scherer G, Yutzey KE. 2007. Sox9 is required for precursor cell expansion and extracellular matrix organization during mouse heart valve development. *Developmental Biology* **305**: 120–132.

Luna-Zurita L, Prados B, Grego-Bessa J, Luxán G, del Monte G, Benguría A, Adams RH, Perez-Pomares JM, la Pompa de JL. 2010. Integration of a Notch-dependent mesenchymal gene program and Bmp2-driven cell invasiveness regulates murine cardiac valve formation. *J Clin Invest* **120**: 3493–3507.

Ma L, Lu M-F, Schwartz R, Martin J. 2005. Bmp2 is essential for cardiac cushion epithelial-mesenchymal transition and myocardial patterning. *Development* **132**: 5601–5611.

Ma Q, Bin Zhou, Pu WT. 2008. Reassessment of Isl1 and Nkx2-5 cardiac fate maps using a Gata4-based reporter of Cre activity. *Developmental Biology* **323**: 98–104.

McCulley DJ, Kang J-O, Martin JF, Black BL. 2008. BMP4 is required in the anterior heart field and its derivatives for endocardial cushion remodeling, outflow tract septation, and semilunar valve development. *Developmental Dynamics* **237**: 3200–3209.

Moskowitz IP, Wang J, Peterson MA, Pu WT, Mackinnon AC, Oxburgh L, Chu GC, Sarkar M, Berul C, Smoot L, et al. 2011. Transcription factor genes Smad4 and Gata4 cooperatively regulate cardiac valve development. *Proceedings of the National Academy of Sciences* **108**: 4006–4011.

Muzumdar MD, Tasic B, Miyamichi K, Li L, Luo L. 2007. A global double-fluorescent Cre reporter mouse. *genesis* **45**: 593–605.

Nakamura T, Colbert M, Robbins J. 2006. Neural Crest Cells Retain Multipotential Characteristics in the Developing Valves and Label the Cardiac Conduction System. *Circulation Research* **98**: 1547–1554.

Niessen K, Fu Y, Chang L, Hoodless PA, McFadden D, Karsan A. 2008. Slug is a direct Notch target required for initiation of cardiac cushion cellularization. *The Journal of Cell Biology* **182**: 315–325.

Norris RA, Moreno-Rodriguez RA, Sugi Y, Hoffman S, Amos J, Hart MM, Potts JD, Goodwin RL, Markwald RR. 2008. Periostin regulates atrioventricular valve maturation. *Developmental Biology* **316**: 200–213.

Omeis IA, Hsu YC, Perin MS. 1996. Mouse and human neuronal pentraxin 1 (NPTX1): conservation, genomic structure, and chromosomal localization. *Genomics* **36**: 543–545.

Padang R, Bagnall RD, Richmond DR, Bannon PG, Semsarian C. 2012. Rare non-synonymous variation in the transcriptional activation domains of GATA5 in bicuspid aortic valve disease. *Journal of Molecular and Cellular Cardiology* **53**: 277–281.

Person AD, Klewer SE, Runyan RB. 2005. Cell biology of cardiac cushion development. *International review of cytology*.

Phillips HM, Mahendran P, Singh E, Anderson RH, Chaudhry B, Henderson DJ. 2013. Neural crest cells are required for correct positioning of the developing outflow cushions and pattern the arterial valve leaflets. *Cardiovascular Research* **99**: 452–460.

Potts JD, Dagle JM, Walder JA, Weeks DL, Runyan RB. 1991. Epithelial-mesenchymal transformation of embryonic cardiac endothelial cells is inhibited by a modified antisense oligodeoxynucleotide to transforming growth factor …. Vol. 88 of, pp. 1516–1520.

Pyagay P, Heroult M, Wang Q, Lehnert W, Belden J, Liaw L, Friesel R, Lindner V. 2005. Collagen Triple Helix Repeat Containing 1, a Novel Secreted Protein in Injured and Diseased Arteries, Inhibits Collagen Expression and Promotes Cell Migration. *Circulation Research* **96**: 261–268.

Ramsdell AF, Markwald RR. 1997. Induction of endocardial cushion tissue in the avian heart is regulated, in part, by TGFbeta-3-mediated autocrine signaling. *Developmental Biology* **188**: 64–74.

Rivera-Feliciano J, Lee K-H, Kong SW, Rajagopal S, Ma Q, Springer Z, Izumo S, Tabin CJ, Pu WT. 2006. Development of heart valves requires Gata4 expression in endothelial-derived cells. *Development* **133**: 3607–3618.

Roberts A, Goff L, Pertea G, Kim D, Kelley DR, Pimentel H, Salzberg SL, Rinn JL, Pachter L, Trapnell C. 2012. Differential gene and transcript expression analysis of RNA-seq experiments with TopHat and Cufflinks. *Nature Protocols* **7**: 562–578.

Roberts W, Ko J. 2005. Frequency by Decades of Unicuspid, Bicuspid, and Tricuspid Aortic Valves in Adults Having Isolated Aortic Valve Replacement for Aortic Stenosis, With or Without Associated Aortic Regurgitation. *Circulation* **111**: 920–925.

Robinson MD, McCarthy DJ, Smyth GK. 2009. edgeR: a Bioconductor package for differential expression analysis of digital gene expression data. *Bioinformatics* **26**: 139–140.

Runyan RB, Markwald RR. 1983. Invasion of mesenchyme into three-dimensional collagen gels: a regional and temporal analysis of interaction in embryonic heart tissue. *Developmental Biology* **95**: 108–114.

Satta J, Melkko J, Pöllänen R, Tuukkanen J, Pääkkö P, Ohtonen P, Mennander A, Soini Y. 2002. Progression of human aortic valve stenosis is associated with tenascin-C expression. *JAC* **39**: 96–101.

Sánchez-Tilló E, Lázaro A, Torrent R, Cuatrecasas M, Vaquero EC, Castells A, Engel P, Postigo A. 2010. ZEB1 represses E-cadherin and induces an EMT by recruiting the SWI/SNF chromatin-remodeling protein BRG1. *Oncogene* **29**: 3490–3500.

Sierro F, Biben C, Martínez-Muñoz L, Mellado M, Ransohoff R, Li M, Woehl B, Leung H, Groom J, Batten M, et al. 2007. Disrupted cardiac development but normal hematopoiesis in mice deficient in the second CXCL12/SDF-1 receptor, CXCR7. Vol. 104 of, pp. 14759–14764.

Siu SC, Silversides CK. 2010. Bicuspid Aortic Valve Disease. *JAC* **55**: 2789–2800.

Sizarov A, Lamers WH, Mohun TJ, Brown NA, Anderson RH, Moorman AFM. 2012. Three-dimensional and molecular analysis of the arterial pole of the developing human heart. *Journal of Anatomy* **220**: 336–349.

Snider P, Hinton RB, Moreno-Rodriguez RA, Wang J, Rogers R, Lindsley A, Li F, Ingram DA, Menick D, Field L, et al. 2008. Periostin Is Required for Maturation and Extracellular Matrix Stabilization of Noncardiomyocyte Lineages of the Heart. *Circulation Research* **102**: 752–760.

Snider P, Standley KN, Wang J, Azhar M, Doetschman T, Conway SJ. 2009. Origin of Cardiac Fibroblasts and the Role of Periostin. *Circulation Research* **105**: 934–947.

Stankunas K, Hang CT, Tsun Z-Y, Chen H, Lee NV, Wu JI, Shang C, Bayle JH, Shou W, Iruela-Arispe ML, et al. 2008. Endocardial Brg1 Represses ADAMTS1 to Maintain the Microenvironment for Myocardial Morphogenesis. *Developmental Cell* **14**: 298–311.

Stankunas K, Ma GK, Kuhnert FJ, Kuo CJ, Chang C-P. 2010. VEGF signaling has distinct spatiotemporal roles during heart valve development. *Developmental Biology* **347**: 325–336.

Stephens EH, Kearney DL, Grande-Allen KJ. 2012. Insight into pathologic abnormalities in congenital semilunar valve disease based on advances in understanding normal valve microstructure and extracellular matrix. *Cardiovascular Pathology* **21**: 46–58.

Stewart S, Gomez AW, Armstrong BE, Henner A, Stankunas K. 2014. Sequential and Opposing Activities of Wnt and BMP Coordinate Zebrafish Bone Regeneration. *Cell Reports* **6**: 482–498.

Sumi-Ichinose C, Ichinose H, Metzger D, Chambon P. 1997. SNF2beta-BRG1 is essential for the viability of F9 murine embryonal carcinoma cells. *Molecular and Cellular Biology* **17**: 5976–5986.

Tadano M, Edamatsu H, Minamisawa S, Yokoyama U, Ishikawa Y, Suzuki N, Saito H, Wu D, Masago-Toda M, Yamawaki-Kataoka Y, et al. 2005. Congenital Semilunar Valvulogenesis Defect in Mice Deficient in Phospholipase C. *Molecular and Cellular Biology* **25**: 2191–2199.

Takeuchi JK, Lickert H, Bisgrove BW, Sun X, Yamamoto M, Chawengsaksophak K, Hamada H, Yost HJ, Rossant J, Bruneau BG. 2007. Baf60c is a nuclear Notch signaling component required for the establishment of left-right asymmetry. *Proc Natl Acad Sci USA* **104**: 846–851.

Takeuchi JK, Lou X, Alexander JM, Sugizaki H, n PD-OI, Holloway AK, Mori AD, Wylie JN, Munson C, Zhu Y, et al. 2011. Chromatin remodelling complex dosage modulates transcription factor function in heart development. *Nature Communications* **2**: 187–11.

Theodoris CV, Li M, White MP, Liu L, He D, Pollard KS, Bruneau BG, Srivastava D. 2015. Human Disease Modeling Reveals Integrated Transcriptional and Epigenetic Mechanisms of NOTCH1 Haploinsufficiency. *Cell* **160**: 1072–1086.

Thomas JT, Canelos P, Luyten FP, Moos M. 2009. Xenopus SMOC-1 Inhibits Bone Morphogenetic Protein Signaling Downstream of Receptor Binding and Is Essential for Postgastrulation Development in Xenopus. *Journal of Biological Chemistry* **284**: 18994–19005.

Thomas PS, Sridurongrit S, Ruiz-Lozano P, Kaartinen V. 2012. Deficient Signaling via Alk2 (Acvr1) Leads to Bicuspid Aortic Valve Development. *PLoS ONE* **7**: e35539.

Timmerman LA, Grego-Bessa J, Raya A, Bertran E, Perez-Pomares JM, Diez J, Aranda S, Palomo S, McCormick F, Izpisua-Belmonte JC, et al. 2004. Notch promotes epithelial-mesenchymal transition during cardiac development and oncogenic transformation. *Genes & Development* **18**: 99–115.

Tkatchenko TV, Moreno-Rodriguez RA, Conway SJ, Molkentin JD, Markwald RR, Tkatchenko AV. 2009. Lack of periostin leads to suppression of Notch1 signaling and calcific aortic valve disease. *Physiological Genomics* **39**: 160–168.

Tokumura A, Majima E, Kariya Y, Tominaga K, Kogure K, Yasuda K, Fukuzawa K. 2002. Identification of Human Plasma Lysophospholipase D, a Lysophosphatidic Acid-producing Enzyme, as Autotaxin, a Multifunctional Phosphodiesterase. *Journal of Biological Chemistry* **277**: 39436–39442.

Tolstorukov MY, Sansam CG, Lu P. 2013. Swi/Snf chromatin remodeling/tumor suppressor complex establishes nucleosome occupancy at target promoters.

Tumbar T, Guasch G, Greco V, Blanpain C, Lowry WE, Rendl M, Fuchs E. 2004. Defining the Epithelial Stem Cell Niche in Skin. *Science* **303**: 359–363.

Umezu-Goto M, Kishi Y, Taira A, Hama K, Dohmae N, Takio K, Yamori T, Mills GB, Inoue K, Aoki J, et al. 2002. Autotaxin has lysophospholipase D activity leading to tumor cell growth and motility by lysophosphatidic acid production. *The Journal of Cell Biology* **158**: 227–233.

Venkatesh DA, Park KS, Harrington A, Miceli-Libby L, Yoon JK, Liaw L. 2008. Cardiovascular and Hematopoietic Defects Associated With Notch1 Activation in Embryonic Tie2-Expressing Populations. *Circulation Research* **103**: 423–431.

Votteler M, Berrio DAC, Horke A, Sabatier L, Reinhardt DP, Nsair A, Aikawa E, Schenke-Layland K. 2013. Elastogenesis at the onset of human cardiac valve development. *Development* **140**: 2345–2353.

Waldo K, Miyagawa-Tomita S, Kumiski D, Kirby ML. 1998. Cardiac neural crest cells provide new insight into septation of the cardiac outflow tract: aortic sac to ventricular septal closure. *Developmental Biology* **196**: 129–144.

Wang J, Gardner BM, Lu Q, Rodova M, Woodbury BG, Yost JG, Roby KF, Pinson DM, Tawfik O, Anderson HC. 2009. Transcription factor NFAT1 deficiency causes osteoarthritis through dysfunction of adult articular chondrocytes. *J Pathol* **219**: 163–172.

Wang J, Sridurongrit S, Dudas M, Thomas P, Nagy A, Schneider MD, Epstein JA, Kaartinen V. 2005. Atrioventricular cushion transformation is mediated by ALK2 in the developing mouse heart. *Developmental Biology* **286**: 299–310.

Wang Y, Wu B, Chamberlain AA, Lui W, Koirala P, Susztak K, Klein D, Taylor V, Zhou B. 2013. Endocardial to Myocardial Notch-Wnt-Bmp Axis Regulates Early Heart Valve Development ed. M. Katoh. *PLoS ONE* **8**: e60244.

Wirrig EE, Snarr BS, Chintalapudi MR, O'Neal JL, Phelps AL, Barth JL, Fresco VM, Kern CB, Mjaatvedt CH, Toole BP, et al. 2007. Cartilage link protein 1 (Crtl1), an extracellular matrix component playing an important role in heart development. *Developmental Biology* **310**: 291–303.

Wright EM, Snopek B, Koopman P. 1993. Seven new members of the Sox gene family expressed during mouse development. *Nucleic Acids Research* **21**: 744–744.

Wu B, Wang Y, Lui W, Langworthy M, Tompkins KL, Hatzopoulos AK, Baldwin HS, Zhou B. 2011. Nfatc1 Coordinates Valve Endocardial Cell Lineage Development Required for Heart Valve Formation. *Circulation Research* **109**: 183–192.

Wu B, Zhang Z, Lui W, Chen X, Wang Y, Chamberlain AA, Moreno-Rodriguez RA, Markwald RR, O'Rourke BP, Sharp DJ, et al. 2012. Endocardial Cells Form the Coronary Arteries by Angiogenesis through Myocardial-Endocardial VEGF Signaling. *Cell* **151**: 1083–1096.

Xi Q, He W, Zhang XH-F, Le H-V, Massagué J. 2008. Genome-wide impact of the BRG1 SWI/SNF chromatin remodeler on the transforming growth factor beta transcriptional program. *J Biol Chem* **283**: 1146–1155.

Xiong Y, Li W, Shang C, Chen RM, Han P, Yang J, Stankunas K, Wu B, Pan M, Bin Zhou, et al. 2013. Brg1 Governs a Positive Feedback Circuit in the Hair Follicle for Tissue Regeneration and Repair. *Developmental Cell* **25**: 169–181.

Xiong Y, Zhou B, Chang C-P. 2011. Analysis of the Endocardial-to-Mesenchymal Transformation of Heart Valve Development by Collagen Gel Culture Assay. Vol. 843 of, pp. 101–109, Cardiovascular Development: Methods and Protocols, Totowa, NJ.

Ya J, Erdtsieck-Ernste EB, de Boer PA, van Kempen MJ, Jongsma H, Gros D, Moorman AF, Lamers WH. 1998. Heart defects in connexin43-deficient mice. *Circulation Research* **82**: 360–366.

Yamada M, Revelli J-P, Eichele G, Barron M, Schwartz RJ. 2000. Expression of Chick Tbx-2, Tbx-3, and Tbx-5 Genes during Early Heart Development: Evidence for BMP2 Induction of Tbx2. *Developmental Biology* **228**: 95–105.

Yu P, Beppu H, Kawai N, Li E, Bloch K. 2005. Bone Morphogenetic Protein (BMP) Type II Receptor Deletion Reveals BMP Ligand-specific Gain of Signaling in Pulmonary Artery Smooth Muscle Cells. *Journal of Biological Chemistry* **280**: 24443–24450.

Yu S, Crawford D, Tsuchihashi T, Behrens TW, Srivastava D. 2011. The chemokine receptor CXCR7 functions to regulate cardiac valve remodeling. *Developmental Dynamics* **240**: 384–393.

Zaidi S, Choi M, Wakimoto H, Ma L, Jiang J, Overton JD, Romano-Adesman A, Bjornson RD, Breitbart RE, Brown KK, et al. 2013. De novo mutations in histone-modifying genes in congenital heart disease. *Nature* **498**: 220–223.

Zhang H-Y, Kluge M, Timpl R, Chu M-L, Ekblom P. 1993. The extracellular matrix glycoproteins BM-90 and tenascin are expressed in the mesenchyme at sites of endothelial-mesenchymal conversion in the embryonic mouse heart. *Differentiation* **52**: 211–220.

Zhang J, Chang JYF, Huang Y, Lin X, Luo Y, Schwartz RJ, Martin JF, Wang F. 2010. The FGF-BMP Signaling Axis Regulates Outflow Tract Valve Primordium Formation by Promoting Cushion Neural Crest Cell Differentiation. *Circulation Research* **107**: 1209–1219.